

NASA
CR
159467
c.1

TECH LIBRARY KAFB, NM
0062902

NASA CONTRACTOR REPORT

NASA CR-159467

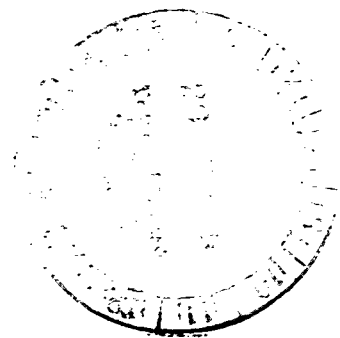
LOAN COPY: RETURN TO
AFWL TECHNICAL LIBRARY
KIRTLAND AFB, NM

**A THREE DIMENSIONAL TURBULENT COMPRESSIBLE FLOW MODEL FOR
EJECTOR AND FLUTED MIXERS**

W. L. Rushmore and S. W. Zelazny

*Prepared by
BELL AEROSPACE TEXTRON
Buffalo, New York
for Lewis Research Center*

NATIONAL AERONAUTICS AND SPACE ADMINISTRATION • WASHINGTON, D. C. • DECEMBER 1978





0062902

| | | | |
|--|--|--|------------|
| 1. Report No. | 2. Government Accession No. | 3. Recipient's Catalog No. | |
| 4. Title and Subtitle A Three-Dimensional Turbulent Compressible Flow Model for Ejector and Fluted Mixers | | 5. Report Date December 1978 | |
| | | 6. Performing Organization Code | |
| 7. Author(s) W.L. Rushmore, S.W. Zelazny | | 8. Performing Organization Report No. | |
| 9. Performing Organization Name and Address Bell Aerospace Textron Division of Textron Inc. P.O. Box One Buffalo, New York 14240 | | 10. Work Unit No. | |
| | | 11. Contract or Grant No. | |
| 12. Sponsoring Agency Name and Address National Aeronautics & Space Admin. Washington, D.C. 20546 | | 13. Type of Report and Period Covered Contractor Report | |
| | | 14. Sponsoring Agency Code | |
| 15. Supplementary Notes Lewis Technical Monitor: Norbert O. Stockman Final Report | | | |
| 16. Abstract A three-dimensional, finite element computer code was developed to analyze ejector and axisymmetric fluted mixer systems whose flow fields are not significantly influenced by streamwise diffusion effects. A two equation turbulence model was used to make comparisons between theory and data for various flow fields which are components of the ejector system, i.e., (a) turbulent boundary layer in a duct, (b) rectangular nozzle (free jet), (c) axisymmetric nozzle (free jet), (d) hypermixing nozzle (free jet), and (e) plane wall jet. Likewise, comparisons of the code with analytical results and/or other numerical solutions were made for components of the axisymmetric fluted mixer system. These included: (a) developing pipe flow, (b) developing flow in an annular pipe, (c) developing flow in an axisymmetric pipe with conical center body and no fluting, and (d) developing fluted pipe flow. Finally, two demonstration cases are presented which show the code's ability to analyze both the ejector and axisymmetric fluted mixers. | | | |
| 17. Key Words (Selected by Author(s)) Three-Dimensional Flow Turbulent Ejector Fluted Mixers Numerical Solution | | 18. Distribution Statement | |
| 19. Security Classif. (of this report) Unclassified | 20. Security Classif. (of this page) Unclassified | 21. No. of Pages | 22. Price* |

TABLE OF CONTENTS

| | Page |
|--|------|
| SUMMARY | 1 |
| INTRODUCTION | 1 |
| NOMENCLATURE | 2 |
| METHOD OF ANALYSIS | 3 |
| Governing Equations | 4 |
| Effective Diffusion Coefficient Models | 6 |
| Pressure Variations in Ducted Flow | 8 |
| Generalized Boundary Conditions | 8 |
| Variable Geometry Coordinate Transformation – Rectangular | 9 |
| Variable Geometry Coordinate Transformation – Axisymmetric | 10 |
| NUMERICAL RESULTS | 11 |
| Case 1. Turbulent Boundary Layer in a Duct | 11 |
| Case 2. Rectangular Nozzle (Two-Dimensional Flow) | 12 |
| Case 3. Axisymmetric Nozzle | 13 |
| Case 4. Hypermixing Nozzle | 14 |
| Case 5. Plane Wall Jet | 14 |
| Case 6. Developing Pipe Flow | 15 |
| Case 7. Developing Flow in an Annular Pipe | 15 |
| Case 8. Developing Flow in an Axisymmetric Pipe with Conical Center Body and No Fluting | 16 |
| Case 9. Developing Fluted Pipe Flow | 17 |
| EJECTOR ANALYSIS | 17 |

TABLE OF CONTENTS (Contd)

| | Page |
|--|------|
| AXISYMMETRIC FLUTED MIXER ANALYSIS | 18 |
| CONCLUDING REMARKS..... | 19 |
| APPENDIX A – COMOC DATA DECK PREPARATION | 20 |
| APPENDIX B – DEFINITION OF EJECTOR/DIFFUSER PARAMETERS | 34 |
| REFERENCES | 40 |

ILLUSTRATIONS

| Figure | | Page |
|--------|---|------|
| 1 | Schematic of Ejector in Wing Configuration | 96 |
| 2 | Axisymmetric Fluted Mixer Configuration | 97 |
| 3 | Variable Geometry Transformation in the y-Direction | 98 |
| 4 | Coordinate Transformation for Axisymmetric Flows from (y,z) to (η,ξ) Plane .. | 99 |
| 5 | Comparison between COMOC Predicted and Experimental Integral Parameters for the Turbulent Boundary Layer Developing in a Duct | 100 |
| 6 | Comparison between COMOC Predicted and Experimental Velocity Profile at x Equal 241.3 cm, for the Turbulent Boundary Layer Developing in a Duct | 101 |
| 7 | Comparison between COMOC Predicted and Experimental Integral Parameters for the Turbulent Boundary Layer Developing in a Duct for Gradient and No Slip Wall Boundary Conditions | 102 |
| 8 | Comparison between COMOC Predicted and Experimental Maximum Velocity Decay and Half-Jet Growth for the Rectangular Nozzle | 103 |
| 9 | Comparison between COMOC Predicted and Experimental Centerline Turbulent Kinetic Energy for the Rectangular Nozzle | 104 |
| 10 | Comparison between COMOC Predicted and Experimental Shape of TKE Profile at x/D Equal 70 for the Rectangular Nozzle | 105 |
| 11 | Comparison between COMOC Predicted and Experimental Decay of Centerline Velocity for the Axisymmetric Nozzle | 106 |
| 12 | Hypermixing Nozzle Geometry | 107 |
| 13 | Comparison with Eastlake Hypermixing Data | 107 |
| 14 | Configuration and Definition of Parameters for the Wall Jet Developing in a Duct | 108 |
| 15 | Comparison between COMOC Predicted and Experimental Skin Friction and Velocity Profile the Wall Jet Developing in a Duct | 109 |
| 16 | Comparison between COMOC Predicted and Experimental Maximum Velocity Decay and Half-Jet Growth for the Wall Jet Developing in a Duct | 110 |
| 17 | Comparison between COMOC Predicted and Experimental TKE Profile for the Wall Jet Developing in a Duct | 111 |
| 18 | Finite Elements for 90° Quadrant | 112 |
| 19 | Developing Flow in a Pipe | 113 |
| 20 | Fully Developed Axial Velocity Profile for Annular Pipe at x/a = 71 | 114 |
| 21 | Decay of Maximum Radial Velocity for Annular Pipe | 115 |
| 22 | Axial Velocity Profiles for Conical Center Pipe Flow | 116 |
| 23 | Maximum Secondary Velocity Comparison for Conical Center Pipe Flow | 117 |
| 24 | Fluted Pipe Geometry | 118 |
| 25 | Growth of Centerline Velocity for Fluted Pipe Flow | 119 |
| 26 | Axial Velocity Profiles for Fluted Pipe Flow | 120 |
| 27 | Maximum Secondary Velocities for Fluted Pipe Flow | 121 |
| 28 | Ejector/Diffuser Configuration | 122 |
| 29 | Axisymmetric Fluted Mixer Geometry | 123 |
| 30 | Axial Velocity Profiles for Fluted Mixer | 124 |

ILLUSTRATIONS (Contd)

| Figure | | Page |
|--------|---|------|
| 31. | Static Temperature Profiles for Fluted Mixer | 125 |
| 32. | Node Numbering of Finite Elements for Case IV | 126 |
| 33 | Finite Elements and Nodes for Changing Boundary Condition | 127 |

TABLES

| Number | | Page |
|--------|---|------|
| I | Ejector Results at $x = 0.0, 15.2,$ and 27.9 cm | 43 |
| II | Summary of Computer Time Required for Test Cases | 55 |
| III | Data Deck for Case I | 56 |
| IV | Data Deck for Case II | 59 |
| V | Data Deck for Case III | 62 |
| VI | Data Deck for Case IV | 65 |
| VII | Output from Case I | 69 |
| VIII | Output from Case II | 73 |
| IX | Output from Case III | 75 |
| X | Output from Case IV | 77 |
| XI | NAMEO1 Output for Case I | 93 |
| XII | NAMEO2 Output for Case I | 94 |

SUMMARY

A three-dimensional, finite element computer code was developed to analyze ejector and axisymmetric fluted mixer systems whose flow fields are not significantly influenced by streamwise diffusion effects. A two equation turbulence model was used to make comparisons between theory and data for various flow fields which are components of the ejector system, i.e., (a) turbulent boundary layer in a duct, (b) rectangular nozzle (free jet), (c) axisymmetric nozzle (free jet), (d) hypermixing nozzle (free jet), and (e) plane wall jet. Likewise, comparisons of the code with analytical results and/or other numerical solutions were made for components of the axisymmetric fluted mixer system. These included: (a) developing pipe flow, (b) developing flow in an annular pipe, (c) developing flow in an axisymmetric pipe with conical center body and no fluting, and (d) developing fluted pipe flow. Finally, two demonstration cases are presented which show the code's ability to analyze both the ejector and axisymmetric fluted mixers.

INTRODUCTION

Solution of the compressible three-dimensional boundary layer equations for flows over arbitrarily shaped external and internal configurations is a current design and analysis requirement for numerous important systems applications. It is only in the last few years that efficient numerical techniques coupled with large high speed computers have become available thereby making solution of these problems feasible, e.g., see the Proceedings of the Conference on Aerodynamic Analysis Requiring Advanced Computers, 1975 (ref. 1). Three-dimensional boundary layer solutions have been used to aid in understanding and/or designing both internal and external flow environments. For example, three-dimensional boundary layer solutions have been used to characterize mixing in scramjet combustors and chemical laser optical cavities, Zelazny et al. (refs. 2 and 3).

The recent development of hypermixing nozzles (refs 4 and 5) for ejectors has made the application of ejectors to VTOL aircraft appear attractive. For example, ejectors are being used in the wing and canard of supersonic aircraft to provide the thrust augmentation for VTOL capability (ref. 6). Also, fluted nozzle mixers are being used in various systems (turbine exhaust, etc.) to conserve fuel by mixing a hot core flow with a cold outer flow, thus getting more thrust from the resulting homogeneous exit mixture.

The overall objective of the present investigation, therefore, was to develop a computer program having the demonstrated capability of solving three-dimensional, compressible, viscous, mixing flow problems such as those characterizing the ejector system shown in figure 1, and the axisymmetric fluted mixer shown in figure 2. This goal was accomplished by extending and modifying the existing COMOC (Computational Mechanics of Continua) finite element program developed in earlier studies (refs. 2, 7, 8, and 9) to the ejector and axisymmetric fluted mixer system classes.

The report is subdivided into six sections plus the Appendices and References. The nomenclature used immediately follows this introduction.

The governing conservation equations and models for the effective diffusion coefficients (laminar plus turbulent) are presented in the METHOD OF ANALYSIS. Also presented in this section are a description of the generalized boundary conditions and the coordinate transformation used to analyze geometries whose cross section varies with distance downstream. The finite element solution algorithm used to solve the governing equations is described in detail in reference 2.

The ejector system is comprised of several component parts (turbulent wall jet, hypermixing nozzle, etc.). Experimental data characterizing these components were used to compare against theoretical predictions obtained using the COMOC computer code. A description of these experimental results and the details of the theoretical predictions are presented in the NUMERICAL RESULTS section. Also presented in this section are comparisons of the COMOC code with other numerical codes that model certain aspects of the axisymmetric fluted mixer system. Key results and recommendations for future efforts are presented in CONCLUDING REMARKS. Finally, APPENDICES A and B are included wherein the required input and output control for the COMOC code is described in a card-by-card sequence.

NOMENCLATURE

| | |
|----------------|--|
| A | Emperical constant = 23.5 |
| C_1^d, C_2^d | Emperical constants = 1.44, 1.92 |
| c_f | Skin friction coefficient |
| $c_{p, i}$ | Specific heat of ith species |
| d | Dissipation rate of turbulent kinetic energy |
| h_i | Static enthalpy of ith species |
| $h_{O, i}$ | Heat of formation of ith species |
| H | Total enthalpy |
| k | Turbulent kinetic energy (TKE) |
| ℓ | Mixing length |
| L | Length scale |
| N_k, N_d | Emperical constants = 1.0, 1.3 |
| N_{Pr}^e | Effective Prandtl number |
| N_{Re} | Reynold's number |
| N_{Sc}^e | Effective Schmidt number |
| r | Radial coordinate |
| T | Static temperature |
| T_O | Total temperature |
| u | Axial velocity in x-direction |
| v | Transverse velocity in y-direction |
| v_r | Transverse velocity in r-direction |
| v_θ | Transverse velocity in θ direction |
| w | Transverse velocity in z-direction |
| W_i | Molecular weight of ith species |
| (x, y, z) | Rectangular coordinates |
| Y_i | Mass fraction of ith species |
| δ | Boundary layer thickness |
| δ^* | Displacement thickness |

| | |
|----------------------|---|
| $\tilde{\delta}$ | Edge of constant shear stress region |
| ϵ | Kinematic eddy viscosity |
| θ | Azimuthal coordinate, momentum thickness |
| κ | Von Kármán constant = 0.435 |
| λ | Empirical constant = 0.09 |
| μ | Laminar viscosity |
| μ^e | Effective viscosity = $\mu + \rho \epsilon$ |
| ν | Kinematic viscosity |
| ρ | Density |
| τ | Shear stress |
| ω | Von Driest Damping Coefficient |
| (ξ, ζ, η) | Coordinate system in transformed domain |
| $()_e$ | Evaluated at edge of boundary layer |
| $()_T$ | Turbulent value |
| $()_\infty$ | Reference value |
| $()_*$ | Nondimensional quantity in wall shear stress formulation |
| $()^e$ | Effective quantity, equal to sum of laminar and turbulent value |
| $()^*$ | Nondimensional quantity in annular pipe formulation |
| $(\tilde{ })$ | Quantity evaluated at $y = \tilde{\delta}$ |
| $()'$ | Differentiation with respect to ξ |

METHOD OF ANALYSIS

Many researchers are now giving attention to numerical solution of three-dimensional parabolic and/or boundary-region flow fields. Most procedures employ a finite difference solution algorithm for variously combined forms of the continuity, momentum and energy equations. Several researchers have obtained solutions for the three-dimensional boundary-region flow of single-species fluids. A brief description of several methods (refs. 10 to 17) that have been employed is given in reference 2.

The system of partial differential equations governing such three-dimensional, confined unidirectional flows of a compressible, reacting fluid is obtained as an approximation to the full three-dimensional Navier-Stokes equations. This approximation, referred to as the "parabolic Navier-Stokes equations," describes steady, confined three-dimensional flows wherein (1) a predominant flow direction is discernible; (2) diffusion of mass, momentum, and energy in the predominant flow direction is negligible compared with convection; and (3) no disturbances are propagated upstream, e.g., recirculation is not considered.

Solution of the three-dimensional parabolic Navier-Stokes equations is obtained wherein the streamwise pressure variation is computed using the approach presented in the subsection Pressure Variation in Ducted Flows. This version of the computer code which computes an axial pressure gradient for confined flows is referred to as COMOC-3DPNS. If a pressure distribution is known *a priori* then that section of the code which computes streamwise pressure variations may be bypassed. The resulting

equations are herein referred to as the three-dimensional boundary region equations and represent a subset of the 3DPNS system. This variant of the code is referred to as COMOC-3DBR. Details of the numerical solution algorithm used to solve the differential equation system may be found in references 2 and 8.

Governing Equations

The parabolic Navier-Stokes equation system for a multiple-species, compressible, nonreacting flow takes the form:

Continuity

$$\frac{\partial}{\partial x}(\rho u) + \frac{\partial}{\partial y}(\rho v) + \frac{\partial}{\partial z}(\rho w) = 0 \quad (1)$$

u Momentum

$$\rho u \frac{\partial u}{\partial x} + \rho v \frac{\partial u}{\partial y} + \rho w \frac{\partial u}{\partial z} = -\frac{\partial \bar{p}}{\partial x} + \frac{\partial}{\partial y} \left(\frac{\mu^e}{N_{Re}} \frac{\partial u}{\partial y} \right) + \frac{\partial}{\partial z} \left(\frac{\mu^e}{N_{Re}} \frac{\partial u}{\partial z} \right) \quad (2)$$

v Momentum

$$\rho u \frac{\partial v}{\partial x} + \rho v \frac{\partial v}{\partial y} + \rho w \frac{\partial v}{\partial z} = -\frac{\partial p}{\partial y} + \frac{\partial}{\partial y} \left(\frac{\mu^e}{N_{Re}} \frac{\partial v}{\partial y} \right) + \frac{\partial}{\partial z} \left(\frac{\mu^e}{N_{Re}} \frac{\partial v}{\partial z} \right) \quad (3)$$

w Momentum

$$\rho u \frac{\partial w}{\partial x} + \rho v \frac{\partial w}{\partial y} + \rho w \frac{\partial w}{\partial z} = -\frac{\partial p}{\partial z} + \frac{\partial}{\partial y} \left(\frac{\mu^e}{N_{Re}} \frac{\partial w}{\partial y} \right) + \frac{\partial}{\partial z} \left(\frac{\mu^e}{N_{Re}} \frac{\partial w}{\partial z} \right) \quad (4)$$

Energy

$$\begin{aligned} \rho u \frac{\partial H}{\partial x} + \rho v \frac{\partial H}{\partial y} + \rho w \frac{\partial H}{\partial z} = & \frac{\partial}{\partial y} \left(\frac{\mu^e}{N_{Re} N_{Pr}^e} \frac{\partial H}{\partial y} \right) + \frac{\partial}{\partial z} \left(\frac{\mu^e}{N_{Re} N_{Pr}^e} \frac{\partial H}{\partial z} \right) \\ & - \frac{U_\infty^2}{H_\infty} \frac{\partial}{\partial y} \left[\frac{1 - N_{Pr}^e}{N_{Pr}^e} \frac{\mu^e}{2N_{Re}} \left(\frac{\partial u^2}{\partial y} + \frac{\partial v^2}{\partial y} + \frac{\partial w^2}{\partial y} \right) \right] \\ & - \frac{U_\infty^2}{H_\infty} \frac{\partial}{\partial z} \left[\frac{1 - N_{Pr}^e}{N_{Pr}^e} \frac{\mu^e}{2N_{Re}} \left(\frac{\partial u^2}{\partial z} + \frac{\partial v^2}{\partial z} + \frac{\partial w^2}{\partial z} \right) \right] \\ & - \frac{\partial}{\partial y} \left(\frac{N_{Sc}^e - N_{Pr}^e}{N_{Sc}^e N_{Pr}^e} \frac{\mu^e}{N_{Re}} \sum h_i \frac{\partial Y_i}{\partial y} \right) - \frac{\partial}{\partial z} \left(\frac{N_{Sc}^e - N_{Pr}^e}{N_{Sc}^e N_{Pr}^e} \frac{\mu^e}{N_{Re}} \sum h_i \frac{\partial Y_i}{\partial z} \right) \end{aligned} \quad (5)$$

Species Continuity

$$\rho u \frac{\partial Y_i}{\partial x} + \rho v \frac{\partial Y_i}{\partial y} + \rho w \frac{\partial Y_i}{\partial z} = \frac{\partial}{\partial y} \left(\frac{\mu^e}{N_{Sc}^e N_{Re}} \frac{\partial Y_i}{\partial y} \right) + \frac{\partial}{\partial z} \left(\frac{\mu^e}{N_{Sc}^e N_{Re}} \frac{\partial Y_i}{\partial z} \right) \quad (6)$$

For parabolic flow in the x-direction, \bar{p} in equation (2) is the mean value over the local (y, z) cross section and the diffusion terms in the x-direction have been neglected implying that recirculation zones are negligible in the flow fields of interest. The variables appearing in equations (1) to (6) are non-dimensionalized with respect to μ_∞ , ρ_∞ , U_∞ , H_∞ , and a length scale L. The Reynolds number N_{Re} , effective Prandtl number N_{Pr}^e , and effective Schmidt number N_{Sc} are defined for a combination of laminar and turbulent contributions as,

$$N_{Re} = \frac{U_\infty \rho_\infty L}{\mu_\infty} \quad (7a)$$

$$\frac{\mu^e}{N_{Pr}^e} = \frac{\mu}{N_{Pr}} + \frac{\rho \epsilon}{(N_{Pr})_T} \quad (7b)$$

$$\frac{\mu^e}{N_{Sc}^e} = \frac{\mu}{N_{Sc}} + \frac{\rho \epsilon}{(N_{Sc})_T} \quad (7c)$$

In equation (7), μ is the laminar viscosity, ϵ is the kinematic eddy viscosity, and the subscript T denotes a turbulent parameter. The stagnation enthalpy is defined in terms of species static enthalpies as

$$H \equiv \sum_i h_i Y_i + \frac{1}{2} (u^2 + v^2 + w^2) \quad (8)$$

The static enthalpy includes the heat of formation $h_{o,i}$ of the ith species in its definition as

$$h_i \equiv \int_{T_0}^T c_{p,i} dt + h_{o,i} \quad (9)$$

An equation of state is obtained by assuming perfect-gas behavior for each species and using Dalton's Law,

$$p = \rho RT \sum_i \frac{Y_i}{W_i} \quad (10)$$

where R is the universal gas constant and W_i is the molecular weight of the ith species.

Effective Diffusion Coefficient Models

Closure of the governing equations requires introducing relationships to define the effective viscosity, and the turbulent Prandtl, and Schmidt numbers. In this investigation it was assumed that mass and thermal energy, both scalar quantities, diffuse at the same rate. Hence, the turbulent Lewis number, $(N_{Le})_T$, is equal to unity. The validity of this assumption is supported by numerous experimental studies and is generally used in most turbulence modeling efforts. This assumption requires $(N_{Pr})_T = (N_{Sc})_T$. It is then only necessary to specify $(N_{Pr})_T$. Generally, it is sufficient to define $(N_{Pr})_T$ equal to a constant in the range from 0.7 to 1.0. For this study, the value of $(N_{Pr})_T = 0.7$ is used.

Four different approaches to modeling ϵ are considered: (1) ϵ equal to a constant (usually some multiple of the laminar viscosity, μ), (2) mixing length theory (MLT), (3) a one-equation turbulence model coupled with an empirical turbulent length scale relation, and (4) the two-equation turbulence model reported by Launder and Spalding (ref. 18).

Mixing Length Theory - The two-dimensional MLT in the (x, y) coordinates, ϵ is given by:

$$\epsilon = \ell^2 \left| \frac{\partial u}{\partial y} \right| \quad (11)$$

The mixing length is defined as

$$\ell \equiv \begin{cases} \kappa y \omega & (0 \leq y \leq \lambda \delta / \kappa) \\ \lambda \delta \omega & (y > \lambda \delta / \kappa) \end{cases} \quad (12)$$

where

$$\begin{aligned} \kappa &= 0.435 \\ \lambda &= 0.09 \\ \delta &= \text{boundary-layer thickness} \end{aligned}$$

The Van Driest damping coefficient is

$$\omega \equiv 1 - \exp\left(-\frac{y^*}{A}\right) \quad (13)$$

where:

$$\begin{aligned} y^* &\equiv \frac{u^* y}{\nu} \\ u^* &= \text{friction velocity, } \sqrt{\rho_w \tau} \\ \tau &= \text{skin friction} \\ \rho &= \text{density at wall} \end{aligned}$$

ν = kinematic viscosity

A \equiv 23.5

One (k) and Two (k&d) Equations Turbulence Models - Dimensional analysis shows that the kinematic viscosity may be expressed as the product of a characteristic velocity (V_t) and the length scale (ℓ_d); hence define

$$\epsilon \equiv C_\tau V_t \ell_d \quad (14a)$$

where C_τ is an empirical constant and the relationship between ℓ_d and ℓ from MLT is given by Launder and Spalding (ref. 18) as

$$\ell_d = C_\tau^{1/2} \ell \quad (14b)$$

The two models both assume that the turbulence velocity V_t is given by

$$V_t = k^{1/2} \quad (15)$$

where k is the turbulent kinetic energy

$$k = \frac{\overline{u'^2} + \overline{v'^2} + \overline{w'^2}}{2} \quad (16)$$

The one equation model assumes an empirical relation for ℓ_d , while the two equation model expresses ℓ_d in terms of k and the dissipation rate of turbulence, d as

$$\ell_d = k^{3/2}/d \quad (17)$$

The turbulent kinetic energy and dissipation are computed from

$$\begin{aligned} \rho u \frac{\partial k}{\partial x} + \rho v \frac{\partial k}{\partial y} + \rho w \frac{\partial k}{\partial z} &= \frac{\partial}{\partial y} \left(\frac{\rho \epsilon}{N_k N_{Re}} \frac{\partial k}{\partial y} \right) \\ &+ \frac{\partial}{\partial z} \left(\frac{\rho \epsilon}{N_k N_{Re}} \frac{\partial k}{\partial z} \right) + \frac{\rho \epsilon}{N_{Re}} \left[\left(\frac{\partial u}{\partial y} \right)^2 + \left(\frac{\partial u}{\partial z} \right)^2 \right] \end{aligned} \quad (18)$$

$$\begin{aligned} \rho u \frac{\partial d}{\partial x} + \rho v \frac{\partial d}{\partial y} + \rho w \frac{\partial d}{\partial z} &= \frac{\partial}{\partial y} \left(\frac{\rho \epsilon}{N_d N_{Re}} \frac{\partial d}{\partial y} \right) \\ &+ \frac{\partial}{\partial z} \left(\frac{\rho \epsilon}{N_d N_{Re}} \frac{\partial d}{\partial z} \right) + \frac{C_1^d d}{N_{Re} k} \left[\left(\frac{\partial u}{\partial y} \right)^2 + \left(\frac{\partial u}{\partial z} \right)^2 \right] - \frac{C_2^d d^2}{2} \end{aligned} \quad (19)$$

where it is assumed that the production of turbulent kinetic energy is due to the $\overline{u'v'}$ component of shear stress, i.e., $\partial u/\partial z$ is negligible compared to $\partial u/\partial y$. This assumption is reasonable for the flow

regimes examined herein using the k and d model. The empirical constants used in equations (14), (18), and (19) as suggested in reference 18 are as follows: $C_\tau = 0.09$, $C_1^d = 1.44$, $C_2^d = 1.92$, $N_k = 1.0$, and $N_d = 1.3$.

Pressure Variation in Ducted Flow

For internal flows, characterized by boundary-layer thicknesses which are small in comparison with the overall internal duct dimension, the axial pressure distribution can be accurately approximated by inviscid flow solutions. However, when the flow is confined in a duct whose lateral dimension is not large with respect to the boundary layer thickness, this approach is invalid. Here, boundary-layer development directly influences the pressure distribution within the duct, and an axial pressure gradient is induced by viscous effects. For these flows, a quasi-one-dimensional integral treatments of equations (3) and (5) has been suggested wherein for steady flows, equations (3) and (5) are integrated across the duct transverse dimensions to obtain a relation for the mean value of axial pressure gradient (three-dimensional parabolic Navier-Stokes variant). Details of the method are described in references 17 and 19.

Generalized Boundary Conditions

The finite element solution algorithm considers the following generalized boundary condition for the variable q.

$$a_1 q + a_2 \frac{\partial q}{\partial n} - a_3 = 0 \quad (20)$$

where a_1 , a_2 , a_3 are user specified constants and $\partial q/\partial n$ is the local outward pointing normal derivative.

For turbulent flows near walls where the velocity gradient becomes very large, it was found useful to replace the no-slip boundary condition for the axial velocity. In its place, the following boundary condition on the velocity gradient at the wall was used.

$$\left. \frac{\partial u}{\partial y} \right|_{\text{wall}} = \frac{\tau_w}{\mu} \quad (21)$$

where τ_w is the local value of the wall shear stress and is computed from the following relation given by Patankar and Spalding (ref. 19).

$$\tau_w = \kappa^2 \rho_1 u_1^2 (R_*^{-1} - 0.156R_*^{-0.45} + 0.08723R_*^{-0.3} + 0.0371R_*^{-0.18}) F_p \quad (22)$$

where κ is von Karman's constant (used in defining the mixing length) $R_* = \kappa^2 \tilde{R}$, $\tilde{R} = \frac{u_1 \delta}{\nu_1}$. The subscript 1 corresponds to evaluation at a distance δ from the wall (δ is defined to be the edge of the constant shear stress region). The effect of pressure gradient on the shear stress is included in equation (22) by the parameter F_p given by

$$F_p = \left[\frac{1 - 4F_* R_*}{(12.8^{2.5} + R_*^{2.5}) 0.4} \right]^{1.6} ; F_* = \frac{\tilde{\delta}}{\rho_1 u_1^2} \frac{d\bar{p}}{dx} \quad (23)$$

Variable Geometry Coordinate Transformation - Rectangular

By an appropriate transformation of variables (essentially coordinate stretching) the cross section in the (y, z) plane may be allowed to grow as a specified function of x. This proves useful in computing internal flows (wall jets, etc.) when the rate of growth of the solution field can be approximated *a priori*. It is also essential in computing confined flows in diffusers or other variable area ducts. It should be noted that the finite element grid is established at the initial cross-sectional geometry (whatever its shape) and then the finite elements in the cross-section expand and/or contract as the flow is followed downstream. At the present time, the COMOC code can handle constant area flows with any cross-sectional geometry. However, the variable cross section option presently is limited to rectangular or axisymmetric geometries.

The coordinate transform for the ejector system is defined as follows. Consider a flow in a domain bounded in the y direction by walls with a specified geometry $y = f_1(x)$ and $y = f_2(x)$ and bounded in the z direction by walls $z = g_1(x)$ and $z = g_2(x)$ (see Figure 3). The transformations from the (x, y, z) space to the (ξ, η, ζ) space are given by:

$$\begin{aligned} \xi &= x \\ \eta &= \frac{y - f_1(x)}{f_2(x) - f_1(x)} \\ \zeta &= \frac{z - g_1(x)}{g_2(x) - g_1(x)} \end{aligned} \quad (24)$$

Then, for example, equation (2) in the transformed plane becomes

$$\begin{aligned} \rho u \frac{\partial u}{\partial \xi} + F_1 \rho v \frac{\partial u}{\partial \eta} + G_1 \rho w \frac{\partial u}{\partial \zeta} &= - \frac{d\bar{p}}{d\xi} + \rho u \left[(F_2 + \eta F_3) \frac{\partial u}{\partial \eta} \right. \\ &\left. + (G_2 + \zeta G_3) \frac{\partial u}{\partial \zeta} \right] + F_1^2 \frac{\partial}{\partial \eta} \left(\frac{\mu^e}{N_{Re}} \frac{\partial u}{\partial \eta} \right) + G_1^2 \frac{\partial}{\partial \zeta} \left(\frac{\mu^e}{N_{Re}} \frac{\partial u}{\partial \zeta} \right) \end{aligned} \quad (25)$$

where:

$$\begin{aligned} F_1(\xi) &= \frac{1}{f_2(\xi) - f_1(\xi)} & G_1(\xi) &= \frac{1}{g_2(\xi) - g_1(\xi)} \\ F_2(\xi) &= \frac{f_1'(\xi)}{f_2(\xi) - f_1(\xi)} & G_2(\xi) &= \frac{g_1'(\xi)}{g_2(\xi) - g_1(\xi)} \end{aligned} \quad (26)$$

$$F_3(\xi) = \frac{f'_2(\xi) - f'_1(\xi)}{f_2(\xi) - f_1(\xi)} \quad G_3(\xi) = \frac{g'_2(\xi) - g'_1(\xi)}{g_2(\xi) - g_1(\xi)}$$

Variable Geometry Coordinate Transformation - Axisymmetric

The coordinate transform for the axisymmetric fluted mixer system is performed using the same approach used for rectangular geometries. Consider a flow in an axisymmetric domain bounded in the radial direction by walls with a specified geometry (see figure 4). The transformation from the (x, y, z) to the (ξ, η, ζ) domain is then found as follows. All points in the (y, z) plane can be specified in polar coordinates as (see figure 4).

$$\begin{aligned} y &= r \sin\theta \\ z &= r \cos\theta \end{aligned} \quad (27)$$

Likewise, the corresponding point in the corresponding (η, ζ) plane is given by:

$$\begin{aligned} \eta &= \bar{r} \sin\theta \\ \zeta &= \bar{r} \cos\theta \end{aligned} \quad (28)$$

where

$$\bar{r} = \frac{r - r_1(x)}{r_2(x) - r_1(x)} = \frac{\sqrt{y^2 + z^2} - r_1(x)}{r_2(x) - r_1(x)} \quad (29)$$

Thus, the coordinate transformation is given by

$$\begin{aligned} \xi &= x \\ \eta &= \bar{r} \sin\theta = \bar{r} \frac{y}{\sqrt{y^2 + z^2}} = \frac{y}{r_2(x) - r_1(x)} \left[1 - \frac{r_1(x)}{\sqrt{y^2 + z^2}} \right] \\ \zeta &= \bar{r} \cos\theta = \bar{r} \frac{z}{\sqrt{y^2 + z^2}} = \frac{z}{r_2(x) - r_1(x)} \left[1 - \frac{r_1(x)}{\sqrt{y^2 + z^2}} \right] \end{aligned} \quad (30)$$

Finally, for example, equation (2) in the transformed plane becomes

$$\begin{aligned} \rho u \frac{\partial u}{\partial \xi} + (\rho u F_4 + \rho v F_6 + \rho w F_8) \frac{\partial u}{\partial \eta} + (\rho u F_5 + \rho v F_7 + \rho w F_9) \frac{\partial u}{\partial \zeta} = \\ - \frac{dp}{d\xi} + \left(F_6 \frac{\partial}{\partial \eta} + F_7 \frac{\partial}{\partial \zeta} \right) \left(\frac{\mu^e}{N_{Re}} F_6 \frac{\partial u}{\partial \eta} + \frac{\mu^e}{N_{Re}} F_7 \frac{\partial u}{\partial \zeta} \right) \\ + \left(F_8 \frac{\partial}{\partial \eta} + F_9 \frac{\partial}{\partial \zeta} \right) \left(\frac{\mu^e}{N_{Re}} F_8 \frac{\partial u}{\partial \eta} + \frac{\mu^e}{N_{Re}} F_9 \frac{\partial u}{\partial \zeta} \right) \end{aligned} \quad (31)$$

where:

$$F_4 = -\eta \left[\frac{r'_2(\xi) - r'_1(\xi)}{r_2(\xi) - r_1(\xi)} + \frac{r'_1(\xi)}{(r_2(\xi) - r_1(\xi)) \sqrt{\eta^2 + \zeta^2}} \right] \quad (32a)$$

$$F_5 = -\zeta \left[\frac{r'_2(\xi) - r'_1(\xi)}{r_2(\xi) - r_1(\xi)} + \frac{r'_1(\xi)}{(r_2(\xi) - r_1(\xi)) \sqrt{\eta^2 + \zeta^2}} \right] \quad (32b)$$

$$F_6 = \frac{r_1(\xi)\eta^2 + [r_2(\xi) - r_1(\xi)] (\eta^2 + \zeta^2)^{3/2}}{[r_2(\xi) - r_1(\xi)] [\eta^2 + \zeta^2] [r_1(\xi) + (r_2(\xi) - r_1(\xi)) \sqrt{\eta^2 + \zeta^2}]} \quad (32c)$$

$$F_7 = \frac{r_1 \zeta \eta}{[r_2(\xi) - r_1(\xi)] [\eta^2 + \zeta^2] [r_1(\xi) + (r_2(\xi) - r_1(\xi)) \sqrt{\eta^2 + \zeta^2}]} \quad (32d)$$

$$F_8 = \text{Same as } F_7 \quad (32e)$$

$$F_9 = \frac{r_1(\xi)\zeta^2 + [r_2(\xi) - r_1(\xi)] (\eta^2 + \zeta^2)^{3/2}}{[r_2(\xi) - r_1(\xi)] [\eta^2 + \zeta^2] [r_1(\xi) + (r_2(\xi) - r_1(\xi)) \sqrt{\eta^2 + \zeta^2}]} \quad (32f)$$

NUMERICAL RESULTS

A good test of the accuracy of a numerical model is a direct comparison of theoretical predictions with experimental data. To this end, predictions for nine different flow conditions were obtained, table II. These particular test cases were chosen for one or both of the following reasons: the data were well documented in that turbulence initial conditions for the TKE equations were either specified or obtainable using algebraic relations from other given data; a given case represents one of the possible component parts of the more complex ejector or axisymmetric fluted mixer system. Where applicable, more than one of the turbulence models described above was used.

Test Cases

Case 1. Turbulent Boundary Layer in a Duct - The data for this case were selected from the Proceedings of the Stanford conference on the Computation of Turbulent Boundary Layers (ref. 21) and provide a well defined description of incompressible boundary layer development. The specific case (Number 2400 of ref. 21) represents an initial equilibrium boundary layer in a moderate positive pressure gradient (specified) where the pressure gradient is abruptly decreased to zero and the flow relaxes towards a new equilibrium condition. Since the pressure distribution is given, the three-dimensional boundary region variant of the COMOC computer code was used. The initial velocity profile was used to generate initial conditions for ϵ and ϱ_d using the MLT model. The initial k&d profiles were then obtained algebraically from equations (14), (15) and (17). The gradient boundary condition relating the velocity gradient at the wall to the local value of the wall shear stress was used. The transverse velocity component v is obtained by numerically integrating the two-dimensional form of the continuity equation.

Data available for comparison include the axial (x) development of the velocity profile, skin friction coefficient $C_f/2$, displacement thickness δ^* , and momentum thickness θ , where:

$$C_f/2 = \frac{\tau_w}{\rho u_e^2} \quad (33)$$

$$\delta^* = \int_0^\delta \left(1 - \frac{\rho u}{\rho_e u_e}\right) dy \quad (34)$$

$$\theta = \int_0^\delta \frac{\rho u}{\rho_e u_e} \left(1 - \frac{u}{u_e}\right) dy \quad (35)$$

By definition, δ is the local boundary layer thickness defined as the distance y from the wall to the point in the boundary layer profile where u/u_e equal 0.99 and u_e, ρ_e are the inviscid values at the outer edge of the boundary layer.

Results were obtained using the MLT model and the two-equation TKE model. Figure 5 shows the skin friction $C_f/2$, δ^* and θ , while figure 6 depicts the final velocity profile at 241.3 cm downstream. As can be seen, both models accurately predict (within 5%) both the final shape of the velocity profile as well as the parameters describing its axial development. Figure 7 shows a comparison of two runs made, both of which used the MLT model. However, one run was made using the gradient boundary condition. The finite element discretization for both cases was the same. As can be seen, the prediction of δ^* and θ are within 5% of the data for both cases. However, the skin friction coefficient $C_f/2$ drops off very rapidly using the no-slip boundary condition (at a distance of 132.1 cm, the predicted value is less than half the measured value). Better agreement could be obtained using the no slip wall only by adding several more nodes in the near wall region. This would greatly increase the amount of computer time required since the integration step size stability is controlled by the minimum spacing between the nodes in the transverse direction. This emphasizes the benefits obtained in using the gradient boundary condition.

Case 2. Rectangular Nozzle (Two-Dimensional Flow) - The data for this case is given by Bradbury (ref. 22). He obtained self-similar velocity and TKE profiles by empirically curve fitting his experimental data. He gives the following results:

$$\frac{u - u_1}{u_0} = f(\eta) = \exp [-0.6749\eta^2 (1 + 0.0269\eta^4)] \quad (36)$$

$$\frac{k}{u_0^2} = g(\eta) \quad (37)$$

where

$$\eta = y/\delta$$

$$u_0 \sim \text{centerline velocity inside jet}$$

$$u_1 \sim \text{freestream velocity}$$

δ ~ y location inside jet where $f(\eta) = 1/2$

$g(\eta)$ ~ given in graphic form

The computations were started at x/D equal to 20 (where D is the nozzle exit width in the y -direction). Initial profiles for u and k were obtained from the empirical curves. The initial value of ℓ_d was obtained from the empirical relation:

$$\ell_d = |y_2 - y_1| \quad (38)$$

where

y_1 = point in jet profile where $f(\eta) = 0.1$

y_2 = point in jet profile where $f(\eta) = 0.9$

Then the initial d profile may be obtained using equation (17). Again, the transverse velocity is computed by numerically integrating the two-dimensional form of the continuity equation.

Results were obtained using the two-equation TKE model and also using the TKE equation (18) combined with equation (38), from which ℓ_d is computed at each x station based on the local shape of the velocity profile. Figure 8 shows results using both models for the centerline velocity decay and the half-jet thickness growth compared with the experimental data. The two-equation model gives excellent agreement for u_0/u_1 and overpredicts δ/D by less than 5% at x/D equal to 70. The one-equation model overpredicts u_0/u_1 by 6% and underpredicts δ/D by 7% at x/D equal 70. However, the true test of both models is in how well they compare with the turbulence data.

Figure 9 gives the results of the centerline turbulence kinetic energy (k_c) scaled by u_0^2 for both models. The two-equation model shows an initial drop in this value then a steady increase so that at x/D equal 70 the value is 8% higher than the experimental value. The one-equation model shows an initial drop and then the value remains constant at 10% lower than the experimental value. The discrepancy in both models may be due to the values of 0.1 and 0.9 used to compute ℓ_d in equation (38). These values are poorly defined and further refinement could give better agreement for both models since these values are used to generate an initial d profile for the two-equation model. The shape of the k profile for both models at x/D equal 70 is shown in figure 10. The profiles have been scaled with respect to k_c so that the magnitude differences depicted in figure 9 are eliminated. Both models accurately predict the shape of the profile (to within 10%) as well as the location of the maximum turbulence kinetic energy.

Case 3. Axisymmetric Nozzle - This case provides a good check on the three-dimensional solution capability of the analysis. Although the flow field may be characterized using only two spatial coordinates (the radius r and axis x), solutions were obtained using a rectangular coordinate system (x, y, z). The specific case considered is an incompressible jet into a stationary medium (quiescent jet). Calculations were started at 106.7 cm downstream of an 8.89 cm diameter jet ($x/D = 12$) where the flow may be described using the similarity solutions reported by Schlichting (ref. 23). The similarity solution is valid for a constant effective viscosity ϵ . Therefore, solutions were obtained by integrating the three velocity components using a constant value of ϵ and also the two-equation TKE model. Initial values for the two-equation model were obtained algebraically by using the known

value of ϵ and by estimating the initial value of ℓ_d from the velocity profile. Figure 11 shows the predictions for both models compared to the similarity solution.

Case 4. Hypermixing Nozzle - Figure 12 shows the hypermixing nozzle being considered. Data are available from Eastlake (ref. 24) giving velocity profiles in the y, z plane at distances 3.0 and 5.0 in. downstream from the nozzle. With the exception of the jet exit speed and nozzle geometry, no initial condition data were available for this case. The procedure used to establish initial conditions was to first assume a constant value of ϵ for the turbulence model. This value was varied until reasonable agreement was obtained with the experimental data for the maximum velocity decay. It was assumed (arbitrarily) that the turbulence kinetic energy in the hypermixing nozzle exit plane was 1.5% and equations (14), (15), and (17) were used to compute the initial turbulence dissipation. Having defined the starting conditions, calculations were then made to predict the flow field development downstream using the two-equation turbulence model. Both magnitude and shape of the velocity profiles in transverse direction were reasonably predicted, figure 13, with a maximum difference between data and theory of 5% for the peak velocity. Of course, these calculations only demonstrate the capability of the code to analyze the hypermixing configuration rather than validate the turbulence models or manner in which the initial conditions were obtained. Analysis of turbulence data for this configuration would be required to address the question relating to the accuracy of the turbulence models and initial conditions. Such an effort was beyond the scope of this study.

Case 5. Plane Wall Jet - This flow provides an excellent check of the turbulence model being used. Consider a two-dimensional flow where the turbulent component of the shear stress is assumed to be given by:

$$\overline{-\rho u'v'} = \rho \epsilon \frac{\partial u}{\partial y} \quad (39)$$

An obvious implication of equation (39) is that the turbulent stress goes to zero at the maximum velocity location in the $u(y)$ profile for a turbulent wall jet. It has been pointed out experimentally by Harris (ref. 25) that the turbulent stress does not go to zero at this point. Indeed, the turbulent stress is quite large and is caused by the asymmetry of the velocity profile about the maximum velocity point.

The plane turbulent wall jet is shown in figure 14, along with a definition of the flow parameters. Initial profiles for u , k , and d were obtained as follows. Experimental data are available for self-similar velocity profiles (ref. 26), mean turbulent kinetic energy (ref. 27), and turbulent shear stress profiles (ref. 28). From these profiles and equations (14) and (17), initial profiles for u , k , and d at $x/L = 25$ were obtained and then numerically integrated to $x/L = 100$. The solution domain was allowed to grow with x using the variable geometry coordinate transformation. In this way, at x/L equal 100 there were still the same number of node points in the turbulent boundary layer portion of the jet as at the initial station. Both the no slip wall and the gradient boundary condition were used to provide another check on the accuracy of the gradient boundary condition.

Shown in figure 15a are numerical results for the axial skin friction C_f given by $2\tau_w/\rho u_j^2$, compared with experimental data of reference 26. As can be seen, the results obtained using the gradient boundary condition remain within the spread of the data. It should be pointed out that both numerical curves were obtained using only four node points in the initial u profile between the wall and the maximum velocity. This explains why the no slip boundary condition results for the skin friction are over an order-of-magnitude smaller than the data at x/L equal 100, i.e., the

discretization was inadequate. Shown in figure 15b are the velocity profiles at $x/L = 100$ for both cases compared with the data of Schwartz and Cosart (ref. 28). Again, the gradient boundary condition results show the flow field remaining self-similar, while the no-slip boundary condition results showed marked deviation from the self-similar profile. Figures 16a and 16b show the maximum velocity decay and half-jet growth compared with the data of reference 26. Figure 17a shows the maximum turbulent kinetic energy (k_{max}) compared to the experimental self-similar value. This value increases initially to a value 9% larger at x/L equal 30 then decreases to a value only 1% larger at x/L equal 100. Figure 17b also shows the turbulent kinetic energy profile at x/L equal 100.

Case 6. Developing Pipe Flow – The experimental data for this case are taken from Nikuradse (ref. 23) who shows the development of the velocity profile from its initial slug value to the fully developed parabolic profile. For this case, a two-dimensional finite difference code in polar coordinates was also used to make comparisons between the predicted secondary velocity decay computed using finite element and difference techniques.

For axisymmetric flows, the continuity equation is rewritten in polar coordinates, assuming the circumferential velocity component (v_θ) is negligible, to give

$$\frac{\partial}{\partial x} (\rho r u) + \frac{\partial}{\partial r} (\rho r v_r) = 0 \quad (40)$$

The radial velocity v_r is related to v and w by

$$v = v_r \sin \theta \quad (41)$$

$$w = v_r \cos \theta$$

where

$$\theta = \tan^{-1} \left(\frac{y}{z} \right) \quad (42)$$

The method of solution used by the COMOC code for axisymmetric flow is to integrate the u momentum equation (2) downstream, then compute v_r from the continuity equation (40) in polar coordinates, and finally obtain v and w from equation (41). For cases 6, 7, and 8, the assumption of zero circumferential velocity, v_θ , is exact since the flows are two dimensional. However, case 9 is three dimensional and will determine how much accuracy is lost when making the assumption that $v_\theta = 0$. The COMOC code was run for both a 45° and 90° wedge of the circular cross section pipe (using angular symmetry) with this method of computing v and w . The finite element discretization for the 90° wedge is shown in figure 18. The solution was started at x equal zero assuming a slug profile for u and a flow Reynolds number ($Re = \frac{2\rho\bar{u}a}{\mu}$) of 500 where \bar{u} is the initial slug velocity and a is the pipe radius. The results for the growth of the centerline velocity u_C , compared with the finite difference solution, are shown in figure 19a. The decay of the maximum radial velocity v_r is shown in figure 19b. Both COMOC runs were made with the same number of elements. Therefore, the 45° wedge had finer resolution. As can be seen, both the 45° and 90° wedge give excellent agreement with the 2D finite difference code.

Case 7. Developing Flow in an Annular Pipe – The analytical solution for a fully developed flow in an annular pipe is given by:

$$u^*(r^*) = - \left(\frac{Re}{8} \right) \left(\frac{dp^*}{dx^*} \right) \left[(1 - r^*)^2 - \frac{(1 - r_0^{*2}) 1}{1 nr_0^*} r^* \right] \quad (43)$$

where

$$\begin{aligned}
 u^* &= u/\bar{u} \\
 r^* &= r/a \\
 r_0^* &= r_0/a \\
 x^* &= x/a \\
 Re &= \frac{2\rho a \bar{u}}{\mu} \\
 p^* &= \frac{p}{\rho \bar{u}^2}
 \end{aligned} \tag{44}$$

and \bar{u} is the initial slug velocity, a is the outer pipe radius, and r_0 is the inner pipe radius.

The pressure gradient $\frac{dp}{dx}$ may be found in terms of the mean velocity \bar{u} , Reynolds number Re , and r_0 as follows.

$$\bar{u}^* \equiv \frac{\bar{u}}{\bar{u}} = 1 = \frac{\int_{r_0^*}^1 r^* u^* dr^*}{\int_{r_0^*}^1 r^* dr^*} \tag{45}$$

using equations (43) and (44) gives

$$\bar{u}^* = 1 = - \frac{Re}{16(1-r_0^{*2})} \frac{dp^*}{dx^*} \left[(1-r_0^{*4}) + \frac{(1-r_0^{*2})^2}{1nr_0^*} \right] \tag{46}$$

Therefore,

$$\frac{dp^*}{dx^*} = \frac{-16(1-r_0^{*2})}{Re \left[(1-r_0^{*4}) + (1-r_0^{*2})/1nr_0^* \right]} \tag{47}$$

The two dimensional finite differences and COMOC codes were run with $Re = 500$, $\bar{u} = 0.5468$, and $r_0^* = 0.25$. The fully developed value of $dp^*/dx^* = -0.0938$ was obtained with both codes.

Figure 20 shows the axial velocity profiles for both codes at $x = 71a$ compared to the analytical solution. The COMOC solution domain is a 90° wedge with 51 node points (73 elements). The decay of the maximum radial velocity (w along θ equal 0° and v along θ equal 90°) is shown in figure 21.

Case 8. Developing Flow in an Axisymmetric Pipe with Conical Center Body and no Fluting – This case can be viewed as a combination of cases 6 and 7. At the initial x station, the pipe has an annular shape. This annulus then conically decreases in size until at some downstream station the pipe cross section changes from annular to circular. See figure 29b for a side view. For this problem, the variable geometry option for axisymmetric flows in COMOC was used to account for the conical center. The 2D finite difference code was also modified to compute variable geometry flows

in the radial direction. Shown in figure 22 is a comparison between the two codes for the u velocity profiles at several stations. The conical center has an initial radius of $r_0/a = 0.25$ at $x/a = 0$, and its radius decreases linearly to zero at $x/a = 10.0$. Figure 23 shows the comparison of the secondary velocity decay between the two codes.

Case 9. Developing Fluted Pipe Flow – The configuration for this flow is shown in figure 24. Two flows, of differing velocity, are separated by a fluting. At $x = 0$, the fluting ends and the two flows then merge in the downstream x direction. This flow is three dimensional in nature and was chosen to test the validity of the assumption that v_θ is negligible when computing v_r from the continuity equation (40) in polar coordinates. A three dimensional finite difference code used in reference 29 was used as a comparison to test this assumption. While this code was written for more elaborate flows, it can be used to solve for the flow in a straight pipe in cylindrical coordinates. Thus, both v_r and v_θ may be computed for the configuration of figure 24. The results of these computations are shown in figure 25 where axial growth of the centerline velocity, non-dimensionalize by a reference velocity \bar{u} , for both codes is presented. Figure 26 shows the u velocity profiles for both codes at several locations. As can be seen, both codes predict the fully developed parabolic profile at a distance of 50 pipe radii downstream. Figure 27 shows the key results for this case. Here the maximum radial velocity v_r for both codes is presented as well as the maximum angular velocity v_θ for the finite difference code. As can be seen, the agreement for v_r is excellent (less than 8% difference), while the finite difference code predicts a value of v_θ no larger than 6% of v_r . Thus, the assumption that v_θ is negligible in equation (40) has been justified for this flow configuration.

EJECTOR ANALYSIS

Application of the code to aid in optimization of ejector design or compare theory with ejector data was beyond the scope of this investigation. However, a demonstrator case was considered to illustrate how COMOC might be employed to support ejector design studies. Consider a typical ejector configuration (ref. 30) composed of free jets, wall jets, a constant area mixing section, and a diffuser, figure 28. Each component of this system was analyzed in the test cases described above. Here our objective was to demonstrate the capability of the model to analyze the integrated components and their interaction. The exit plane (y, z) consists of a bank of nozzles (one of which is depicted in figure 28) spaced 7.62 cm in the z -direction. Each 25.4 cm high nozzle consists of a hypermixing nozzle (which is broken up into eight 2.54 cm segments) with a 2.54 cm rectangular nozzle at the top and bottom. Boundary layer control wall jets (0.155 cm) are placed along the bottom and top walls. The mixing section is 25.4 cm long in the x -direction, followed by a diffuser with a total angle of 19.6 degrees.

The desired information for this system is the thrust augmentation obtainable for various exit plane conditions (velocities, static pressure, temperature, etc.). The procedure used is as follows:

- (1) Exit plane conditions for the nozzle bank and wall jet are assumed to be given.
- (2) A guess is made for the value of the secondary (entrained) velocity.
- (3) The flow is then computed through the mixing section to the diffuser exit.
- (4) If the exit static pressure is correctly predicted to be ambient, then the thrust augmentation, skewness, etc. are computed for the system. If the exit pressure is not correctly predicted to be

ambient, then a new value for the secondary velocity is selected and the calculation repeated. An alternate approach would be to calculate the length required to give ambient static pressure at the exit rather than fix the length of the diffuser section *a priori*.

The initial conditions required at the nozzle exit plane are obtained in the following manner:

(1) The exit velocities (hypermixing, boundary layer control, and secondary) and the exit pressure were obtained using the one dimensional code developed by Salter for the same geometry (ref. 31). These values are:

$$u_p \equiv \text{hypermixing velocity} = 173.7 \text{ m/sec}$$

$$u_{BL} \equiv \text{boundary layer control velocity} = 173.7 \text{ m/sec}$$

$$u_S \equiv \text{secondary flow velocity} = 51.8 \text{ m/sec}$$

$$\text{Exit Static Pressure} = 99626 \text{ N/m}^2$$

(2) It is assumed that the boundary layer control nozzle and the rectangular nozzle at the base of the hypermixing section possess fully developed turbulent wall jet and boundary layer profiles, respectively, at the jet exit. This assumption allows use of a relatively coarse grid spacing in the near-wall region at the nozzle exit plane and considerable savings in computer time due to the absence of steep velocity gradients. The initial velocity, turbulent kinetic energy (k), and dissipation (d) profiles can then be determined from the approach previously used in cases 1 and 2 (see Numerical Results Section).

(3) The initial k and d values for the hypermixing nozzle are obtained from the results of check case 4. The initial values of k and d for the present configuration were obtained by using the same nondimensional values of k/u_p^2 and db/u_p^3 from case 4, where b is the nozzle exit width.

These values are:

$$k/u_p^2 = 1.46 \times 10^{-2}$$

$$db/u_p^3 = 2.10 \times 10^{-4}$$

(4) The values for k and d in the secondary flow were nominally taken to be 10% of the hypermixing values.

The ejector/diffuser system, figure 28, was analyzed by employing the COMOC restart option by making three separate runs each requiring 5 hours of IBM 360/65 computer time. Table I gives the initial and computed values of the velocities (u , v , w), turbulence quantities (k & d), etc. at $x = 0.0$, 15.2 , and 27.9 cm (see figure 28).

AXISYMMETRIC FLUTED MIXER ANALYSIS

Figure 29 illustrates the geometry for a 90° sector of an axisymmetric fluted mixer which was selected to establish the feasibility of using COMOC to characterize the three-dimensional flow field development. The outer fan flow, figure 29, is used to cool the inner core flow as it mixes downstream from the mixer exit plane. The radius of the center plug is assumed to decrease linearly from 12.7 cm at the exit plane to zero at 76.2 cm downstream. The radius of the outer cowl wall is assumed to be constant at 50.8 cm. The solution domain is continued an additional 76.2 cm downstream from the end of the center plug. The initial conditions for this system are assumed to be:

Core Flow

$u = 260 \text{ m/sec}$
 $T_o = 707^\circ\text{K}$
Mach Number = 0.5
 $P = 41364 \text{ N/m}^2$

Fan Flow

$u = 179 \text{ m/sec}$
 $T_o = 333^\circ\text{K}$
Mach Number = 0.5
 $P = 41364 \text{ N/m}^2$

The inner and outer walls are assumed to be adiabatic. The inner wall axial velocity condition changes from no slip on the centerbody wall to zero gradient (symmetry) on the centerline at the end of the center body. The turbulent diffusion rates were assumed to be equal to 100 times the laminar value rather than using a higher order turbulence model (represented a savings of 50% in computer time). This assumption is not required nor recommended when performing fluted mixer design studies. The results for the axial velocity and static temperature profiles along the radial lines $\theta = 0^\circ$ and $\theta = 22.5^\circ$ at $x = 0.0, 76.2$ and 152.4 cm are shown in figures 30 and 31.

CONCLUDING REMARKS

A three dimensional computer code has been developed for analyzing ejector/diffuser and axisymmetric fluted mixer systems. Some specific results are:

(1) A general three dimensional finite element model employing the two equation turbulence model was developed which characterizes flow field development not significantly influenced by streamwise diffusion effects.

(2) This model was used to examine various flow fields and a comparison made between the model and data, i.e., (a) turbulent boundary layer in a duct, (b) rectangular nozzle (free jet), (c) axisymmetric nozzle (free jet), (d) hypermixing nozzle (free jet), (e) plane wall jet.

(3) It was found that the initial conditions have a first order effect on the numerical results. Here a specific problem area is the initial turbulence parameter profiles required in the two equation turbulence model.

(4) The CPU time for the nine test cases, the ejector system, and the axisymmetric fluted mixer presented above is presented in Table II. Also shown in this table are the number of integrated variables, number of finite elements, and the number of integration steps for each case. It should be emphasized that the code can most efficiently be used to aid in providing design guidance to a specific device only after the theoretical predictions are compared to data representative of the device of interest. Two demonstration cases were analyzed to show the interaction of the different component parts for these devices. Detailed solutions do not come cheaply, i.e., 15 hours of computer time on the IBM 360/65 were required for the ejector demonstration case.

APPENDIX A

COMOC DATA DECK PREPARATION

A description of the data deck preparation for the 3DBR and 3DPNS versions of COMOC was reported in references 2 and 7, respectively. The 3DBR version is for flows where the pressure field is given and no area constraints are imposed upon the flow. The 3DPNS version reported in reference 7 considered constant area ducted flows. In modifying the code to consider variable area, ducted injector/diffuser systems and axisymmetric fluted nozzle mixer systems, several changes were required in the input and output subroutines, i.e., data deck preparation. For this reason, data decks for four different problems that typify these system classes have been chosen to demonstrate the required modifications. These decks and their pertinent features are:

| Four Test Cases | |
|---|---|
| Case | Key Features |
| I. Turbulent Boundary Layer | <ul style="list-style-type: none"> ● Two-Equations (k&d) Turbulence Model ● Gradient Boundary Condition ● Boundary Conditions for k&d at Node off the Wall ● Boundary Layer Integral Parameter Output |
| II. Diverging Channel Flow | <ul style="list-style-type: none"> ● Variable Geometry ● Flow Separation |
| III. Rectangular Nozzle Ejector | <ul style="list-style-type: none"> ● Ejector Performance Parameters Output ● Constant Turbulent Viscosity Option |
| IV. 90° Sector of Axisymmetric, Conical Center, Fluted Mixer System | <ul style="list-style-type: none"> ● Finite Element Setup and Variable Geometry for Nonrectangular Cross Section ● Generation of Cross Flow Velocities from Continuity Equations in Polar Coordinates |

Tables III-VI are a listing of the data decks used to run Cases I-IV. Tables VII-X are the output generated by each of these decks. Details and a complete description of these tables are given below.

DATA DECK DESCRIPTION

Examining Tables III - VI, it is seen that the data deck may be conveniently divided into 27 separate sections. The purpose of each section, as well as the definition of terms as applied to each test case, are given below.

Section 1.

Starting in Column 1, FEBL, used to start execution of COMOC.

Section 2.

Starting in Column 1, 3DPNS (Cases II, III, IV) for ducted flows where the pressure is computed internally or, 3DBR (Case I) in flows where the static pressure field is given.

Section 3.

Starting in Column 1, FENAME. This section consists of two parts for inputting integer and fixed point variables. For the first part, on the next card starting in Column 2, \$NAMEO1, followed on succeeding cards with the input integer parameters. There is no designated column for these variables, as long as a comma follows immediately after each variable. A complete list of all the possible integer variables is given in Table XI, which was outputted for Case I. For the four test cases presented here, the required integer variables are as follows. The pertinent case (s) for each input variable are in parentheses following the definition of the variable.

| | | |
|---------------------|---|---|
| IGAS (I,II,III,IV) | 0 | Default, isoenergetic flow with constant c_p |
| | 1 | General flow |
| IFR (I,II,III,IV) | 0 | Default, equilibrium composition or complete reaction |
| | 1 | Frozen composition |
| KBNOTW (I) | 0 | Default |
| | 1 | Use gradient boundary condition for variable 1 (U1) |
| KBNOS (IV) | 0 | Default |
| | n | Number of initial nodes for U1 (KBNOS) and/or H (KBNOSH) whose boundary condition changes from a fixed value to symmetry (zero gradient) at $X1=TIMESW$ for axisymmetric fluted mixers. |
| KDUMP (I,II,III,IV) | 0 | Default, suppress printout of input cards |
| | 1 | Print input cards |
| LG (IV) | 0 | Default, automatically computes number of columns (for computation of U2 from continuity equation solver) from rectangular grid input |
| | n | For axi-flows (NAXI=1), assumes n radial lines for computation of secondary velocities |
| NAXI (V) | 0 | Default |
| | 1 | For axi-flows |
| NBC (I) | 0 | Default |
| | n | Numbers of nodes for which gradient boundary condition (KBNOTW=1) will be used |
| NELEM (IV) | 0 | Default, automatically computes number of elements assuming rectangular grid |
| | 1 | For axi-flows (NAXI=1), node numbers for each element will be input, see Section 4 |

| | | |
|----------------------|---|---|
| NELEMS (IV) | 0 | Default |
| | n | Number of elements to delete when boundary condition changes at $X1=TIMESW$ for axisymmetric fluted mixers |
| NEQKNN (I,II,III,IV) | 1 | Default |
| | n | Number of dependent variables to be integrated in X1 direction |
| NNODE (IV) | 0 | Default, number and location of nodes automatically computed assuming rectangular grid |
| | 1 | For axi-flows ($NAXI=1$), node locations will be individually input, see Section 4 |
| NNODES (IV) | 0 | Default |
| | n | Number of nodes to delete when boundary condition changes |
| NPVSX (I,II,III,IV) | n | Number of entries in pressure table |
| NSCX (I,II,III) | 0 | Uniform X3 interval in rectangular discretization (Default) |
| | 1 | Nonuniform X3 interval in rectangular discretization |
| NSCY (I,II,III) | 0 | Default, uniform X2 interval in rectangular discretization |
| | 1 | Nonuniform X2 interval in rectangular discretization |
| NE1E2 (I) | 0 | Default, laminar flow |
| | 1 | Turbulent flow (see Chapter IV for input for various turbulence models) |
| NU2POS (II) | n | Number of entries in table for variable geometry in X2 direction |
| NU3POS (II) | n | Number of entries in table for variable geometry in X3 direction (Note: even if variable geometry is only being used in one coordinate, NU2POS and NU3POS must both be input as the same value) |

This part of Section 3 for inputting integer variables is ended by a card with \$END starting in Column 2.

The second part of Section 3 consists of inputting noninteger input variables. It begins with the card \$NAMEO2 in Column 2, followed by the input variables in the same format as NAMEO1, and ended by the card \$END starting in Column 2. A complete list of all the possible input variables is given in Table XII, which was computed for Case I. For the four test cases presented here, the required variables and their input units are:

| | |
|----------|-------------------------------------|
| AO (III) | Area of primary flow (F^2) |
| A1 (III) | Area of secondary flow (F^2) |
| A2 (III) | Area of diffuser entrance (F^2) |
| A3 (III) | Area of diffuser exit (F^2) |

| | |
|----------------------|--|
| ADUCT (IV) | Multiplier for confined flow pressure computation. Total area of cross section = ADUCT times the computed area of the input cross section as determined from the sum of all the input elements. ADUCT has a default value of 2.0 (Cases II and III). |
| ALC (IV) | Program computed length scale for non-dimensionalization. For rectangular grids, program automatically computes as shortest distance between adjacent X2 or X3 values of the nodes. For axi-flows (NAXI=1), user input as shortest side of the finite element triangles. |
| BMDOT (III) | Flow rate of boundary layer control nozzle (lbm/s) |
| CMDOT (III) | Flow rate of Coanda nozzle (lbm/s) |
| DELP (I,II,III,IV) | Percent increment of TD at which output is desired |
| PCNT (I) | Percent difference from edge velocity for computation of boundary layer thickness |
| PMDOT (III) | Flow rate of primary nozzle (lbm/s) |
| REFL (I,II,III,IV) | Reference length (F) |
| RHOINF (III) | Reference density (lbm/F ³). If not input, computed from reference temperature and first entry in pressure table. |
| SMDOT (III) | Flow rate of secondary flow (lbm/s) |
| TD (I,II,III,IV) | Length of X1 solution, starting at TO(F) |
| TO (I,II,III,IV) | Initial X1 station (F) |
| TIMESW (IV) | X1 location (in feet) where boundary condition changes for axisymmetric fluted mixers. Default = TO+2*TD |
| TOFINF (I,II,III,IV) | Reference stagnation temperature (°K) |
| UB (III) | Velocity of boundary layer control nozzle (F/s) |
| UC (III) | Velocity of Coanda nozzle (F/s) |
| UINF (I,II,III,IV) | Reference velocity (F/s) |
| UP (III) | Velocity of primary flow (F/s) |
| VSTART (I,II,III,IV) | Percent increment of TD at which transverse velocity (U2) computation starts - Default = 100% |
| X2SCLE (II,III) | Multiplier on X2 to convert rectangular discretization to feet |
| X3SCLE (II,III) | Multiplier on X3 to convert rectangular discretization to feet |
| X2SHFT (II) | Shifts X2 coordinates by an amount X2SHFT(F)/ALC, where ALC is the program computed length scale (see entry 3 in Table XI) |

After the END card for NAMEO2, Section 3 is ended by the card FEDIMN starting in Column 1 calling the subroutines FEDIMN which computes dimensionalizing quantities, vector lengths, etc. based upon the variables input in NAMEO1 and NAMEO2.

Section 4.

This section computes the node location and finite elements. It begins with the card LINK1 in Column 1 and 1 in Column 10. Three modes may then be used.

Mode 1: Automatic Uniform Rectangular Discretization

Occurs for NSCX = NSCY = 0 (Case II), where user set X2SCLE = desired element width in the X2 direction and X3SCLE = desired element height in the X3 direction. On the next card in any column (i.e., input for this card is in free format), indicate the number of the first node in the X2 direction (always 1). Skip one or more places and add the last number in the X2 direction. Place a comma immediately after the last X2 node number. Repeat for X3 direction, e.g., if we desired 2 columns of 11 nodes in the X2 direction, the card would appear as:

1 11, 1 2,

The sequence is completed by placing a "T" either on this card or a following card.

Mode 2: Automatic Nonuniform Rectangular Discretization

Occurs for NSCX=NSCY=1, cases (I, III). Set X3 discretization first; X2 second. Data are input in sets of 3 integers separated by a comma after the third integer. The first integer identifies the interval number between nodes, the next two indicate interval width (or height) as a dimensionless ratio. The first integer in successive groups need not be consecutive, i.e., if the first 5 intervals are to be the same distance apart, then it is allowable to skip from 1 to 5 for the first integer. For example (see Table I), there is one interval of width 1/60 in the X3 direction and 20 intervals of height 4/1200, 4/1200, 4/1200, 8/1200, 1/120, 1/120, 1/60, 1/60, 1/60, 1/60, 1/30, 1/30, 1/30, 1/30, 1/30, 1/30, 1/30, 1/30, 1/30, 1/30 in the X2 direction. Hence, the grid is 21 nodes high (X2) by 2 nodes wide (X3). These dimensionless intervals are converted to feet by being multiplied by X2SCLE and X3SCLE.

Mode 3: Nonuniform, Nonrectangular Discretization

Occurs for NNODE=1, NELEM=1, in NAMEO1 (Case IV). For this mode, the three node numbers for each element are entered in integer form (free format with no commas) ended by a "T". On the next card, in Column 5, put a 1. On successive cards (in Format 2E20.8), input the values of X3 and X2 for each node, starting with node number 1. End this input with any large number greater than 10^{10} . The numbering system used to generate the finite elements and node locations for Case IV is shown in Figure 32.

Section 5.

Starting in Column 1 COMTITLE, which designates that the following card will be a title card (Columns 1-80) printed on the cover page of the output. End this section with a DONE card, i.e., starting in Column 1, the letters DONE.

Section 6.

Starting in Column 1 DESCRIPT, then in Columns 11-13 the integers 204 followed by one or more spaces and a "T". Note that any message may be placed on this card after the "T" without affecting the data. Up to ten successive title cards may then be added which will be printed at the head of each output print station. End this section with a DONE card.

Section 7.

Starting in Column 1 DESCRIPT, then in Columns 11-13, the integers 332 followed by one or more blanks and a "T". The following cards are the output heading descriptors which are printed at the beginning of each print station. This section is ended by a DONE card.

Section 8.

Starting in Column 1 IONUMB, followed by -1 in Columns 9 and 10. The next cards print the appropriate variables from NAMEO2 (see Table XI) in the spaces provided (5 per output line in free format) in the output heading descriptors of Section 7. A "999" gives a line of x-x's across the page, while a "200" leaves the space blank. This section is ended by a "T".

Section 9.

Starting in Column 1 MPARA, followed by -1 in Columns 9 and 10. These cards multiply each input variable from Section 8 by the corresponding values (mostly conversion factors) from NAMEO2. Note that entry 2 in NAMEO2 multiplies the variable by 1.0. This section is ended by a "T".

Section 10.

Starting in Column 1 DESCRIPT, then in Column 11 the number 203, followed by one or more blanks and a "T". The succeeding cards give the titles to be printed above the output variables (integrated or computed). The format is 5H16 (5 variable titles per card). This section is ended by a DONE card.

Section 11.

This section designates which variables are to be printed out at all node point locations. Any variable ending with the numerals 248 represents a dependent variable, those with a 249 represent the derivative of the dependent variable. The numerals preceding the 248 or 249 designate which dependent variable is to be printed. See Section 16, for a list of the corresponding integer value for each dependent variable. The following computed variables may also be printed out at each node.

| <u>Location</u> | <u>Variable</u> | <u>Location</u> | <u>Variable</u> |
|-----------------|--------------------|-----------------|--------------------------|
| 285 | Static temperature | 1247 | Effective viscosity |
| 320 | Static enthalpy | 334 | Effective Prandtl number |
| 284 | Density | 314 | Effective Schmidt number |
| 278 | c_p | 292 | Laminar viscosity |

This section is ended by a "T".

Section 12.

Starting in Column 1 IOMULT, followed by -1 in Column 8. The following cards multiply the input variables from section 11 by the appropriate values in NAMEO2. For division, put a minus sign in front of the integer value. This section is completed with a "T".

Section 13.

Starting in Column 1 COMOC. This card prints the COMOC logo at the beginning of the output print.

Section 14.

Starting in Column 1 DESCRIPT. The following title cards (Columns 1-80) are printed once at the start of the run. A maximum of four title cards is allowed. This section is completed with a DONE card.

Section 15.

Starting in Column 1 VX3ST designating that the next card will give the X1 locations (in feet) at which the pressure will be input. If the 3DBR option is used (Case I), this pressure profile will be used for the complete calculation. If the 3DPNS option is used (II, III, IV), this pressure profile is used to specify the initial pressure and to compute the initial pressure gradient. The X1 locations are input in free format separated by one or more spaces and are terminated by a "T". The next card has, starting in Column 1 VPVSX, followed by a card with the corresponding pressure values (in PSFA) terminated by a "T".

Section 16.

Starting in Column 1 IPINT and in Column 11 put -1. The following card designates the integer array numbers of the dependent variables. The first NEQKNN of these values are integrated and also U2. Starting in any column, list the integer values of the dependent variables which correspond to the following key:

| <u>Integer</u> | <u>Variable</u> |
|----------------|----------------------------|
| 1 | U1 |
| 2 | U2 |
| 3 | U3 |
| 4 | H |
| 5 | k |
| 6 | d |
| 7 | Open |
| 8 | Y ^{O₂} |
| 9 | Y ^{H₂} |
| 10 | Y ^{N₂} |

A free format is used, the sequence being terminated with a "T".

Section 17.

Boundary conditions are required at each boundary node point for all integrated, dependent variables. The following input instructions refer to any dependent variable. There are three modes under which the boundary condition may be defined: (1) zero normal gradient, (2) value fixed to its initial value, (3) normal gradient defined as a finite value, i.e., the gradient boundary conditions.

Mode 1: Zero Gradient Boundary Condition

This represents the default boundary condition, hence any boundary node whose boundary condition for a particular dependent variable is not input will automatically be given a zero normal gradient.

Mode 2: Boundary Node Fixed to its Initial Value

This mode may be input in two ways. First, for rectangular grids, we define the boundaries of the cross section as TOP, BOTTOM, LEFT, and RIGHT. The code has been programmed so that the fixed boundary condition for the nodes along a given boundary are not required to have the same boundary condition. To use this option (see Cases I, II, III) on the first card, put KBNO in Column 1, then in Column 11 put the integer number of the dependent variable whose boundary condition is to be defined. The next card may have the general image as follows:

| | | | | | | | |
|-------------------|-----------|-----------|-----------|-----------|-----------|-----------|-----------|
| Column = <u>1</u> | <u>11</u> | <u>21</u> | <u>31</u> | <u>41</u> | <u>51</u> | <u>61</u> | <u>71</u> |
| Card = BOTTOM | NB | TOP | NT | RIGHT | NR | LEFT | NL |

This general card designates that the first NB nodes of the bottom row, NT nodes of the top row, NR nodes of the right column, and NL nodes of the left column will be held constant and equal to their input values. By leaving out any of the integers (NB, NT, NR, NL) all the nodes on that particular boundary are held constant. For those nodes not defined, the default boundary condition (Mode 1) applies. This input is terminated by a DONE card.

The second option for this mode is to pick specific nodes in the cross section to be kept fixed to their input values (as in Case IV), or to be recomputed by some algebraic relation (as in Case I). The input for this option is on the first card KBNO in Column 1 followed by the integer number of the dependent variable in Column 11. The next card is ADD starting in Column 1. The following card has the integer numbers of the nodes in free format separated by blanks and terminated by a "T". This option is then completed by a DONE card.

Mode 3: Gradient Boundary Condition

This option is used when KBNOTW=1. It sets the derivative of U1 at the wall equal to the wall shear stress (computed in WLFLXS) divided by the laminar viscosity at the wall. The input form (see Case I) is as follows. On the first card, starting in Column 1, IBORD. The next card, again in Column 1, BOTTOM, -TOP in Column 21, and DONE in Column 41. These two cards orient the elements so that the gradient boundary condition may be properly applied. For the next card, starting in Column 1, KBNO, followed on the same card by a 1 in Columns 10 and 12. For the final card, starting in Column 1, BOTTOM, 0 in Columns 11, 13, and 15, 0.0 in Column 18, 2 in Column 23, 0.0 in Column 27, 2 in Column 34, 0 in Column 39, and a "T" in Column 41.

Section 18.

This section contains the format for inputting the initial values of the variables at each node point. The format for each variable is as follows:

Stagnation Temperature (Case III)

On the first card, starting in Column 1, VTEMP. If the stagnation temperature is input in °R, then in Column 11 put a -58. This divides the input values by the 58th entry in NAMEO2 which is TOFINF, the reference temperature in °R. The next card has the values of the stagnation temperature for each node. The order that the values appear on the card(s) correspond to the order of the node numbers. For Modes 1 and 2 of Section 4 (Rectangular Grid), this order proceeds from the bottom node of the left column across the bottom row, then to the next row (left to right), etc. For Mode 3 of Section 4, the node numbering follows from the order of the cards for which the values of X2 and X3 are prescribed. Repeated values may be defined as n·A, where the n successive nodes would each have a value of A. This data set is terminated by a "T". If this data set is not prescribed, then each node is assumed to have an input stagnation temperature of TOFINF.

Integrated Variables (Including U2)

The input for these variables is as follows. Starting in Column 1 VYY, then in Column 11 the appropriate nondimensionalizing factor (-27 for velocities, etc.). Note, that if Columns 11-14 are left blank, then the input values are nondimensional. The succeeding cards contain the values of the variable at each node in the same format as the stagnation temperature, terminated by a "T". The final card has a VYYEND in Column 1, followed by the integer value n in Column 11, where n denotes the appropriate integer (see key in Section 16) for each variable.

Section 19.

This section sets the laminar viscosity equal to a constant value at each node point, see Case II. Starting in Column 1 put VSUTHLD, on the following card in any column after 1 put 4*0.0 then one or more blanks, and finally the constant value in free format. This section is terminated by a "T".

Section 20.

This section inputs a turbulent viscosity at each node point, see Case III. On the first card, starting in Column 1, VEPSILON, followed by -38 in Columns 11-13, if the turbulent viscosity is to be input in dimensional units (LBM/F-S). If input is nondimensional form, leave Columns 11-13 blank. On the next card input the values for each node, in the same order as for the velocities, etc. Terminate this section with a "T".

Section 21.

This section inputs the table for a variable cross-sectional area solution domain in the X2 direction (see Summary of Key Items for Input for a more general description of the input options for variable area). On the first card, starting in Column 1 VU2POS. The next card contains the X1 locations, in feet, where the values of X2 are to be input. The number of input values is equal to NU2POS in NAMEO1. They are input in free format, and terminated with a "T". On the next card, starting in Column 1, VU2VAL. The following card contains the values of X2, in feet, at the top of the solution domain for each corresponding X1 station. The final card contains the values of X2 at the bottom of

the solution domain, terminated by a "T". Variable geometry in the X3 direction is similarly input using VU3POS and VU3VAL cards.

For axisymmetric fluted mixer flows (NAXI=1), the variable geometry in the radial direction is input as follows. The first card is VU3POS, followed by a card with the X1 locations (in feet) for specifying the inner and outer radii of the duct, the number of entries being equal to NU3POS in NAMEO1. They are entered in free format and terminated by a "T". The next card contains VU3VAL starting in Column 1. The following two cards contain the inner and outer radii, respectively, of the duct (in feet) at the corresponding X1 locations. The last card is terminated with a "T".

Section 22.

This section sets up the node locations for computing the U2 and U3 velocities along radial lines from the continuity equation in polar coordinates (NAXI=1, see Case IV). On the first card, starting in Column 1, CNTPTS, followed by -1 in Column 11. The next card has the integer number of nodes in each radial line (there are LG entries) completed by a "T". The next card, starting in Column 1, is CNTNDS, followed by -1 in Column 11. The final cards contain the integer numbers of the nodes along each line, terminated by a "T". See Figure 32 for the notation used to obtain the numbering for Case IV.

Section 23.

For the first card, starting in Column 1, LINKCALL, followed by -1 in Column 11. The next card describes the calls to various subroutines performed at each integration step. The calls are inputted as pairs of two integers followed by a comma. The end of the calling sequence is determined by the single integer 0, followed by one or more blanks and a "T". The purpose of the subroutine called by each integer pair is as follows:

| <u>Integer</u> | <u>Pair</u> | <u>Subroutine Called</u> | <u>Purpose</u> |
|----------------|-------------|---|---|
| 2 | 4 | CONTES | Computes U2 Velocity from continuity equation knowing U1 and U3 (NAXI=0). Or, computes U2 and U3 from continuity equation in polar coordinates knowing U1 (NAXI=1). |
| 5 | 6 | SETDIF | Computes diffusion coefficients |
| 2 | 15 | TBRTHK | Computes integral parameters for boundary layer flows |
| 2 | 9 | DRHOBL (IGAS=0) DRHOGS ₀ (IGAS=1) | Computes nodal values of density |
| 2 | 3 | WLFLXS | Computes skin friction and wall shear stress |
| 1 | 5 | DPDX | Computes pressure gradient, as either input (3DBR) or calculated (3DPNS) |
| 1 | 6 | SOURCE | Computes source term for each dependent variable |
| 2 | 19 | WLSTAR | Computes k&d at 1st node off the wall |
| 5 | 1 | NWGEOM | Computes new coordinates for variable geometry |
| 5 | 11 | OUTPAR | Computes ejector performance parameters |

The next card has starting in Column 1 LINK3, followed by a 4 in Column 10. This calls the sub-routine DIMEN which finalizes all the nondimensionalization. The final card has starting in Column 1, LINK1, followed by a 3 in Column 10. This card establishes which nodes for each variable are to be integrated as well as setting up the coordinates in the proper nondimensional form.

Section 24.

Starting in Column 1, QKNINT. This card directs the program to the integration loop.

Section 25.

Starting in Column 1, DESCRIPT, followed by a 3 in Column 10. The following cards denote the printout which will appear at the end of the program output. This section is ended with a DONE card.

Section 26.

Starting in Column 1, COMOC. This card prints the COMOC logo after the output of Section 25.

Section 27.

Starting in Column 1, EXIT. This tells the program that the output is complete and to end execution.

OUTPUT DESCRIPTION

The previous sections dealt with preparing the input data decks for Cases I-IV shown in Tables III - VI. These data decks produce the output format at each print station as shown in Tables VII - X. The output resulting from pertinent sections of the input data decks has been labeled on these tables.

SUMMARY OF KEY ITEMS FOR INPUT

This section will summarize and provide a more complete description for inputting some of the more important aspects of the flow systems under investigation.

1. Turbulence Modeling

The COMOC code currently has five different turbulence models available to the user. A description of each as well as input instructions follows.

1-a. Mixing Length Theory: This model computes the turbulent viscosity from classical mixing length theory, including von Driest damping in the near wall region and intermittency in the outer freestream region. This option is used by setting NE1E2=1, in NAMEO1. For this model k&d are not to be integrated and hence should not be included in IPINT (Section 16) or in the determination of the number of variables to be integrated (NEQKNN).

1-b. Two-Equation (k&d) Model with Initial Profiles for k&d Computed from Mixing Length Theory: This option is used in case I. Here the turbulent viscosity is obtained at each downstream station by integrating the k&d equations. However, the initial profiles are obtained by using mixing length theory at the initial X1 station to compute the mixing length and turbulent viscosity. Algebraic relations are then used to compute the initial k&d profiles. To use this option input NE1E2=1 in NAMEO1, include

k&d when determining the number of equations to be integrated (NEQKNN) and finally by including 5 and 6 in the first NEQKNN entries of IPINT (Section 16).

1-c. Two-Equation (k&d Model with Initial Profiles for (k&d) Input at Each Node Point: For this option the initial profiles for k&d are input following the format in Section 18. If k&d are to be input in dimensional form (F^2/S^2 and F^2/S^3) then the nondimensional factors for Column 11 on the VYY cards are, -90 and -89, respectively. Also required are that NE1E2=1 and ITKE=1 in NAMEO1. NEQKNN and IPINT (Section 16) include k&d as for Case 1-b.

1-d. One-Equation (k) Turbulence Model: For this case the turbulent viscosity is obtained from k (integrated) and a mixing length ℓ computed algebraically for free shear flows. For this case the initial k profile is input as in Case 1-c above. In NAMEO1 include NE1E2=1, ITKE=1, and IFSL=1. Also include k when determining NEQKNN and hence in IPINT.

1-e. Constant Turbulent Viscosity Model: This option was used in Case III. Here the turbulent viscosity at each node is input in VEPSILON (Section 20). No additional input in NAMEO1 is required and k&d should not be included in NEQKNN or IPINT.

2. Boundary Conditions for Turbulent Flows

Turbulent flows are characterized by steep gradients in the near wall region. For this reason it was found to be advantageous to replace the no-slip wall velocity boundary condition for U1, and to calculate the values of k&d at the node off the wall from algebraic relations. This requires fewer node points in the near wall region and hence allows faster running times. The gradient boundary condition is used by inputting KBNOTW=1, and NBC=n where n is the number of columns, in NAMEO1, and by using Mode 3 of Section 17 for the U1 boundary condition at the wall. The computation of k&d off the wall is done algebraically by calling 2 19 in LINKCALL (Section 23). Hence, the nodes off the wall for k&d need not be integrated and may be eliminated (Mode 2 - second option, of Section 17).

3. Variable Geometry

Rectangular or axisymmetric flows whose cross section does not remain constant in the X1 direction may be computed using a coordinate transformation. For rectangular flows, the required input for this option is as follows. In NAMEO1, set NU2POS=NU3POS=n, where n is the number of entries in the table of X1 vs X2 and/or X3. In the LINKCALL card (Section 23) include the integer pair 5 1, which calls the subroutine for recomputing the coordinates at each X1 station as well as computing the additional terms in the differential equation resulting from the coordinate transformation. For rectangular flows, two options are possible. The first treats variable geometry flows which are symmetrical about the centerline. For this case in NAMEO2 put ADUCT=2.0 (default). The flow is then calculated in the bottom half of the cross-sectional solution domain only. The input cards with the X1 vs X2 and/or X3 values are read in as in Section 21 (see Case II). For nonsymmetrical flows, the entire cross-sectional domain must be included. This option is set by putting ADUCT=1.0 in NAMEO2. The X1 vs X2 and/or X3 tables are then read in as before. Variable geometry for axi flows whose inner and/or outer radii vary with X1 may likewise be calculated using the input described in Section 21.

4. Ejector Parameter Output

For ejector/diffuser systems, several parameters are of interest, i.e., thrust augmentation, skewness, etc. (see Appendix B for the definition of these terms). These parameters are computed and printed out at each output station as follows. The enlarged output print of Section 7, 8, and 9 is used (see Case III). In the LINKCALL (Section 23) include the integer pair 5 11, which calls the subroutine to compute the parameters. Also required in input are A0, A1, A2, A3, UB, UC, UP, BMDOT, CMDOT, PMDOT, and SMDOT in NAMEO2.

5. Node and Element Input for Axisymmetric Flows

For axisymmetric flows, Mode 3 of Section 4 is used. This requires NAXI=1, NNODE=1, NELEM=1 in NAMEO1, and the specification of ALC in NAMEO2. Also, for the computation of U2 and U3 from the continuity equation in radial coordinates, Section 22 giving the node numbers along radial lines is required (see Case IV).

6. Changing Boundary Condition for Axisymmetric Flows

At the downstream X location where the inner wall (conical center) ends, the boundary condition for those nodes that were along the wall changes from no slip to symmetry, i.e., zero gradient. Also at this station, those finite elements and nodes that were along the wall require further examination. Figure 33 shows these elements and nodes at the initial X station and at the station where the inner wall ends. The nodes are depicted by the numbers 31 to 40, and the elements by the circled numbers from 49 to 56. As can be seen, at the X station where the inner wall ends, the elements 50, 52, 54 and 56 shrink to zero area. This causes computational problems and therefore these elements must be deleted from the computational domain at this X station. Also, nodes 36, 37, 38, 39, and 40 become physically identical. This will not cause problems as each node is computed independently. However, since element 56 has been deleted, node 40 is no longer used and must also be deleted.

The input instruction to perform these procedures are as follows:

6-a. The variable geometry for axisymmetric flows (NAXI=1) is calculated by inputting the inner and outer radii as functions of X1 as per Section 21 and by calling the subroutine NWGEOM by inputting the integer pair 5 1 in the LINKCALL as per Section 23.

6-b. The X1 station in feet where the inner wall ends and hence the boundary condition changes is input as the value of TIMESW in NAMEO2.

6-c. The number of initial nodes whose boundary condition changes at X1=TIMESW is input as the integer KBNOS in NAMEO1. For the example shown in Figure 33, KBNOS=5. It should be noted that the last KBNOS nodes change their boundary condition input as per Section 4 (Mode 3). Therefore, care must be taken when setting up the node locations to insure that these nodes are read in last. Also, even though node 40 is deleted at X1=TIMESW, it is still included in the determination of KBNOS.

6-d. The number of elements to be deleted at X1=TIMESW is input as the integer NELEMS in NAMEO1. For the example in Figure 2, NELEMS=4. Again, the last NELEMS elements input as per Section 4 (Mode 3) are deleted.

6-e. The number of nodes to be deleted at $X1=TIMESW$ is input as the integer `NNODES` in `NAMEO1` (`NNODES=1` for the example in Figure 33). Again, the last `NNODES` nodes of the input are deleted.

CONCLUDING REMARKS

This manual is intended to provide the user who is not familiar with `COMOC` with a step-by-step outline of how to prepare an input data deck. The test cases presented were chosen for two reasons. First, they represent typical problems when dealing with ejector/diffuser or fluted nozzle mixer systems. Secondly, they contained all the pertinent options currently in effect in the `COMOC` code.

APPENDIX B

DEFINITION OF EJECTOR/DIFFUSER PARAMETERS

1. Ejector Inlet Area Ratio

The following discussion presents definitions of ejector terminology with respect to ejector station locations shown in Figure B-1, which along with the references used herein may be found at the end of Appendix B.

There is no ambiguity in the definition of inlet area ratio, A_1/A_0 , when the ejector consists of a single primary nozzle discharging axially into a symmetric mixing chamber, and the primary nozzle is assumed to be ideal (von Karman, 1969; Bevilaqua, 1973). Under these conditions, the inlet area ratio is defined as the ratio of the secondary stream cross-sectional area at the nozzle exit plane, to the primary nozzle exit area.

The first difficulty arises when the performance of an actual primary nozzle is considered. If the primary flow is subsonic and the nozzle is conical, the primary stream will initially contract until there is a static pressure balance between the primary and secondary flows. The use of inlet area ratio as a performance correlation parameter arises from a one - dimensional analysis in which the static pressures of the two streams are assumed to be equal over the areas A_0 and A_1 (e.g., Campbell & O'Hain, 1967). Better correlation could be expected, therefore, if the primary nozzle effective area were used rather than the geometric area (Salter 1972). McClintock and Hall Hood, (1966), in discussing the performance of ejectors with supersonic primary flows, suggested that the fully expanded area should be used for ejector performance calculation. It is, however, more customary to define the inlet area ratio as a geometric area ratio, and to include supplementary curves of primary nozzle performance (Campbell, et. al, 1973).

When the primary flow consists of multiple jets discharging into the ejector at a number of different locations, the task of correlating performance on the basis of flow areas at some station where the pressure is assumed to be equalized would be a formidable task. It would be necessary to determine the expansion of each jet to the common reference plane, and to calculate each jet velocity at that plane. Under these conditions Quinn (1972) chose to define inlet area ratio as

$$\frac{A_1}{A_0} = \frac{\text{Total duct area at the primary exit plane}}{\text{Sum of geometric primary and boundary layer nozzle areas}}^{-1} \quad (1)$$

From the practical aspects of ejector design and performance evaluation, inlet area ratio should be defined in terms of geometric areas, and Quinn's definition for the case of multiple injection appears to be the most appropriate. We suggest, therefore, that inlet area ratio should be defined as

$$\text{IAR} = \frac{\text{Ejector duct area at primary nozzle exit plane}}{\text{Total geometric area of primary, Coanda and Boundary layer nozzles}}^{-1} \quad (2)$$

2. Diffuser Area Ratio

Ambiguity could arise here too if an attempt were made to define the ratio in terms of areas normal to the flow directions. For example, at the diffuser exit under conditions where the diffuser doors are deflected backward, one might define the exit area as the plane normal to the diffuser centerline through the trailing edge of the forward door (Bell, 1973). This definition results in the diffuser area ratio being a function of the deflection angle even when the diffusion angle is kept con-

stant. The reason for this definition was an attempt to correlate ejector performance independent of deflection angle. For the purposes of design and performance estimation, it is more desirable to express the diffuser area ratio in terms of the physical diffuser inlet and exit boundaries. We suggest that diffuser area ratio should be defined as:

$$\text{DAR} = \frac{\text{Cross-sectional area at Station 3}}{\text{Cross-sectional area at Station 2}} \quad (3)$$

3. Gross Thrust

Gross thrust is the thrust produced by the flow leaving the ejector. A simple integration of the momentum flux over the diffuser exit plane area (Station 3) would not yield the correct gross thrust value because the stream lines may be diverging and the pressure may be varying over this area. The most direct way to determine the gross thrust value is to integrate the momentum flux over the surface where the static pressure is everywhere equal to the ambient pressure, i.e., over Station 3'.

If $\vec{n}_{3'}$ is the unit vector normal to the surface 3' then

$$\text{Gross Thrust} = \int_{A_{3'}} \vec{U}_{3'} (\rho_{3'} U_{3'}) \cdot \vec{n}_{3'} d\sigma \quad (4)$$

4. Momentum Drag

Momentum drag is the loss in momentum of the freestream due to the presence of the ejector.

$$\text{Momentum drag} = \dot{m}_1 \vec{V}_\infty = \vec{V}_\infty \int_{A_1} \rho_1 \vec{U}_1 \cdot \vec{n}_1 d\sigma \quad (5)$$

5. Net Thrust

In the case of a propulsion unit whose exhaust is aligned such that the gross thrust acts along the flight path, the net thrust is defined as the difference between the gross thrust and momentum drag. When the gross thrust acts at an angle to the freestream direction, the resultant force may be computed by vector subtraction. It is suggested that, rather than computing net thrust, the magnitudes and directions of the gross thrust and ram drag should be given. Pitching moments may then be computed from the sum of the two moments about any desired point.

6. Mass Flow and Mass Flow Ratio

The mass flow rate through any surface is obtained by the integration of the components of (ρU) normal to the surface, over the surface area.

$$m = \int_A (\rho \vec{U}) \cdot \vec{n} d\sigma \quad (6)$$

The total primary mass flow rate is $(\dot{m}_p + \dot{m}_c)$. The question is now raised as to whether or not the boundary layer control flow should be included in the definition of mass flow ratio. From a practical point of view, all air supplied to the ejector jets must be supplied by power plants on board the aircraft. If this air were not used in an ejector, it could be employed to produce useful thrust. For example, if the boundary layer control air were extracted from the engine bleed ports, there would be a reduction in engine performance, either in the form of a direct thrust loss, or in an increase in fuel consumption if the power lever were advanced to maintain the same thrust. It is reasonable, then to consider all of the injected mass flow in the definition of mass flow ratio. In addition, this

definition would be consistent with the inlet area ratio definition. From these considerations, it is recommended that the following definition should be used:

$$\text{Mass Flow Ratio} = \frac{\text{Total ejector discharge mass flow rate}}{\text{Total injected mass flow rate}} \quad (7)$$

7. Thrust Augmentation Ratio

Von Karman (1949) defined thrust augmentation ratio as the ratio of the actual thrust produced to the primary jet momentum with the nozzle installed in the ejector. He commented that this is "somewhat arbitrary." Campbell and O'Hain (1967) and all subsequent ARL literature, define thrust augmentation ratio as the ratio of ejector thrust to the isentropic primary thrust that would result if the same primary mass flow rate were discharged to atmospheric pressure, from the same stagnation conditions. Since the local pressure at the nozzle exit plane is lower than ambient pressure, this definition implies a larger nozzle area when discharging to ambient pressure. The reasons for this definition are two-fold. First, a certain mass flow rate at known stagnation conditions is provided by the aircraft power plant. If the engine is to run at its design point when operating in conjunction with an ejector, the primary nozzles must be sized correctly to allow the same mass flow through the system. ARL's definition is, therefore, the ratio of ejector thrust to that which could be produced by the same engine exhausting through an isentropic nozzle. The second reason for adopting this definition is its convenience. The ejector thrust is measured during a test and the isentropic thrust is computed from the stagnation conditions and mass flow. Another definition used by Boeing/NASA (Campbell 1973) is the ratio of ejector thrust to actual primary thrust with the ejector shrouds removed. In this approach, the primary thrust is reduced due to the lower mass flow (unless the nozzles are choked), and the primary nozzle thrust efficiency is included. This definition leads to a larger value of thrust augmentation ratio than ARL's. Alperin and Marlotte (1971) discuss various definitions and conclude that a parameter based on engine power is the most appropriate. Their definition consists of the ratio of ejector thrust to reference engine thrust based on the same reference engine power. As indicated by Alperin, a problem with this definition is that it requires an assumption as to the reference engine nozzle area.

It is our recommendation that ARL's definition of thrust augmentation should be used, and that all jets discharging into the ejector should be considered in the evaluation of the denominator. Denoting V_{is} as the isentropic velocity of a jet, which can be calculated from its stagnation pressure, stagnation temperature, and ambient pressure, then thrust augmentation ratio ϕ , is defined as:

$$\phi = \frac{\text{Ejector Gross Thrust}}{\sum_i (\dot{m} V_{is})_i} \quad i = p, c, b \quad (8)$$

No attempt will be made to define net thrust augmentation ratio, because of the lack of a suitable definition for net thrust.

8. Propulsion Efficiency

The basic definition of propulsive efficiency is the ratio of output work rate to input energy rate. The output work rate consists of that due to the component of gross thrust in the direction of flight and that due to momentum drag. Thus,

$$\text{Output work rate} = \vec{F}_G \cdot \vec{V}_\infty - \vec{D}_m \cdot \vec{V}_\infty \quad (9)$$

where \vec{F}_G is the gross thrust vector and \vec{D}_m is the momentum drag.

Input energy rate is the sum of the input energy rates of all of the jets. To be consistent with our definition of thrust augmentation ratio, it is recommended that isentropic jet velocities should be used for the calculation of input energy rates. Then propulsive efficiency is:

$$\eta_{PR} = \frac{\vec{F}_G \cdot \vec{V}_\infty - \vec{D}_m \cdot \vec{V}_\infty}{1/2 \sum_i (\dot{m} V_{is}^2)_i} \quad i = c, p, b \quad (10)$$

9. Energy Transfer Efficiency

This is the ratio of the rate of energy addition to the freestream by the ejector to the input energy rate of the jets, i.e.,:

$$\eta_{TR} = \frac{\dot{m}_T |\vec{V}_{3'}|^2 - \dot{m}_s |\vec{V}_\infty|^2}{\sum_i (\dot{m} V_{is}^2)_i} \quad i = c, p, b \quad (11)$$

where $\vec{V}_{3'}$, is the integrated average velocity in Station 3.

10. Skewness

Skewness is a convenient means of expressing the "flatness" of the velocity profile at any station. It has been denoted in the literature by λ (Von Karman, 1949), K_m (London, 1955 and SAE, 1960) and by β (Quinn, 1972, and Bevilaqua, 1973).

Skewness is defined as the ratio of the actual integrated momentum to the bulk average momentum at the station under consideration. Von Karman was the first investigator to demonstrate the importance of this parameter on ejector performance. He showed that high inlet skewness was beneficial, and suggested that the high efficiency of the Coanda ejector was largely explained by this phenomenon and "has little to do with the mysterious flow of the fluid around sharp edges." Bevilaqua (1974) has demonstrated the importance of low values of skewness at entrance to the diffuser.

The bulk average momentum at any station is

$$\dot{m} \bar{V} = \frac{m}{A} \int_A \vec{U} \cdot \vec{n} d\sigma \quad (12)$$

and the actual momentum is $\int_A (\rho \vec{U}) \cdot \vec{U} d\sigma$. Skewness is defined, therefore, as

$$\beta = \frac{A}{\dot{m}} \frac{\int_A (\rho \vec{U}) \cdot \vec{U} d\sigma}{\int_A \vec{U} \cdot \vec{n} d\sigma} \quad (13)$$

11. Loss Factor

This is defined for any component as the ratio of total pressure loss across the component to the dynamic pressure at entrance to that component. Thus,

$$LF = \frac{\Delta P}{q} \quad (14)$$

where ΔP is the loss in total pressure, and q is defined by

$$q = \frac{1}{2} \int_A (\rho \vec{U}) \cdot \vec{U} d\sigma \text{ at entry}$$

12. Ideal Isentropic Nozzle Thrust

This parameter was discussed under "Thrust Augmentation Ratio," where the following definition was recommended:

$$F_{is} = \sum_i (\dot{m} V_{is})_i \quad i = p, c, b \quad (15)$$

13. Actual Isentropic Nozzle Thrust

This is defined as the sum of the isentropic thrusts of all of the jets discharging into the ejector. One of the program output parameters will be a complete description of the pressure field in the ejector. The local pressure at each nozzle exit location will be used, in conjunction with the stagnation pressures, temperatures, and mass flow rates, to calculate the actual isentropic nozzle thrusts.

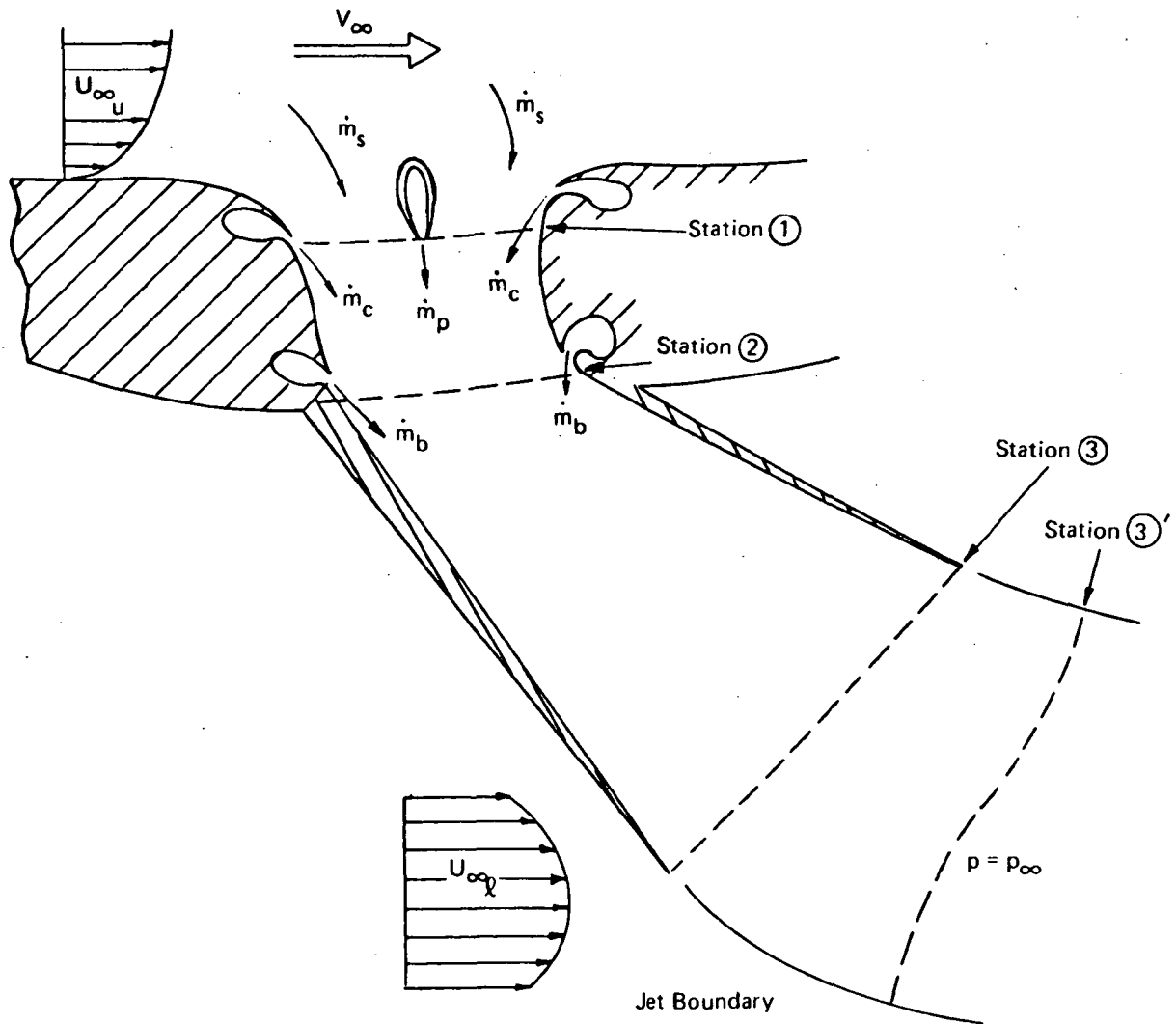


Figure B-1. Ejector Schematic

REFERENCES FOR APPENDIX B

- Alperin, M. and Marlotte, G., "A Jet Flap Diffuser Ejector," AFFDL-TR-71-66, June 1971.
- Bell Aerospace Textron, "1973 IR&D Final Report - CTA - Lift Augmentation System Development," Project No. 18, BAC Report 2500-927036, December 1973.
- Bevilaqua, P.M., "A Comparison Test of the Hypermixing Nozzle," ARL TR 74-0006, January 1974.
- Campbell, J., et al., "Design Integration and Noise Studies for Jet STOL Aircraft," NASA CR-114534, 1973.
- Campbell, W. and Von O'Hain, H., "Thrust Augmentation for V/STOL - ARL's Research and Concepts," ARL Report 67-0065, April 1967.
- London, A., "Exhaust-Stack Ejectors for Marine Gas Turbine Installations," Stanford University Tech. Report No. 26, 1955.
- McClintock, F. and Hall Hood, J., "Aircraft Ejector Performance," J. Aero. Sci., Vol. 13, No. 11, November 1946.
- Quinn, B., "Cold Thrust Augmentation Briefing," presented to the Industry at WPAFB, Ohio, 13 April, 1972.
- Salter, G., "Analysis of the Wing Ejector under Static and In-Flight Conditions," Bell Aerospace Report 7500-927053, November 1972.
- Von Karman, T., "Theoretical Remarks on Thrust Augmentation," Reissner Anniversary Volume Contributions to Applied Mechanics, Published by J.W. Edwards, Ann Arbor, Michigan, 1949.

REFERENCES

1. Proceedings of the Conference on Aerodynamic Analyses Requiring Advanced Computers, Parts I and II, NASA SP-347, March 1975.
2. Zelazny, S.W., Baker, A.J. and Rushmore, W.L., "Modeling of Three-Dimensional Mixing and Reacting Ducted Flows," NASA CR-2661, April 1976 (see also AIAA 76-49, January 1976, for abbreviated version.)
3. Zelazny, S.W. and Rushmore, W.L., "Three-Dimensional Mixing Effects in Laser Optical Cavities," presented at the AFWL Tri-Service Chemical Laser Symposium, February 1976.
4. Quinn, B., "Compact Ejector Thrust Augmentation," *Journal of Aircraft*, Vol. 10, No. 8, August 1973, pp. 481-486.
5. Bevilaqua, P.M., "An Evaluation of Hypermixing Nozzles for V/STOL Aircraft Augmentors," AIAA Paper No. 73-654.
6. Thronson, L.W., "Compound Ejector Thrust Augmentor Development," ASME Paper No. 73-GT-67.
7. Baker, A.J. and Zelazny, S.W., "A Theoretical Study of Mixing Downstream of Transverse Injection into a Supersonic Boundary Layer," NASA CR-112254, 1972.
8. Baker, A.J. and Zelazny, S.W., "COMOC: Three-Dimensional Boundary Region Variant. Theoretical Manual and User's Guide," NASA CR-132450, 1974.
9. Orzechowski, J.A. and Baker, A.J., "COMOC: Three-Dimensional Boundary Region Variant. Programmer's Manual," NASA CR-132449, 1974.
10. Pal, A. and Rubin, S.G., "Viscous Flow Along a Corner. Part I. Asymptotic Features of the Corner Layer Equations," AFOSR-69-1225TR, U.S. Air Force, May 1969. (Available from DDC as AD 693 630.)
11. Cresci, R.J., Rubin, S.G., Nardo, C.T., and Lin, T.C., "Hypersonic Interaction Along a Rectangular Corner," *AIAA J.*, Vol. 7, No. 12, 1969, pp. 2241-2246.
12. Rubin, S.G. and Lin, T.C., "A Numerical Method for Three-Dimensional Viscous Flow. Application to the Hypersonic Leading Edge," *Journal of Computational Physics*, Vol. 9, No. 2, 1972, pp. 339-364.
13. Caretto, L.S., Curr, R.M., and Spalding, D.B., "Two Numerical Methods for Three-Dimensional Boundary Layers," *Computational Methods Applied Mechanics and Engineering*, Vol. 1, No. 1, 1972, pp. 39-57.
14. Curr, R.M., Sharma, D., and Tatchell, D.G., "Numerical Predictions of Some Three-Dimensional Boundary Layers in Ducts," *Computational Methods Applied Mechanics and Engineering*, Vol. 1, No. 2, 1972.

15. Patankar, S.V. and Spalding, D.B., "A Calculation Procedure for Heat, Mass and Momentum Transfer in Three-Dimensional Parabolic Flows," *International Journal of Heat and Mass Transfer*, Vol. 15, No. 10, 1972, pp. 1787-1806.
16. Amsden, A.A. and Harlow, F.H., "The SMAC Method: A Numerical Technique for Calculating Incompressible Fluid Flows," LA-4370, Los Alamos Scientific Laboratory, University of California, 1970.
17. Baker, A.J., "Finite Element Solution Theory for Three-Dimensional Boundary Flows," *Computational Methods Applied Mechanics and Engineering*, Vol. 4, No. 3, 1974, pp. 367-386.
18. Launder, B.E. and Spalding, D.B., *Lectures in Mathematical Models of Turbulence*, Academic Press, Inc., 1972.
19. Patankar, S.V. and Spalding, D.B., *Heat and Mass Transfer in Boundary Layers*, Second Edition, Int. Textbook Company, Ltd., London, 1970.
20. Launder, B.E., Reece, G.J., and Rodi, W., "Progress in the Development of a Reynolds-Stress Turbulence Closure," *Journal of Fluid Mechanics*, Vol. 68, Part 3, 1975, pp. 537-566.
21. Coles, D.E. and Hirst, E.A., *Proceedings of Turbulent Boundary Layers - 1968 AFOSR-IFP - Stanford Conference*, Stanford University, California, 1968.
22. Bradbury, L.J.S., "The Structure of a Self-Preserving Turbulent Plane Jet," *Journal of Fluid Mechanics*, Vol. 22, 1965, pp. 31-64.
23. Schlichting, H., *Boundary Layer Theory*, 4th Edition, McGraw-Hill, New York, 1960.
24. Eastlake, C.N. II, "The Macroscopic Characteristics of Some Subsonic Nozzles and the Three-Dimensional Turbulent Jets They Produce," *Aerospace Research Labs Reports*, ARL 71-0058, March 1971.
25. Harris, G.L., "The Turbulent Wall Jet in a Moving Stream," *AGARDograph*, May 1965, pp. 131-158.
26. Myers, G.E., Schauer, J.J., and Eustis, R.H., "Plane Turbulent Wall Jet Flow Development and Friction Factor," *Journal of Basic Engineering*, March 1963, pp. 47-54.
27. Ng, K.H. and Spalding, D.B., "Turbulence Model for Boundary Layers Near Walls," *The Physics of Fluids*, Vol. 15, 1972, pp. 20-30.
28. Schwartz, W.H. and Cosant, W.P., "The Two-Dimensional Turbulent Wall Jet," *Journal of Fluid Mechanics*, Vol. 10, Part 4, 1961, pp. 481-495.
29. Rushmore, W.L., "Theoretical Investigation of Curve Pipe Flows," PhD Dissertation, State University of New York at Buffalo, 1975.

30. Campbell, D.R. and Quinn, B., "Test Results of a VTOL Propulsion Concept Utilizing a Turbofan Powered Augmenter," *Journal of Aircraft*, August 1974, pp. 467-471.
31. Salter, G.R., "Method of Analysis of V/STOL Aircraft Ejectors," *AIAA Journal of Aircraft*, Vol. 12, No. 12, December 1975.

Table I
Ejector Results at x = 0.0, 15.2, and 27.9 cm

C C M O C

THREE-DIMENSIONAL PARACILIC NAVIER-STOKES VARIANT

HYPERMIXING NOZZLE + WALL JET PART 2

| REFERENCE | ENGLISH-FT | ENGLISH-IN | M-K-S | C-G-S |
|--|---------------------|-------------|----------------------------|---------------|
| LENGTH | | | | |
| ..FEET.. | ..IN.. | ..M.. | ..CM.. | |
| 0.83330E-01 | 0.99996E+00 | 0.25399E-01 | 0.25399E+01 | |
| VELOCITY | | | | |
| ..FT/SEC.. | ..M/S.. | ..CM/S.. | ..G/CC.. | |
| 0.57000E+03 | 0.17374E+03 | 0.17374E+03 | 0.17374E+05 | |
| DENSITY | | | | |
| ..LBM/FT3.. | ..KG/M3.. | ..KELVIN.. | ..G/CC.. | |
| 0.82476E-01 | 0.13213E+01 | 0.13213E+01 | 0.13213E-02 | |
| TEMPERATURE | | | | |
| ..RANKINE.. | ..KELVIN.. | ..KJ/KG.. | ..KJ/KG.. | |
| 0.50000E+03 | 0.27778E+03 | 0.10000E+01 | 0.10000E+01 | |
| ENTHALPY | | | | |
| ..RTU/LRM.. | ..RTU/LRM-R | ..KJ/KG-K.. | ..KJ/KG-K.. | |
| 0.43022E+00 | 0.24000E+00 | 0.10042E+01 | 0.10042E+01 | |
| FR07. SPEC. HEAT | | | | |
| ..LBM/FT-S.. | ..NT-S/M2.. | 0.17528E-04 | 0.17528E-03 | |
| 0.11779E-04 | 0.17528E-04 | ..NT/M2.. | ..TORR.. | |
| VISCOSITY | | | | |
| ..DSF.. | ..PST.. | ..NT/M2.. | ..TORR.. | |
| 0.20808E+04 | 0.1449E+02 | 0.99629E+05 | 0.7472E+03 | |
| LOCAL PRESSURE | | | | |
| 0.24984E+01 | ..DPDX1.. | ..MAX. H2.. | ..MIX. EFF.. | |
| LOCAL SOLUTION | | | | |
| 0.52004E+00 | 0.0 E+00 | 0.0 E+00 | 0.0 E+00 | |
| X1/LREF | | | | |
| 0.0 E+00 | ..EPSTION.. | ..DX1M/LREF | ..DX1M/LREF | |
| 0.0 E+00 | 0.50004E+00 | 0.0 E+00 | 0.0 E+00 | |
| THE FOLLOWING PARAMETERS ARE N3-DIMENSIONAL BY DEFINITION. | | | | |
| THE FOLLOWING PAR. ARE IN THE SPECIFIED DIMENSIONAL UNITS | | | | |
| INPUT AREA RATIO | | | | |
| 0.20106E+02 | DIFFUSER AREA RATIO | 0.16996E+01 | VELOCITY RATIO | 0.37372E+00 |
| MASS FLOW RATIO | | | | |
| 0.82801E+01 | THRUST AUGMENTATION | 0.39927E+01 | ENERGY TRANSFER EFFICIENCY | 0.10219E+01 |
| PROPULSION EFFICIENCY | | | | |
| 0.0 F+00 | 0.0 F+00 | 0.10219E+01 | 0.12887E+01 | |
| THE FOLLOWING PAR. ARE IN THE SPECIFIED DIMENSIONAL UNITS | | | | |
| MOMENTUM DRAG | | | | |
| 0.0 E+00 | Y - COMPONENT | 0.0 E+00 | Z - COMPONENT | (LBM-FT/SEC2) |
| AVERAGE VELOCITY | | | | |
| 0.21302E+03 | Y | 0.52689E+01 | Z | (FT/SEC) |
| GROSS THRUST | | | | |
| 0.50297E+03 | X - COMPONENT | 0.0 E+00 | Z - COMPONENT | (LBM-FT/SEC2) |
| 0.50297E+03 | Y - COMPONENT | 0.0 E+00 | Z - COMPONENT | (LBM-FT/SEC2) |
| THE FOLLOWING PAR. ARE IN THE SPECIFIED DIMENSIONAL UNITS | | | | |

Table I
Ejector Results at $x = 0.0, 15.2,$ and 27.9 cm (cont)

| F I | III/IIIEF | F I | F I | F I | F I | F I | F I | F I | F I | |
|---------|-----------|---------|---------|---------|---------|---------|---------|---------|---------|---------|
| -0.0000 | 0.02982 | 0.02982 | 0.02982 | 0.02982 | 0.10000 | 0.10000 | 0.02982 | 0.02982 | 0.02982 | |
| -0.5000 | 0.02982 | 0.02982 | 0.02982 | 0.02982 | 0.09667 | 0.09667 | 0.02982 | 0.02982 | 0.02982 | |
| -1.0000 | 0.02982 | 0.02982 | 0.02982 | 0.02982 | 0.10000 | 0.10000 | 0.02982 | 0.02982 | 0.02982 | |
| -1.5000 | 0.02982 | 0.02982 | 0.02982 | 0.02982 | 0.09667 | 0.09667 | 0.02982 | 0.02982 | 0.02982 | |
| -2.0000 | 0.02982 | 0.02982 | 0.02982 | 0.02982 | 0.10000 | 0.10000 | 0.02982 | 0.02982 | 0.02982 | |
| -2.5000 | 0.02982 | 0.02982 | 0.02982 | 0.02982 | 0.09667 | 0.09667 | 0.02982 | 0.02982 | 0.02982 | |
| -3.0000 | 0.02982 | 0.02982 | 0.02982 | 0.02982 | 0.10000 | 0.10000 | 0.02982 | 0.02982 | 0.02982 | |
| -3.5000 | 0.02982 | 0.02982 | 0.02982 | 0.02982 | 0.09667 | 0.09667 | 0.02982 | 0.02982 | 0.02982 | |
| -4.0000 | 0.02982 | 0.02982 | 0.02982 | 0.02982 | 0.10000 | 0.10000 | 0.02982 | 0.02982 | 0.02982 | |
| -4.5000 | 0.02982 | 0.02982 | 0.02982 | 0.02982 | 0.09667 | 0.09667 | 0.02982 | 0.02982 | 0.02982 | |
| -4.9160 | 0.05551 | 0.05551 | 0.05551 | 0.05551 | 0.09060 | 0.09060 | 0.05551 | 0.05551 | 0.05551 | |
| -4.9580 | 0.06956 | 0.06956 | 0.06956 | 0.06956 | 0.08200 | 0.08200 | 0.06956 | 0.06956 | 0.06956 | |
| -4.9790 | 0.07400 | 0.07400 | 0.07400 | 0.07400 | 0.07430 | 0.07430 | 0.07400 | 0.07400 | 0.07400 | |
| -4.9860 | 0.07253 | 0.07253 | 0.07253 | 0.07253 | 0.07011 | 0.07011 | 0.07253 | 0.07253 | 0.07253 | |
| -4.9930 | 0.06660 | 0.06660 | 0.06660 | 0.06660 | 0.06340 | 0.06340 | 0.06660 | 0.06660 | 0.06660 | |
| -5.0000 | 0.0 | 0.0 | 0.0 | 0.0 | 0.0 | 0.0 | 0.0 | 0.0 | 0.0 | |
| F I | 0.0 | 0.05000 | 0.10000 | 0.13000 | 0.14330 | 0.15670 | 0.17000 | 0.20000 | 0.25000 | 0.30000 |

| E I | III/IIIEF | E 0 | E 0 | E 0 | E 0 | E 0 | E 0 | E 0 | E 0 | |
|---------|-----------|---------|---------|---------|---------|---------|---------|---------|---------|---------|
| -0.0000 | 0.0 | 0.0 | 0.0 | 0.0 | 0.0 | 0.0 | 0.0 | 0.0 | 0.0 | |
| -0.5000 | 0.0 | 0.0 | 0.0 | 0.0 | 0.0 | 0.0 | 0.0 | 0.0 | 0.0 | |
| -1.0000 | 0.0 | 0.0 | 0.0 | 0.0 | 0.0 | 0.0 | 0.0 | 0.0 | 0.0 | |
| -1.5000 | 0.0 | 0.0 | 0.0 | 0.0 | 0.0 | 0.0 | 0.0 | 0.0 | 0.0 | |
| -2.0000 | 0.0 | 0.0 | 0.0 | 0.0 | 0.0 | 0.0 | 0.0 | 0.0 | 0.0 | |
| -2.5000 | 0.0 | 0.0 | 0.0 | 0.0 | 0.0 | 0.0 | 0.0 | 0.0 | 0.0 | |
| -3.0000 | 0.0 | 0.0 | 0.0 | 0.0 | 0.0 | 0.0 | 0.0 | 0.0 | 0.0 | |
| -3.5000 | 0.0 | 0.0 | 0.0 | 0.0 | 0.0 | 0.0 | 0.0 | 0.0 | 0.0 | |
| -4.0000 | 0.0 | 0.0 | 0.0 | 0.0 | 0.0 | 0.0 | 0.0 | 0.0 | 0.0 | |
| -4.5000 | 0.0 | 0.0 | 0.0 | 0.0 | 0.0 | 0.0 | 0.0 | 0.0 | 0.0 | |
| -4.9160 | 0.0 | 0.0 | 0.0 | 0.0 | 0.0 | 0.0 | 0.0 | 0.0 | 0.0 | |
| -4.9580 | 0.0 | 0.0 | 0.0 | 0.0 | 0.0 | 0.0 | 0.0 | 0.0 | 0.0 | |
| -4.9790 | 0.0 | 0.0 | 0.0 | 0.0 | 0.0 | 0.0 | 0.0 | 0.0 | 0.0 | |
| -4.9860 | 0.0 | 0.0 | 0.0 | 0.0 | 0.0 | 0.0 | 0.0 | 0.0 | 0.0 | |
| -4.9930 | 0.0 | 0.0 | 0.0 | 0.0 | 0.0 | 0.0 | 0.0 | 0.0 | 0.0 | |
| -5.0000 | 0.0 | 0.0 | 0.0 | 0.0 | 0.0 | 0.0 | 0.0 | 0.0 | 0.0 | |
| E I | 0.0 | 0.05000 | 0.10000 | 0.13000 | 0.14330 | 0.15670 | 0.17000 | 0.20000 | 0.25000 | 0.30000 |

Table I
Ejector Results at x = 0.0, 15.2, and 27.9 cm (cont)

| DISP*ALC/HPREF**3 E - 3 | |
|-------------------------|---|
| E I | |
| -0.0000 | 0.00147 0.00147 0.00147 0.00147 0.01470 0.01470 0.00147 0.00147 0.00147 0.00147 0.00147 0.00147 |
| -0.0500 | 0.00147 0.00147 0.00147 0.00147 0.01470 0.01470 0.00147 0.00147 0.00147 0.00147 0.00147 0.00147 |
| -1.0000 | 0.00147 0.00147 0.00147 0.00147 0.01470 0.01470 0.00147 0.00147 0.00147 0.00147 0.00147 0.00147 |
| -1.5000 | 0.00147 0.00147 0.00147 0.00147 0.01470 0.01470 0.00147 0.00147 0.00147 0.00147 0.00147 0.00147 |
| -2.0000 | 0.00147 0.00147 0.00147 0.00147 0.01470 0.01470 0.00147 0.00147 0.00147 0.00147 0.00147 0.00147 |
| -2.5000 | 0.00147 0.00147 0.00147 0.00147 0.01470 0.01470 0.00147 0.00147 0.00147 0.00147 0.00147 0.00147 |
| -3.0000 | 0.00147 0.00147 0.00147 0.00147 0.01470 0.01470 0.00147 0.00147 0.00147 0.00147 0.00147 0.00147 |
| -3.5000 | 0.00147 0.00147 0.00147 0.00147 0.01470 0.01470 0.00147 0.00147 0.00147 0.00147 0.00147 0.00147 |
| -4.0000 | 0.00147 0.00147 0.00147 0.00147 0.01470 0.01470 0.00147 0.00147 0.00147 0.00147 0.00147 0.00147 |
| -4.5000 | 0.05320 0.05320 0.05320 0.05320 0.0896 0.0896 0.05320 0.05320 0.05320 0.05320 0.05320 0.05320 |
| -4.9160 | 0.15900 0.15900 0.15900 0.15900 0.15900 0.15900 0.15900 0.15900 0.15900 0.15900 0.15900 0.15900 |
| -4.9580 | 0.26500 0.26500 0.26500 0.26500 0.26500 0.26500 0.26500 0.26500 0.26500 0.26500 0.26500 0.26500 |
| -4.9790 | 0.33000 0.33000 0.33000 0.33000 0.33000 0.33000 0.33000 0.33000 0.33000 0.33000 0.33000 0.33000 |
| -4.9860 | 0.44300 0.44300 0.44300 0.44300 0.44300 0.44300 0.44300 0.44300 0.44300 0.44300 0.44300 0.44300 |
| -4.9930 | 0.24300 0.24300 0.24300 0.24300 0.24300 0.24300 0.24300 0.24300 0.24300 0.24300 0.24300 0.24300 |
| -5.0000 | 0.0 0.0 0.0 0.0 0.0 0.0 0.0 0.0 0.0 0.0 0.0 0.0 |
| E I | 0.0 0.05000 0.10000 0.13000 0.14330 0.15670 0.17000 0.20000 0.25000 0.30000 0.30000 0.30000 |
| FFF*MIJ/HPREF E - 4 | |
| E I | |
| -0.0000 | 0.03048 0.03048 0.03048 0.03048 0.30393 0.30393 0.03048 0.03048 0.03048 0.03048 0.03048 0.03048 |
| -0.0500 | 0.03048 0.03048 0.03048 0.03048 0.30393 0.30393 0.03048 0.03048 0.03048 0.03048 0.03048 0.03048 |
| -1.0000 | 0.03048 0.03048 0.03048 0.03048 0.30393 0.30393 0.03048 0.03048 0.03048 0.03048 0.03048 0.03048 |
| -1.5000 | 0.03048 0.03048 0.03048 0.03048 0.30393 0.30393 0.03048 0.03048 0.03048 0.03048 0.03048 0.03048 |
| -2.0000 | 0.03048 0.03048 0.03048 0.03048 0.30393 0.30393 0.03048 0.03048 0.03048 0.03048 0.03048 0.03048 |
| -2.5000 | 0.03048 0.03048 0.03048 0.03048 0.30393 0.30393 0.03048 0.03048 0.03048 0.03048 0.03048 0.03048 |
| -3.0000 | 0.03048 0.03048 0.03048 0.03048 0.30393 0.30393 0.03048 0.03048 0.03048 0.03048 0.03048 0.03048 |
| -4.0000 | 0.03048 0.03048 0.03048 0.03048 0.30393 0.30393 0.03048 0.03048 0.03048 0.03048 0.03048 0.03048 |
| -4.5000 | 0.07402 0.07402 0.07402 0.07402 0.07402 0.07402 0.07402 0.07402 0.07402 0.07402 0.07402 0.07402 |
| -4.9160 | 0.07103 0.07103 0.07103 0.07103 0.07103 0.07103 0.07103 0.07103 0.07103 0.07103 0.07103 0.07103 |
| -4.9580 | 0.04377 0.04377 0.04377 0.04377 0.04377 0.04377 0.04377 0.04377 0.04377 0.04377 0.04377 0.04377 |
| -4.9790 | 0.02230 0.02230 0.02230 0.02230 0.02230 0.02230 0.02230 0.02230 0.02230 0.02230 0.02230 0.02230 |
| -4.9860 | 0.01492 0.01492 0.01492 0.01492 0.01492 0.01492 0.01492 0.01492 0.01492 0.01492 0.01492 0.01492 |
| -4.9930 | 0.00389 0.00389 0.00389 0.00389 0.00389 0.00389 0.00389 0.00389 0.00389 0.00389 0.00389 0.00389 |
| -5.0000 | 0.00010 0.00010 0.00010 0.00010 0.00010 0.00010 0.00010 0.00010 0.00010 0.00010 0.00010 0.00010 |
| E I | 0.0 0.05000 0.10000 0.13000 0.14330 0.15670 0.17000 0.20000 0.25000 0.30000 0.30000 0.30000 |

Table I
Ejector Results at x = 0.0, 15.2, and 27.9 cm (cont)

| F I | U1/U1REF | F 0 | F 1 | F 2 | F 3 | F 4 | F 5 | F 6 | F 7 | F 8 | F 9 | F 10 | F 11 | F 12 | F 13 | F 14 | F 15 | F 16 | F 17 | F 18 | F 19 | F 20 |
|---------|----------|---------|---------|---------|---------|---------|---------|----------|---------|---------|-----|------|------|------|------|------|------|------|------|------|------|------|
| -0.0005 | 0.33355 | 0.35714 | 0.30473 | 0.40649 | 0.40861 | 0.40355 | 0.39712 | 0.37149 | 0.31036 | 0.28507 | | | | | | | | | | | | |
| -0.0005 | 0.33971 | 0.35738 | 0.30550 | 0.40931 | 0.41100 | 0.40955 | 0.40467 | 0.38027 | 0.31459 | 0.28530 | | | | | | | | | | | | |
| -0.0005 | 0.34021 | 0.35660 | 0.30574 | 0.41260 | 0.41038 | 0.41741 | 0.41518 | 0.39571 | 0.32368 | 0.28569 | | | | | | | | | | | | |
| -0.0005 | 0.33623 | 0.35287 | 0.39123 | 0.40874 | 0.41308 | 0.41484 | 0.41352 | 0.39664 | 0.32352 | 0.27920 | | | | | | | | | | | | |
| -0.0005 | 0.33168 | 0.34843 | 0.38746 | 0.40515 | 0.40923 | 0.41074 | 0.40815 | 0.38832 | 0.31279 | 0.26942 | | | | | | | | | | | | |
| -0.0000 | 0.32707 | 0.34561 | 0.38062 | 0.41067 | 0.41594 | 0.41794 | 0.41594 | 0.39405 | 0.31234 | 0.26817 | | | | | | | | | | | | |
| -0.0000 | 0.32086 | 0.34173 | 0.39338 | 0.42180 | 0.43082 | 0.43670 | 0.43829 | 0.42743 | 0.32627 | 0.27222 | | | | | | | | | | | | |
| -0.0005 | 0.31171 | 0.33200 | 0.38541 | 0.42505 | 0.43933 | 0.44951 | 0.45492 | 0.43884 | 0.32969 | 0.27018 | | | | | | | | | | | | |
| -0.0005 | 0.30620 | 0.32588 | 0.38606 | 0.43686 | 0.45376 | 0.46875 | 0.47176 | 0.43008 | 0.31571 | 0.27527 | | | | | | | | | | | | |
| -0.0005 | 0.32280 | 0.33761 | 0.40922 | 0.48749 | 0.51625 | 0.52697 | 0.51355 | 0.42378 | 0.33442 | 0.31249 | | | | | | | | | | | | |
| -0.0155 | 0.42574 | 0.41424 | 0.45601 | 0.55157 | 0.59155 | 0.59854 | 0.55888 | 0.46910 | 0.42574 | 0.40731 | | | | | | | | | | | | |
| -0.0155 | 0.42245 | 0.40588 | 0.45110 | 0.54566 | 0.58563 | 0.59139 | 0.58136 | 0.45604 | 0.41600 | 0.39043 | | | | | | | | | | | | |
| -0.0155 | 0.41433 | 0.40387 | 0.44649 | 0.54017 | 0.57864 | 0.58355 | 0.54881 | 0.44528 | 0.40532 | 0.39043 | | | | | | | | | | | | |
| -0.0155 | 0.40975 | 0.40168 | 0.44502 | 0.53470 | 0.57609 | 0.57924 | 0.54421 | 0.444035 | 0.39996 | 0.38506 | | | | | | | | | | | | |
| -0.0155 | 0.40726 | 0.39557 | 0.44095 | 0.53485 | 0.56956 | 0.57387 | 0.53795 | 0.43385 | 0.39766 | 0.37979 | | | | | | | | | | | | |
| -0.0155 | 0.0 | 0.0 | 0.0 | 0.0 | 0.0 | 0.0 | 0.0 | 0.0 | 0.0 | 0.0 | | | | | | | | | | | | |
| E I | 0.0 | 0.05000 | 0.09998 | 0.12098 | 0.14328 | 0.15638 | 0.16098 | 0.17995 | 0.24995 | 0.29995 | | | | | | | | | | | | |

| F I | U1/U1REF | F 0 | F 1 | F 2 | F 3 | F 4 | F 5 | F 6 | F 7 | F 8 | F 9 | F 10 | F 11 | F 12 | F 13 | F 14 | F 15 | F 16 | F 17 | F 18 | F 19 | F 20 |
|---------|----------|----------|----------|----------|---------|---------|---------|----------|----------|----------|-----|------|------|------|------|------|------|------|------|------|------|------|
| -0.0005 | 0.0 | 0.0 | 0.0 | 0.0 | 0.0 | 0.0 | 0.0 | 0.0 | 0.0 | 0.0 | | | | | | | | | | | | |
| -0.0005 | -0.32057 | -0.31897 | -0.11303 | 0.15223 | 0.24880 | 0.28179 | 0.27428 | 0.444350 | -0.31252 | -0.21460 | | | | | | | | | | | | |
| -0.0005 | -0.32359 | -0.32590 | -0.15004 | 0.10728 | 0.20767 | 0.24597 | 0.24972 | 0.42498 | 0.34405 | -0.12225 | | | | | | | | | | | | |
| -0.0005 | -0.30664 | -0.30594 | -0.15702 | 0.09443 | 0.18505 | 0.22092 | 0.21770 | 0.35588 | 0.04541 | -0.06862 | | | | | | | | | | | | |
| -0.0000 | -0.26604 | -0.26664 | -0.15220 | 0.07375 | 0.17034 | 0.20409 | 0.19793 | 0.30115 | 0.03563 | -0.03052 | | | | | | | | | | | | |
| -0.0000 | -0.22016 | -0.23442 | -0.16880 | 0.03706 | 0.13248 | 0.16895 | 0.17203 | 0.28938 | 0.07720 | 0.03827 | | | | | | | | | | | | |
| -0.0000 | -0.17687 | -0.21196 | -0.19481 | -0.00823 | 0.08625 | 0.12455 | 0.13925 | 0.26988 | 0.12022 | 0.19779 | | | | | | | | | | | | |
| -0.0005 | -0.12219 | -0.16472 | -0.16878 | 0.00110 | 0.09044 | 0.12059 | 0.13020 | 0.18273 | 0.09497 | 0.11447 | | | | | | | | | | | | |
| -0.0005 | -0.04445 | -0.07525 | -0.07270 | 0.06675 | 0.13938 | 0.14754 | 0.10628 | 0.06052 | 0.03549 | 0.06642 | | | | | | | | | | | | |
| -0.0005 | 0.03990 | 0.01663 | 0.00537 | 0.07436 | 0.13383 | 0.13498 | 0.05697 | 0.01593 | 0.03605 | 0.05106 | | | | | | | | | | | | |
| -0.0155 | 0.01813 | 0.01247 | 0.00631 | 0.01500 | 0.02297 | 0.02127 | 0.00976 | 0.00427 | 0.01226 | 0.01369 | | | | | | | | | | | | |
| -0.0155 | 0.01072 | 0.00628 | 0.00305 | 0.00700 | 0.01143 | 0.01045 | 0.00441 | 0.00137 | 0.00577 | 0.00664 | | | | | | | | | | | | |
| -0.0155 | 0.00225 | 0.00099 | 0.00024 | 0.00850 | 0.00362 | 0.00531 | 0.00199 | 0.00047 | 0.00262 | 0.00300 | | | | | | | | | | | | |
| -0.0155 | 0.00187 | 0.00260 | 0.00166 | 0.00118 | 0.00410 | 0.00331 | 0.00131 | 0.00027 | 0.00166 | 0.00192 | | | | | | | | | | | | |
| -0.0155 | 0.00023 | 0.00133 | 0.00115 | 0.00003 | 0.00256 | 0.00145 | 0.00064 | 0.00004 | 0.00076 | 0.00089 | | | | | | | | | | | | |
| -0.0155 | 0.0 | 0.0 | 0.0 | 0.0 | 0.0 | 0.0 | 0.0 | 0.0 | 0.0 | 0.0 | | | | | | | | | | | | |
| E I | 0.0 | 0.05000 | 0.09998 | 0.12998 | 0.14328 | 0.15558 | 0.16998 | 0.19995 | 0.24995 | 0.29995 | | | | | | | | | | | | |

Table I
Ejector Results at x = 0.0, 15.2, and 27.9 cm (cont)

| | F - 1 | | | | | | | | | |
|----------|----------|----------|----------|----------|----------|----------|----------|----------|----------|---------|
| U13/URFF | | | | | | | | | | |
| E I | | | | | | | | | | |
| -0.00035 | 0.0 | -0.0172 | -0.14719 | -0.14684 | -0.13905 | -0.12792 | -0.11413 | -0.07813 | -0.02926 | 0.0 |
| -0.05035 | 0.0 | -0.08356 | -0.12659 | -0.11882 | -0.10902 | -0.09620 | -0.08150 | -0.04449 | -0.01166 | 0.0 |
| -0.10035 | 0.0 | -0.06148 | -0.07967 | -0.05834 | -0.04337 | -0.02609 | -0.00792 | 0.03036 | 0.03320 | 0.0 |
| -0.15035 | 0.0 | -0.04154 | -0.04667 | -0.02534 | -0.01182 | 0.00355 | 0.01997 | 0.05530 | 0.05554 | 0.0 |
| -0.20030 | 0.0 | -0.03805 | -0.05199 | -0.04400 | -0.03737 | -0.02888 | -0.01913 | 0.00664 | 0.02445 | 0.0 |
| -0.20000 | 0.0 | -0.04196 | -0.06301 | -0.05677 | -0.04975 | -0.04037 | -0.02934 | 0.00019 | 0.01835 | 0.0 |
| -0.30000 | 0.0 | -0.03264 | -0.03348 | -0.00299 | 0.01687 | 0.03958 | 0.06307 | 0.10975 | 0.07838 | 0.0 |
| -0.34995 | 0.0 | -0.00959 | 0.02105 | 0.07460 | 0.10424 | 0.13605 | 0.16671 | 0.21463 | 0.12228 | 0.0 |
| -0.39995 | 0.0 | 0.00271 | 0.03004 | 0.06262 | 0.07850 | 0.09473 | 0.10928 | 0.12663 | 0.05903 | 0.0 |
| -0.44995 | 0.0 | 0.00726 | 0.01078 | 0.01643 | 0.01893 | 0.02286 | 0.02804 | 0.03529 | 0.01414 | 0.0 |
| -0.49155 | 0.0 | 0.00050 | 0.00201 | 0.00237 | 0.00245 | 0.00325 | 0.00472 | 0.00669 | 0.00209 | 0.0 |
| -0.5375 | 0.0 | 0.00037 | 0.00135 | 0.00156 | 0.00159 | 0.00213 | 0.00308 | 0.00429 | 0.00119 | 0.0 |
| -0.49785 | 0.0 | 0.00021 | 0.00094 | 0.00111 | 0.00108 | 0.00147 | 0.00211 | 0.00293 | 0.00077 | 0.0 |
| -0.49855 | 0.0 | 0.00017 | 0.00074 | 0.00079 | 0.00092 | 0.00119 | 0.00170 | 0.00237 | 0.00062 | 0.0 |
| -0.49925 | 0.0 | 0.00010 | 0.00053 | 0.00076 | 0.00059 | 0.00096 | 0.00117 | 0.00168 | 0.00043 | 0.0 |
| -0.49995 | 0.0 | 0.0 | 0.0 | 0.0 | 0.0 | 0.0 | 0.0 | 0.0 | 0.0 | 0.0 |
| F I | 0.0 | 0.05000 | 0.09998 | 0.12998 | 0.14328 | 0.15658 | 0.16598 | 0.16995 | 0.17495 | 0.29995 |
| U13/URFF | | | | | | | | | | |
| E I | | | | | | | | | | |
| -0.00035 | 0.44022 | 0.45998 | 0.46667 | 0.42686 | 0.40136 | 0.37144 | 0.33893 | 0.25694 | 0.14452 | 0.10573 |
| -0.05005 | 0.43946 | 0.46017 | 0.47194 | 0.43643 | 0.41202 | 0.38274 | 0.35065 | 0.26611 | 0.14501 | 0.10171 |
| -0.10035 | 0.43652 | 0.45984 | 0.47686 | 0.44485 | 0.42113 | 0.39265 | 0.36114 | 0.27587 | 0.14332 | 0.09023 |
| -0.15075 | 0.42632 | 0.45001 | 0.46700 | 0.43473 | 0.41128 | 0.38285 | 0.35150 | 0.26746 | 0.13344 | 0.07440 |
| -0.20700 | 0.40470 | 0.42907 | 0.44521 | 0.41076 | 0.38628 | 0.35690 | 0.32481 | 0.24135 | 0.11530 | 0.06068 |
| -0.25000 | 0.36942 | 0.39736 | 0.41799 | 0.38407 | 0.35977 | 0.33057 | 0.29914 | 0.21868 | 0.10426 | 0.05457 |
| -0.30000 | 0.31640 | 0.35012 | 0.38117 | 0.35743 | 0.33189 | 0.30583 | 0.27778 | 0.20688 | 0.10144 | 0.04959 |
| -0.34995 | 0.24247 | 0.27867 | 0.31550 | 0.29501 | 0.27673 | 0.25481 | 0.23225 | 0.18257 | 0.09095 | 0.04120 |
| -0.39995 | 0.15484 | 0.18669 | 0.21643 | 0.20150 | 0.18607 | 0.16923 | 0.15530 | 0.13545 | 0.05485 | 0.03681 |
| -0.44995 | 0.07441 | 0.09769 | 0.12103 | 0.11524 | 0.10472 | 0.09745 | 0.09074 | 0.09074 | 0.05321 | 0.05072 |
| -0.49155 | 0.07909 | 0.02928 | 0.04226 | 0.04391 | 0.03786 | 0.04372 | 0.04372 | 0.03417 | 0.02289 | 0.02471 |
| -0.49575 | 0.01883 | 0.02006 | 0.03054 | 0.03302 | 0.02926 | 0.02889 | 0.03273 | 0.02543 | 0.01674 | 0.01965 |
| -0.49785 | 0.01323 | 0.01409 | 0.02274 | 0.02572 | 0.02144 | 0.02132 | 0.02431 | 0.01921 | 0.01292 | 0.01598 |
| -0.49855 | 0.01087 | 0.01187 | 0.01745 | 0.01834 | 0.01902 | 0.01819 | 0.02025 | 0.01628 | 0.01114 | 0.01423 |
| -0.49925 | 0.000715 | 0.000741 | 0.01343 | 0.01800 | 0.01256 | 0.01387 | 0.01456 | 0.01216 | 0.00856 | 0.01167 |
| -0.49995 | 0.0 | 0.0 | 0.0 | 0.0 | 0.0 | 0.0 | 0.0 | 0.0 | 0.0 | 0.0 |
| F I | 0.0 | 0.05000 | 0.09998 | 0.12998 | 0.14328 | 0.15658 | 0.16598 | 0.16995 | 0.17495 | 0.29995 |

Table I
Ejector Results at x = 0.0, 15.2, and 27.9 cm (cont)

| F I | DISP#ALC/HIPEFF**3 E - 4 | | | | | | | | | |
|---------|--------------------------|---------|---------|---------|---------|----------|---------|---------|---------|---------|
| -0.0005 | 0.25276 | 0.29699 | 0.33564 | 0.29837 | 0.27114 | 0.24430 | 0.21582 | 0.14248 | 0.14790 | 0.07482 |
| -0.0505 | 0.25295 | 0.30046 | 0.35202 | 0.32175 | 0.30065 | 0.27508 | 0.24756 | 0.17060 | 0.05779 | 0.07719 |
| -1.0005 | 0.24887 | 0.30041 | 0.35977 | 0.32378 | 0.31352 | 0.28835 | 0.26241 | 0.18840 | 0.06314 | 0.07679 |
| -1.5005 | 0.23462 | 0.28413 | 0.33902 | 0.31251 | 0.29206 | 0.26755 | 0.24170 | 0.17376 | 0.06177 | 0.02280 |
| -2.0000 | 0.21330 | 0.26022 | 0.31058 | 0.28165 | 0.26098 | 0.23533 | 0.20893 | 0.14202 | 0.04610 | 0.01569 |
| -2.5000 | 0.18864 | 0.23021 | 0.29348 | 0.26516 | 0.24516 | 0.22055 | 0.19496 | 0.12904 | 0.03980 | 0.01276 |
| -3.0000 | 0.15491 | 0.21125 | 0.27762 | 0.25714 | 0.23955 | 0.21801 | 0.19560 | 0.13770 | 0.04518 | 0.01292 |
| -3.4905 | 0.10537 | 0.15872 | 0.22475 | 0.21171 | 0.15670 | 0.17858 | 0.16129 | 0.12895 | 0.04400 | 0.01131 |
| -3.9905 | 0.05212 | 0.09066 | 0.13853 | 0.13688 | 0.12641 | 0.11481 | 0.10606 | 0.09482 | 0.02533 | 0.00807 |
| -4.4905 | 0.02266 | 0.03806 | 0.07353 | 0.09727 | 0.09311 | 0.09024 | 0.09409 | 0.06576 | 0.02294 | 0.02092 |
| -4.0155 | 0.02919 | 0.01092 | 0.01823 | 0.03116 | 0.02292 | 0.02392 | 0.03986 | 0.02810 | 0.02537 | 0.01692 |
| -4.9375 | 0.01094 | 0.01494 | 0.01348 | 0.02444 | 0.01852 | 0.02027 | 0.03246 | 0.02727 | 0.01065 | 0.01594 |
| -4.0785 | 0.01484 | 0.01110 | 0.01027 | 0.01964 | 0.01440 | 0.01643 | 0.02536 | 0.01816 | 0.01643 | 0.01531 |
| -4.9855 | 0.01247 | 0.00637 | 0.00737 | 0.01597 | 0.01270 | 0.01423 | 0.02159 | 0.01599 | 0.01479 | 0.01479 |
| -4.9325 | 0.00861 | 0.00641 | 0.00672 | 0.01325 | 0.00912 | 0.01122 | 0.01601 | 0.01260 | 0.01207 | 0.01343 |
| -4.9905 | 0.0 | 0.0 | 0.0 | 0.0 | 0.0 | 0.0 | 0.0 | 0.0 | 0.0 | 0.0 |
| E I | 0.0 | 0.05000 | 0.00993 | 0.12008 | 0.14328 | 0.15555 | 0.16998 | 0.19995 | 0.24995 | 0.29995 |
| F I | 0.16066 | 0.14768 | 0.13259 | 0.12971 | 0.12450 | 0.11854 | 0.11147 | 0.09670 | 0.09128 | 0.09437 |
| -0.5005 | 0.15000 | 0.14768 | 0.13259 | 0.12405 | 0.11832 | 0.11150 | 0.10408 | 0.08698 | 0.07625 | 0.07975 |
| -1.0005 | 0.16044 | 0.14740 | 0.13244 | 0.12467 | 0.11853 | 0.11185 | 0.10415 | 0.08465 | 0.06608 | 0.06369 |
| -1.5005 | 0.16237 | 0.14935 | 0.13480 | 0.12672 | 0.12136 | 0.11490 | 0.10712 | 0.08677 | 0.06041 | 0.05086 |
| -2.0000 | 0.16093 | 0.14791 | 0.13373 | 0.12553 | 0.12004 | 0.11343 | 0.10582 | 0.08505 | 0.06044 | 0.04919 |
| -2.5000 | 0.15158 | 0.13837 | 0.12475 | 0.11637 | 0.11064 | 0.10385 | 0.09618 | 0.07766 | 0.05723 | 0.04892 |
| -3.0000 | 0.13541 | 0.12159 | 0.10967 | 0.10179 | 0.09636 | 0.08991 | 0.08267 | 0.05510 | 0.04774 | 0.03989 |
| -3.4905 | 0.11698 | 0.10253 | 0.09281 | 0.08614 | 0.08159 | 0.07615 | 0.07009 | 0.05417 | 0.03940 | 0.03145 |
| -3.9905 | 0.09641 | 0.08050 | 0.07084 | 0.06216 | 0.05740 | 0.05232 | 0.04766 | 0.03455 | 0.03480 | 0.03519 |
| -4.4905 | 0.05172 | 0.05134 | 0.04175 | 0.02842 | 0.02469 | 0.02206 | 0.02114 | 0.02625 | 0.02597 | 0.02578 |
| -4.0155 | 0.00600 | 0.00603 | 0.02054 | 0.01311 | 0.01199 | 0.01139 | 0.00993 | 0.00872 | 0.00434 | 0.00757 |
| -4.9375 | 0.00374 | 0.00565 | 0.01451 | 0.00529 | 0.00970 | 0.009853 | 0.00693 | 0.00609 | 0.00300 | 0.00508 |
| -4.0785 | 0.00248 | 0.00372 | 0.01010 | 0.00701 | 0.00670 | 0.00638 | 0.00489 | 0.00427 | 0.00214 | 0.00350 |
| -4.9855 | 0.00193 | 0.00316 | 0.00864 | 0.00598 | 0.00598 | 0.00598 | 0.00399 | 0.00348 | 0.00177 | 0.00299 |
| -4.9325 | 0.00125 | 0.00180 | 0.00567 | 0.00514 | 0.00364 | 0.00350 | 0.00275 | 0.00247 | 0.00128 | 0.00214 |
| -4.9905 | 0.00001 | 0.00001 | 0.00001 | 0.00001 | 0.00001 | 0.00001 | 0.00001 | 0.00001 | 0.00001 | 0.00001 |
| F I | 0.0 | 0.05000 | 0.00993 | 0.12008 | 0.14328 | 0.15555 | 0.16998 | 0.19995 | 0.24995 | 0.29995 |

Table I
Ejector Results at x = 0.0, 15.2, and 27.9 cm (cont)

| F I | U1/UPEF | F 0 | F 1 | F 2 | F 3 | F 4 | F 5 | F 6 | F 7 | F 8 | F 9 | F 10 | F 11 | F 12 | F 13 | F 14 | F 15 | F 16 | F 17 | F 18 | F 19 | F 20 | |
|----------|----------|----------|----------|----------|----------|----------|----------|----------|----------|----------|-----|------|------|------|------|------|------|------|------|------|------|------|--|
| -0.0091 | 0.36007 | 0.36189 | 0.36501 | 0.36440 | 0.36307 | 0.36107 | 0.35941 | 0.35034 | 0.33364 | 0.32613 | | | | | | | | | | | | | |
| -0.05251 | 0.35984 | 0.36175 | 0.36514 | 0.36485 | 0.36375 | 0.36196 | 0.35948 | 0.35144 | 0.33430 | 0.32644 | | | | | | | | | | | | | |
| -0.10351 | 0.35913 | 0.36129 | 0.36546 | 0.36588 | 0.36509 | 0.36360 | 0.36135 | 0.35350 | 0.33536 | 0.32664 | | | | | | | | | | | | | |
| -0.15522 | 0.35786 | 0.36041 | 0.36569 | 0.36696 | 0.36553 | 0.36335 | 0.36334 | 0.35563 | 0.33615 | 0.32632 | | | | | | | | | | | | | |
| -0.20413 | 0.35624 | 0.35940 | 0.36644 | 0.36902 | 0.36913 | 0.36841 | 0.36674 | 0.35921 | 0.33772 | 0.32625 | | | | | | | | | | | | | |
| -0.25745 | 0.35435 | 0.35952 | 0.36955 | 0.37346 | 0.37455 | 0.37470 | 0.37370 | 0.36661 | 0.34171 | 0.32753 | | | | | | | | | | | | | |
| -0.30884 | 0.35234 | 0.35794 | 0.37440 | 0.38083 | 0.38340 | 0.38485 | 0.38483 | 0.37821 | 0.34747 | 0.32894 | | | | | | | | | | | | | |
| -0.35975 | 0.35076 | 0.35415 | 0.37854 | 0.39197 | 0.39630 | 0.39920 | 0.40003 | 0.39249 | 0.35207 | 0.32838 | | | | | | | | | | | | | |
| -0.41146 | 0.35117 | 0.35074 | 0.39078 | 0.41032 | 0.41723 | 0.42168 | 0.42251 | 0.40934 | 0.35489 | 0.32812 | | | | | | | | | | | | | |
| -0.46246 | 0.35419 | 0.36552 | 0.40669 | 0.44058 | 0.45260 | 0.45936 | 0.45894 | 0.42972 | 0.36178 | 0.33433 | | | | | | | | | | | | | |
| -0.50555 | 0.34955 | 0.35673 | 0.40329 | 0.44375 | 0.46571 | 0.47390 | 0.47242 | 0.41943 | 0.35300 | 0.31682 | | | | | | | | | | | | | |
| -0.50986 | 0.34053 | 0.34417 | 0.37984 | 0.40823 | 0.40730 | 0.40278 | 0.39600 | 0.34100 | 0.27040 | 0.23698 | | | | | | | | | | | | | |
| -0.51201 | 0.33447 | 0.33571 | 0.36614 | 0.38138 | 0.37137 | 0.36223 | 0.35541 | 0.30223 | 0.23116 | 0.19586 | | | | | | | | | | | | | |
| -0.51273 | 0.33270 | 0.33162 | 0.35902 | 0.37040 | 0.35706 | 0.34636 | 0.33971 | 0.28781 | 0.21697 | 0.18099 | | | | | | | | | | | | | |
| -0.51318 | 0.32814 | 0.32864 | 0.35054 | 0.35837 | 0.34189 | 0.32981 | 0.32353 | 0.27312 | 0.20262 | 0.16582 | | | | | | | | | | | | | |
| -0.51410 | 0.0 | 0.0 | 0.0 | 0.0 | 0.0 | 0.0 | 0.0 | 0.0 | 0.0 | 0.0 | | | | | | | | | | | | | |
| F I | 0.0 | 0.04930 | 0.09995 | 0.12995 | 0.14325 | 0.15665 | 0.16995 | 0.19988 | 0.24988 | 0.29988 | | | | | | | | | | | | | |
| F I | 0.0 | 0.0 | 0.0 | 0.0 | 0.0 | 0.0 | 0.0 | 0.0 | 0.0 | 0.0 | | | | | | | | | | | | | |
| -0.0091 | 0.24753 | 0.21217 | 0.26261 | 0.32890 | 0.33716 | 0.34147 | 0.35111 | 0.38561 | 0.30660 | 0.19788 | | | | | | | | | | | | | |
| -0.05251 | 0.19395 | 0.16337 | 0.21505 | 0.28240 | 0.29293 | 0.29991 | 0.31405 | 0.35613 | 0.29403 | 0.19605 | | | | | | | | | | | | | |
| -0.15522 | 0.14582 | 0.11950 | 0.17094 | 0.23746 | 0.24979 | 0.25932 | 0.27507 | 0.32128 | 0.27494 | 0.18941 | | | | | | | | | | | | | |
| -0.20413 | 0.10577 | 0.09268 | 0.13223 | 0.19770 | 0.20099 | 0.21920 | 0.23714 | 0.28456 | 0.25216 | 0.18052 | | | | | | | | | | | | | |
| -0.25745 | 0.07308 | 0.05215 | 0.09810 | 0.16340 | 0.17213 | 0.18090 | 0.19843 | 0.24326 | 0.22299 | 0.16769 | | | | | | | | | | | | | |
| -0.30884 | 0.05069 | 0.03270 | 0.07212 | 0.12842 | 0.13851 | 0.14490 | 0.15978 | 0.19255 | 0.17991 | 0.14428 | | | | | | | | | | | | | |
| -0.35975 | 0.04024 | 0.02424 | 0.05735 | 0.10505 | 0.11176 | 0.11351 | 0.11942 | 0.12975 | 0.11938 | 0.10651 | | | | | | | | | | | | | |
| -0.41146 | 0.03838 | 0.02632 | 0.04988 | 0.08706 | 0.08729 | 0.08303 | 0.08783 | 0.05938 | 0.05206 | 0.05850 | | | | | | | | | | | | | |
| -0.46246 | 0.02831 | 0.01992 | 0.02630 | 0.04146 | 0.03271 | 0.02192 | 0.01187 | -0.01701 | -0.01505 | -0.00285 | | | | | | | | | | | | | |
| -0.50555 | -0.01038 | -0.01994 | -0.06906 | -0.09437 | -0.11376 | -0.11976 | -0.12399 | -0.13012 | -0.13673 | | | | | | | | | | | | | | |
| -0.50986 | -0.0812 | -0.1546 | -0.2942 | -0.4715 | -0.5849 | -0.6676 | -0.6594 | -0.6499 | -0.6671 | -0.7865 | | | | | | | | | | | | | |
| -0.51201 | -0.00705 | -0.01074 | -0.02195 | -0.03437 | -0.04023 | -0.04544 | -0.04379 | -0.04217 | -0.04269 | -0.05204 | | | | | | | | | | | | | |
| -0.51273 | -0.00314 | -0.01036 | -0.01954 | -0.02374 | -0.0222 | -0.03590 | -0.03387 | -0.03262 | -0.03297 | -0.04149 | | | | | | | | | | | | | |
| -0.51338 | -0.00970 | -0.0210 | -0.01390 | -0.02170 | -0.02257 | -0.02469 | -0.02244 | -0.02177 | -0.02201 | -0.02960 | | | | | | | | | | | | | |
| -0.51410 | 0.0 | 0.0 | 0.0 | 0.0 | 0.0 | 0.0 | 0.0 | 0.0 | 0.0 | 0.0 | | | | | | | | | | | | | |
| F I | 0.0 | 0.04099 | 0.09095 | 0.12995 | 0.14325 | 0.15665 | 0.16995 | 0.19988 | 0.24988 | 0.29988 | | | | | | | | | | | | | |

Table I
Ejector Results at x = 0.0, 15.2, and 27.9 cm (cont)

| U3/UREF | | E -2 | | | | | | | | | |
|-------------|---------|----------|----------|----------|----------|----------|----------|----------|----------|---------|--|
| E 1 | | | | | | | | | | | |
| -0.0081 | 0.0 | -0.25847 | -0.42514 | -0.44719 | -0.43713 | -0.41738 | -0.38910 | -0.30513 | -0.14016 | 0.0 | |
| -0.05251 | 0.0 | -0.23544 | -0.37726 | -0.38984 | -0.37948 | -0.36016 | -0.33363 | -0.25289 | -0.10703 | 0.0 | |
| -0.10351 | 0.0 | -0.18717 | -0.28693 | -0.28209 | -0.26563 | -0.24417 | -0.21669 | -0.14338 | -0.03980 | 0.0 | |
| -0.15522 | 0.0 | -0.13619 | -0.19478 | -0.17468 | -0.15519 | -0.13049 | -0.10270 | -0.03620 | 0.02922 | 0.0 | |
| -0.20613 | 0.0 | -0.08956 | -0.10895 | -0.07148 | -0.04634 | -0.01742 | 0.01286 | 0.07782 | 0.10782 | 0.0 | |
| -0.25785 | 0.0 | -0.03637 | -0.00181 | 0.06797 | 0.10646 | 0.14748 | 0.18764 | 0.26208 | 0.23925 | 0.0 | |
| -0.30884 | 0.0 | 0.02548 | 0.13013 | 0.24723 | 0.30658 | 0.36742 | 0.42474 | 0.51913 | 0.42030 | 0.0 | |
| -0.35975 | 0.0 | 0.07679 | 0.23759 | 0.38938 | 0.46338 | 0.53798 | 0.60705 | 0.71343 | 0.53975 | 0.0 | |
| -0.41146 | 0.0 | 0.08623 | 0.24141 | 0.37435 | 0.43668 | 0.49881 | 0.55534 | 0.63838 | 0.44521 | 0.0 | |
| -0.46246 | 0.0 | 0.05068 | 0.13617 | 0.19846 | 0.22558 | 0.25391 | 0.28084 | 0.33044 | 0.21940 | 0.0 | |
| -0.50555 | 0.0 | 0.00731 | 0.02380 | 0.02996 | 0.03078 | 0.03375 | 0.03867 | 0.06933 | 0.05052 | 0.0 | |
| -0.50986 | 0.0 | 0.00449 | 0.01477 | 0.01599 | 0.01599 | 0.01616 | 0.01518 | 0.03300 | 0.02224 | 0.0 | |
| -0.51201 | 0.0 | 0.00274 | 0.00910 | 0.00946 | 0.00823 | 0.00816 | 0.00632 | 0.01763 | 0.01133 | 0.0 | |
| -0.51273 | 0.0 | 0.00198 | 0.00711 | 0.00586 | 0.00573 | 0.00569 | 0.00400 | 0.01262 | 0.00781 | 0.0 | |
| -0.51338 | 0.0 | 0.00150 | 0.00481 | 0.00433 | 0.00340 | 0.00339 | 0.00208 | 0.00777 | 0.00457 | 0.0 | |
| -0.51410 | 0.0 | 0.0 | 0.0 | 0.0 | 0.0 | 0.0 | 0.0 | 0.0 | 0.0 | 0.0 | |
| E 1 | | | | | | | | | | | |
| 0.0 | 0.0 | 0.04999 | 0.09995 | 0.12995 | 0.14325 | 0.15665 | 0.16995 | 0.19988 | 0.24988 | 0.29988 | |
| TKE/UREF**2 | | | | | | | | | | | |
| E 1 | | | | | | | | | | | |
| -0.0081 | 0.18954 | 0.18575 | 0.17534 | 0.16643 | 0.16182 | 0.15681 | 0.15155 | 0.13898 | 0.11803 | 0.10935 | |
| -0.05251 | 0.18791 | 0.18429 | 0.17389 | 0.16459 | 0.15986 | 0.15476 | 0.14946 | 0.13637 | 0.11460 | 0.10577 | |
| -0.10351 | 0.18445 | 0.18125 | 0.17098 | 0.16135 | 0.15639 | 0.15103 | 0.14544 | 0.13179 | 0.10926 | 0.10024 | |
| -0.15522 | 0.18018 | 0.17731 | 0.16753 | 0.15806 | 0.15313 | 0.14777 | 0.14212 | 0.12811 | 0.10417 | 0.09427 | |
| -0.20613 | 0.17330 | 0.17086 | 0.16185 | 0.15273 | 0.14791 | 0.14265 | 0.13708 | 0.12308 | 0.09825 | 0.08754 | |
| -0.25785 | 0.16242 | 0.16064 | 0.15292 | 0.14448 | 0.13993 | 0.13493 | 0.12961 | 0.11609 | 0.09086 | 0.07941 | |
| -0.30884 | 0.14675 | 0.14594 | 0.14019 | 0.13280 | 0.12867 | 0.12407 | 0.11917 | 0.10673 | 0.08175 | 0.06953 | |
| -0.35975 | 0.12526 | 0.12575 | 0.12263 | 0.11656 | 0.11286 | 0.10872 | 0.10437 | 0.09379 | 0.07036 | 0.05783 | |
| -0.41146 | 0.09678 | 0.09880 | 0.09877 | 0.09417 | 0.09076 | 0.08697 | 0.08325 | 0.07554 | 0.05550 | 0.04459 | |
| -0.46246 | 0.06043 | 0.06353 | 0.06568 | 0.06215 | 0.05885 | 0.05544 | 0.05297 | 0.05026 | 0.03642 | 0.03020 | |
| -0.50555 | 0.01635 | 0.01759 | 0.02015 | 0.02124 | 0.02157 | 0.02193 | 0.02220 | 0.02411 | 0.01814 | 0.02130 | |
| -0.50986 | 0.01117 | 0.01280 | 0.01645 | 0.02160 | 0.02914 | 0.03371 | 0.03564 | 0.03610 | 0.03059 | 0.02987 | |
| -0.51201 | 0.00723 | 0.00886 | 0.01176 | 0.01625 | 0.02209 | 0.02506 | 0.02506 | 0.02499 | 0.02128 | 0.02252 | |
| -0.51273 | 0.00608 | 0.00653 | 0.00663 | 0.01328 | 0.01775 | 0.01993 | 0.01935 | 0.01932 | 0.01648 | 0.01853 | |
| -0.51338 | 0.00307 | 0.00527 | 0.00689 | 0.00970 | 0.01236 | 0.01364 | 0.01266 | 0.01279 | 0.01097 | 0.01369 | |
| -0.51410 | 0.0 | 0.0 | 0.0 | 0.0 | 0.0 | 0.0 | 0.0 | 0.0 | 0.0 | 0.0 | |
| E 1 | | | | | | | | | | | |
| 0.0 | 0.0 | 0.04999 | 0.09995 | 0.12995 | 0.14325 | 0.15665 | 0.16995 | 0.19988 | 0.24988 | 0.29988 | |

TABLE II
SUMMARY OF COMPUTER TIME REQUIRED FOR TEST CASES

| Case No. | Description | Number of Integrated Variables | Number of Finite Elements | Number of Integration Steps | CPU Time (sec) |
|----------|--|--------------------------------|---------------------------|-----------------------------|----------------|
| 1 | Turbulent Boundary Layer in a Duct (k&d) | 3 | 40 | 475 | 621.89 |
| | Turbulent Boundary Layer in a Duct (MLT) | 1 | 40 | 513 | 221.42 |
| 2 | Rectangular Nozzle (k&d) | 3 | 40 | 111 | 456.40 |
| | Rectangular Nozzle (k&l) | 2 | 40 | 162 | 309.20 |
| 3 | Axisymmetric Nozzle (k&d) | 3 | 162 | 184 | 3200.00 |
| | Axisymmetric Nozzle (Constant ϵ) | 1 | 162 | 227 | 1185.19 |
| 4 | Hypermixing Nozzle | 4 | 120 | 79 | 1800.00 |
| 5 | Plane Wall Jet | 3 | 40 | 307 | 1412.94 |
| 6 | Developing Pipe Flow (45° Wedge) | 1 | 73 | 558 | 504.15 |
| | Developing Pipe Flow (90° Wedge) | 1 | 73 | 707 | 696.34 |
| 7 | Developing Flow in an Annular Pipe | 1 | 73 | 271 | 278.46 |
| 8 | Developing Flow in an Axisymmetric Pipe with Conical Center and No Fluting | 1 | 56 | 451 | 500.00 |
| 9 | Developing Fluted Pipe Flow | 1 | 73 | 995 | 975.64 |
| - | Ejector System | 4 | 270 | 1520 | 54000.00 |
| - | Axisymmetric Fluted Mixer | 2 | 56 | 227 | 650.93 |

Table III
Data Deck for Case I

6c/25/76

```

1 CASECI
  FEPL
  3CRF
  FNAME
  ENAME01
  NPSK = 4, NSCX = 1, NSCY = 1, NELE2 = 1, KRODIA = 1,
  NEC = 2, NEKNN = 3, TGA5 = 1, IFC = 1, KDUMP=1,
  GENC
  ENAME02
  PCAT = 1.0, UINF = 112.2, TCFINF = 562.0, REFL = .4333,
  VSTART = 0.1, TC = 3.517, TD = 4.0, DELP = 12.5,
  GENC
  FCTPA
  LINKI 1 1 .6C,
  T
  4 1 4 1200, 2 4 1200, 4 8 1200, 5 1 120, 6 1 120, 7 1 60, 10 1 60, 11 1 30,
  20 1 30,
  T
  1 21, 1 2,
  T 21 ROWS AND 2 COLUMNS
5 CMTITLE
  TURBULEN P-L--BRADSHAW RELAXING FLCK-K AND D
  DCNE
  DESCRIPT 204 1 DESCRIPTIVE TITLE AT BEGINING OF OUTPUT.
  TURBULEN P-L--BRADSHAW RELAXING FLCK-K AND D
  DCNE
  DESCRIPT 332 1 TOPAR PARAMETER TITLES FOR OUTPUT
  REFERENCE ENGLISH--FI ENGLISH--IN M-K-S
  LENGTH ..FEET.. ..IN.... C-C-S
  VELOCITY ..FT/SEC.. ..M/S..... ..CM/S....
  DENSITY ..LBM/FT3.. ..KG/M3.... ..G/CC....
  TEMPERATURE ..RANKINE.. ..KELVIN..
  ENTHALPY ..BTU/LBM.. ..KJ/KG....
  FRCZ ..SPEC-HEAT ..BTU/LBM-R ..KJ/KG-K..
  VISCOSITY ..LBM/FT-S.. ..PSF..... ..NT-S/M2...
  LOCAL PRESSURE ..PSI..... ..PCISE....
  LOCAL SOLUTION ..DPOXI.... ..TCFR....
  XI/LREF ..DXI/LREF. ..EPSILON.. ..DXI/LREF
  DCNE
  ICNLPB -1
  999
  5*20C
  95C
  20C 4*43
  200 27 200 2*27
  200 10 200 2*10
  200 58 200 58 200
  200 57 200 57 200
  
```


Table III
Data Deck for Case I (cont)

```

17  ACC      1 2 3 4 T
    DCNE
    KENC      6
    ACC      1 2 3 4 T
    DCNE
    VTEMP     -5E
    VVY      42*562.C T
    VVY      -27
    2*0.0 2*46.56 2*50.83 2*53.41 2*56.43 2*59.58 2*62.05 2*66.42 2*71.58 2*76.52
    2*82.13 2*92.01 2*103.C10 2*109.73 2*111.98 12*112.2
    T INITIAL U1 PROFILE
    VVYENC 1
    LINKCALL -1
    2 4, 5 6, 2 15, 2 4, 2 3, 1 5, 1 6, 2 19, 0 T
    23  LINK2  4
    ICCAC
    LINK1  3
    24  DESCRIPT 3
    REFERENCE LENGTH,LREF
    REFERENCE VISCOSITY,LAMINAR VALUE
    EVALUATED AT REF. TEMPERATURE.
    FREESTREAM VELOCITY AT X0(=LREF)
    STAGNATION TEMPERATURE (CONSTANT,=TREF)
    FREESTREAM DENSITY AT X0(=R*PREF)
    FREESTREAM MACH NUMBER AT X0
    STATIC PRESSURE AT X0
    NUMBER OF NODES
    NUMBER OF FINITE ELEMENTS
    26  DCNE
    CCMCC
    27  EXIT . END
    DIMEN
    GECMFL
    43 FT.
    38 LBW/FT S
    27 FT/S
    58 DEG F
    10 LBW/FT
    154
    9 PSF
    -16
    -14
  
```


Table IV
Data Deck for Case II

```

1 CASE01
  FEFL
2 3DPNS
  FNAME
  &NAME01
  NPV SX = 2, NSCX = 0, NSCY = 0,
  NEQNN = 1, IGA S = 0, IFR = 1,
  NU2POS = 2, NU3POS = 2, KDUMP = 1,
  &END
3 &NAME02
  X2SCALE = 0.1, X3SCALE = 0.1, X2SHFT = -10.0,
  UINF = 100.0, TOFNF = 533.0, REFL = 1.0, RHOINF = 0.008168,
  Y0 = 0.0, TD = 100.0, VSTART = 0.1, DELP = 1.0,
  &END
4 FEDIMN
  LINK1 1
  LINK2 1 11, 1 2,
  &END
5 COMTITLE
  DIVERGING CHANNEL FLOW, RE = 200, SLOPE = 0.1
  &END
6 DESCRIPT 204 Y DESCRIPTIVE TITLE AT BEGINNING OF OUTPUT.
  DIVERGING CHANNEL FLOW, RE = 200, SLOPE = 0.1
  &END
7 DESCRIPT 332 T IOPAR PARAMETER TITLES FOR OUTPUT.
  REFERENCE M-K-S
  LENGTH C-G-S
  VELOCITY ..FEET... M.....
  DENSITY ..FT/SEC.. ..M/S.....
  TEMPERATURE ..LBM/FT3.. ..KG/M3...
  ENTHALPY ..RANKINE.. ..KJ/KG...
  FROZ. SPEC. HEAT ..BTU/LBM.. ..KJ/KG-K...
  VISCOSITY ..LBM/FT-S.. ..NT-S/M2...
  LOCAL PRESSURE ..PSF..... ..TORR...
  LOCAL SOLUTION ..DXI/LREF.. ..EPSILON..
  &END
8 IONUMB -1
  999
  5*200
  999
  200 4*43
  200 27 200 2*27
  200 10 200 2*10
  200 58 200 58 200
  200 97 200 97 200
  200 30 200 30 200
  200 38 200 2*38
  999
  
```

Table IV
Data Deck for Case II (cont)

06/29/76

39 4*36
2*200 100 200 200
11 12 14 85

| I | MPARA | -1 | 162 | 164 | 163 |
|---|-------|----|------|-----|-----|
| 8 | 5*2 | 2 | 2 | 2 | 163 |
| | | 2 | 2 | 2 | 164 |
| | | 2 | 2 | 2 | 170 |
| | | 2 | 2 | 2 | 165 |
| 9 | | 2 | -175 | 2 | 2 |
| | | 2 | 2 | 2 | 176 |
| | | 2 | 2 | 2 | 177 |
| | | 2 | 2 | 2 | 178 |
| | | 2 | 2 | 169 | 168 |
| | | 2 | 2 | 2 | 167 |
| | | 2 | 2 | 2 | 2 |
| | 6*2 | | | | |

TITLES FOR OUTPUT DEPENDENT VARIABLES.
UIPRIME*ALC/UIJNF MU/XHUIJNF

| I | DESCRIPT | 203 | T | U2/UJNF |
|----|-------------------------------------|------------|------|----------|
| 10 | UI/UJNF | | | |
| | DOONE | | | |
| 11 | IOSAVE | -1 | | |
| | | 1248 | 2248 | 1249 292 |
| 12 | IMULT | -1 | | |
| | COMCC | | | |
| 13 | DESCRIPT | | | |
| 14 | DOONE | | | |
| | VX3ST | | | |
| | 0.0 | | 10.0 | |
| 15 | VPV SX | | | |
| | 25.3416 | | | 25.3416 |
| 16 | IPINT | -1 | | |
| | 1 2 | | | |
| | KBNG | 1 | | |
| 17 | BOTTOM | | | DOONE |
| | KBNG | 2 | | |
| | TOP | | | BOTTOM |
| | VTEMP | | | -58 |
| | 22*533. | | | |
| 18 | T INITIAL TOTAL TEMPERATURE PROFILE | | | |
| | VYV | | | -27 |
| | 2*0.0 | 20*105.0 | | |
| | VYVEND | 1 | | |
| 19 | VSUTHLD | | | |
| | 4*0.0 | 0.00408415 | | |

Table IV
Data Deck for Case II (cont)

06/29/76

| | | | | | | | |
|----|---|------------|--|-------|---|-------------|-----|
| 19 | T | VU2POS | 0.0 | 100.0 | T | | |
| 21 | | VU2VAL | 0.0 | 0.0 | | | |
| | | | -1.0 | -11.0 | T | | |
| | | LINKCALL | -1 | | | | |
| 23 | | LINK3 | 5 1, 2 4, 5 6, 2 3, 1 5, 1 6, 0 1 | | | | |
| | | ICOND | | | | | |
| | | LINK1 | | | | | |
| | | LINK2 | | | | | |
| 24 | | DESCRIPT 3 | | | | | |
| | | | REFERENCE LENGTH, LREF | | | 43 FT. | |
| | | | REFERENCE VISCOSITY, LAMINAR VALUE | | | 38 LBM/FT-S | |
| | | | EVALUATED AT REF. TEMPERATURE. | | | 27 FT/S | |
| | | | FREESTREAM VELOCITY AT X0(=UREF) | | | 58 DEG R | |
| 25 | | | STAGNATION TEMPERATURE (CONSTANT, =TREF) | | | 10 LBM/FT3 | |
| | | | FREESTREAM DENSITY AT X0(=RHOREF) | | | 154 | |
| | | | FREESTREAM MACH NUMBER AT X0 | | | 9 | PSF |
| | | | STATIC PRESSURE AT X0 | | | -16 | |
| | | | NUMBER OF NODES | | | -14 | |
| | | | NUMBER OF FINITE ELEMENTS | | | | |
| 26 | | DONE | | | | | |
| | | CONOC | | | | | |
| 27 | | EXIT | | | | | |
| | | | | | | | END |

DIMEN
GEOMFL

Table V
Data Deck for Case III

06/29/70

1 CASECI
FEBL
3DPNS
FENAME

GNAME01
NPVSK=2, NSCH=1, NSCV=1,
NECKNN=1, IGAS=C, IFR=1, KOUPE=1,
GENC

GNAME02
XZSCALE = 0.0092592, XZSCALE = 0.1, VSTART = 0.1,
TC = C.O, TD = 2.E3, DELP = 10.0,
UINF = 203.6, TOFINF = 515.C, REFL = 1.0,
AO = 0.00464, A1 = 0.07869, A2 = 0.08333, A3 = 0.08333,
UE = C.O, LC = C.C, LP = 203.6,
PMCDT = 0.0, CMCDT = C.C, PMCDT = 0.07250, SMOCT = 0.1715,
GENC

FECIPN
LINK1 1
1 1 1,
T
Y

SETUP

4 1 1 1, 5 1 1, 6 2 1, 10 2 1, 11 5 1, 15 5 1, 16 10 1, 20 10 1,
T
Y

1 21, 1 2,
T 21 ROWS AND 2 COLUMNS

CCMTITLE
EJECTOR CLTPLT CHECK CASE

5 CCNE
DESCRPT 204 T DESCRIPTIVE TITLE AT BEGINING OF COUTPUT.

6 CCNE
DESCRPT 322 T TOPAR PARAMETER TITLES FOR COUTPUT.

REFERENCE ENGLISH-FT ENGLISH-IN M-K-S
LENGTH ...FEET... ..IN..... C-6-S
VELOCITY ...FT/SEC... ..M/S..... ...CH....
DENSITY ...LBM/FT3... ..KG/M3.... ...CP/S....
TEMPERATURE ...RANKINE... ..KELVIN... ..C/CC....
ENTHALPY ...BTU/LBM... ..KJ/KG....
FRCT7 SPEC.FEAT ...BTU/LBM-R ..KJ/KG-K...
LOCAL PRESSURE ...LBM/FT-S... ..NT-S/M2...
LOCAL SCLUTION ...PSF..... ..NT/M2....
X1/LREF ...DX1/LPEF... ..DX1M/LREF
THE FOLLOWING PARAMETERS ARE NON-DIMENSIONAL BY DEFINITION.
INPLT AREA RATIO DIFFERENTIAL AREA RATIO VELOCITY RATIO
MASS FLOW RATIO THPLST AUGMENTATION SKWENESS
PROPULSION EFFICIENCY ENERGY TRANSFER EFFICIENCY
REFERENCE AREA REF. MASS FLOW REF. MOMENTUM
THE FOLLOWING PAR. ARE NON-D BY REFERENCE AREA, MASS FLOW OR MOMENTUM.
IDEAL ISENTROPIC NGZZLE THRUST MASS FLOW
MOMENTUM CRAG X - COMPONENT Y - COMPONENT Z - COMPONENT
AVERAGE VELOCITY X
GROSS THRUST X - COMPONENT Y - COMPONENT Z - COMPONENT

7 CCNE

Table V
Data Deck for Case III (cont)

| | | | | |
|-----------|-----------|------------------------------------|--|------|
| 14 | DCNE | EJECTOR OUTPUT CHECK CASE | | |
| | VR3ST | | | |
| 15 | T | 0.0 50.0 | | |
| | VWVSX | | | |
| | T | 2115.0 2115.0 | | |
| 16 | IPINT | -1 | | |
| | I | 1 2 T | | |
| 17 | KENC | 2 | | |
| | BCYTCM | TOP | | DCNE |
| | VTEMP | -58 | | |
| 18 | VVY | 424562.0 T | | |
| | VVYENC | 1 | | |
| | VVEPSILON | 1.2*203.6 30*2E-3 T | | |
| 20 | LINKCALL | -1 | | |
| | LINK2 | 4 | | |
| | LINK3 | 3 | | |
| 23 | LINK4 | 2 4, 5 6, 2 3, 1 5, 1 6, 5 11, 0 T | | |
| | LINK5 | 4 | | |
| | LINK6 | 3 | | |
| 24 | LINK7 | 3 | | |
| | LINK8 | 3 | | |
| | LINK9 | 3 | | |
| 25 | LINK10 | 3 | | |
| | LINK11 | 3 | | |
| | LINK12 | 3 | | |
| | LINK13 | 3 | | |
| | LINK14 | 3 | | |
| | LINK15 | 3 | | |
| | LINK16 | 3 | | |
| | LINK17 | 3 | | |
| | LINK18 | 3 | | |
| | LINK19 | 3 | | |
| | LINK20 | 3 | | |
| | LINK21 | 3 | | |
| | LINK22 | 3 | | |
| | LINK23 | 3 | | |
| | LINK24 | 3 | | |
| | LINK25 | 3 | | |
| | LINK26 | 3 | | |
| | LINK27 | 3 | | |
| | LINK28 | 3 | | |
| | LINK29 | 3 | | |
| | LINK30 | 3 | | |
| | LINK31 | 3 | | |
| | LINK32 | 3 | | |
| | LINK33 | 3 | | |
| | LINK34 | 3 | | |
| | LINK35 | 3 | | |
| | LINK36 | 3 | | |
| | LINK37 | 3 | | |
| | LINK38 | 3 | | |
| | LINK39 | 3 | | |
| | LINK40 | 3 | | |
| | LINK41 | 3 | | |
| | LINK42 | 3 | | |
| | LINK43 | 3 | | |
| | LINK44 | 3 | | |
| | LINK45 | 3 | | |
| | LINK46 | 3 | | |
| | LINK47 | 3 | | |
| | LINK48 | 3 | | |
| | LINK49 | 3 | | |
| | LINK50 | 3 | | |
| | LINK51 | 3 | | |
| | LINK52 | 3 | | |
| | LINK53 | 3 | | |
| | LINK54 | 3 | | |
| | LINK55 | 3 | | |
| | LINK56 | 3 | | |
| | LINK57 | 3 | | |
| | LINK58 | 3 | | |
| | LINK59 | 3 | | |
| | LINK60 | 3 | | |
| | LINK61 | 3 | | |
| | LINK62 | 3 | | |
| | LINK63 | 3 | | |
| | LINK64 | 3 | | |
| | LINK65 | 3 | | |
| | LINK66 | 3 | | |
| | LINK67 | 3 | | |
| | LINK68 | 3 | | |
| | LINK69 | 3 | | |
| | LINK70 | 3 | | |
| | LINK71 | 3 | | |
| | LINK72 | 3 | | |
| | LINK73 | 3 | | |
| | LINK74 | 3 | | |
| | LINK75 | 3 | | |
| | LINK76 | 3 | | |
| | LINK77 | 3 | | |
| | LINK78 | 3 | | |
| | LINK79 | 3 | | |
| | LINK80 | 3 | | |
| | LINK81 | 3 | | |
| | LINK82 | 3 | | |
| | LINK83 | 3 | | |
| | LINK84 | 3 | | |
| | LINK85 | 3 | | |
| | LINK86 | 3 | | |
| | LINK87 | 3 | | |
| | LINK88 | 3 | | |
| | LINK89 | 3 | | |
| | LINK90 | 3 | | |
| | LINK91 | 3 | | |
| | LINK92 | 3 | | |
| | LINK93 | 3 | | |
| | LINK94 | 3 | | |
| | LINK95 | 3 | | |
| | LINK96 | 3 | | |
| | LINK97 | 3 | | |
| | LINK98 | 3 | | |
| | LINK99 | 3 | | |
| | LINK100 | 3 | | |
| | LINK101 | 3 | | |
| | LINK102 | 3 | | |
| | LINK103 | 3 | | |
| | LINK104 | 3 | | |
| | LINK105 | 3 | | |
| | LINK106 | 3 | | |
| | LINK107 | 3 | | |
| | LINK108 | 3 | | |
| | LINK109 | 3 | | |
| | LINK110 | 3 | | |
| | LINK111 | 3 | | |
| | LINK112 | 3 | | |
| | LINK113 | 3 | | |
| | LINK114 | 3 | | |
| | LINK115 | 3 | | |
| | LINK116 | 3 | | |
| | LINK117 | 3 | | |
| | LINK118 | 3 | | |
| | LINK119 | 3 | | |
| | LINK120 | 3 | | |
| | LINK121 | 3 | | |
| | LINK122 | 3 | | |
| | LINK123 | 3 | | |
| | LINK124 | 3 | | |
| | LINK125 | 3 | | |
| | LINK126 | 3 | | |
| | LINK127 | 3 | | |
| | LINK128 | 3 | | |
| | LINK129 | 3 | | |
| | LINK130 | 3 | | |
| | LINK131 | 3 | | |
| | LINK132 | 3 | | |
| | LINK133 | 3 | | |
| | LINK134 | 3 | | |
| | LINK135 | 3 | | |
| | LINK136 | 3 | | |
| | LINK137 | 3 | | |
| | LINK138 | 3 | | |
| | LINK139 | 3 | | |
| | LINK140 | 3 | | |
| | LINK141 | 3 | | |
| | LINK142 | 3 | | |
| | LINK143 | 3 | | |
| | LINK144 | 3 | | |
| | LINK145 | 3 | | |
| | LINK146 | 3 | | |
| | LINK147 | 3 | | |
| | LINK148 | 3 | | |
| | LINK149 | 3 | | |
| | LINK150 | 3 | | |
| | LINK151 | 3 | | |
| | LINK152 | 3 | | |
| | LINK153 | 3 | | |
| | LINK154 | 3 | | |
| | LINK155 | 3 | | |
| | LINK156 | 3 | | |
| | LINK157 | 3 | | |
| | LINK158 | 3 | | |
| | LINK159 | 3 | | |
| | LINK160 | 3 | | |
| | LINK161 | 3 | | |
| | LINK162 | 3 | | |
| | LINK163 | 3 | | |
| | LINK164 | 3 | | |
| | LINK165 | 3 | | |
| | LINK166 | 3 | | |
| | LINK167 | 3 | | |
| | LINK168 | 3 | | |
| | LINK169 | 3 | | |
| | LINK170 | 3 | | |
| | LINK171 | 3 | | |
| | LINK172 | 3 | | |
| | LINK173 | 3 | | |
| | LINK174 | 3 | | |
| | LINK175 | 3 | | |
| | LINK176 | 3 | | |
| | LINK177 | 3 | | |
| | LINK178 | 3 | | |
| | LINK179 | 3 | | |
| | LINK180 | 3 | | |
| | LINK181 | 3 | | |
| | LINK182 | 3 | | |
| | LINK183 | 3 | | |
| | LINK184 | 3 | | |
| | LINK185 | 3 | | |
| | LINK186 | 3 | | |
| | LINK187 | 3 | | |
| | LINK188 | 3 | | |
| | LINK189 | 3 | | |
| | LINK190 | 3 | | |
| | LINK191 | 3 | | |
| | LINK192 | 3 | | |
| | LINK193 | 3 | | |
| | LINK194 | 3 | | |
| | LINK195 | 3 | | |
| | LINK196 | 3 | | |
| | LINK197 | 3 | | |
| | LINK198 | 3 | | |
| | LINK199 | 3 | | |
| | LINK200 | 3 | | |
| | LINK201 | 3 | | |
| | LINK202 | 3 | | |
| | LINK203 | 3 | | |
| | LINK204 | 3 | | |
| | LINK205 | 3 | | |
| | LINK206 | 3 | | |
| | LINK207 | 3 | | |
| | LINK208 | 3 | | |
| | LINK209 | 3 | | |
| | LINK210 | 3 | | |
| | LINK211 | 3 | | |
| | LINK212 | 3 | | |
| | LINK213 | 3 | | |
| | LINK214 | 3 | | |
| | LINK215 | 3 | | |
| | LINK216 | 3 | | |
| | LINK217 | 3 | | |
| | LINK218 | 3 | | |
| | LINK219 | 3 | | |
| | LINK220 | 3 | | |
| | LINK221 | 3 | | |
| | LINK222 | 3 | | |
| | LINK223 | 3 | | |
| | LINK224 | 3 | | |
| | LINK225 | 3 | | |
| | LINK226 | 3 | | |
| | LINK227 | 3 | | |
| | LINK228 | 3 | | |
| | LINK229 | 3 | | |
| | LINK230 | 3 | | |
| | LINK231 | 3 | | |
| | LINK232 | 3 | | |
| | LINK233 | 3 | | |
| | LINK234 | 3 | | |
| | LINK235 | 3 | | |
| | LINK236 | 3 | | |
| | LINK237 | 3 | | |
| | LINK238 | 3 | | |
| | LINK239 | 3 | | |
| | LINK240 | 3 | | |
| | LINK241 | 3 | | |
| | LINK242 | 3 | | |
| | LINK243 | 3 | | |
| | LINK244 | 3 | | |
| | LINK245 | 3 | | |
| | LINK246 | 3 | | |
| | LINK247 | 3 | | |
| | LINK248 | 3 | | |
| | LINK249 | 3 | | |
| | LINK250 | 3 | | |
| | LINK251 | 3 | | |
| | LINK252 | 3 | | |
| | LINK253 | 3 | | |
| | LINK254 | 3 | | |
| | LINK255 | 3 | | |
| | LINK256 | 3 | | |
| | LINK257 | 3 | | |
| | LINK258 | 3 | | |
| | LINK259 | 3 | | |
| | LINK260 | 3 | | |
| | LINK261 | 3 | | |
| | LINK262 | 3 | | |
| | LINK263 | 3 | | |
| | LINK264 | 3 | | |
| | LINK265 | 3 | | |
| | LINK266 | 3 | | |
| | LINK267 | 3 | | |
| | LINK268 | 3 | | |
| | LINK269 | 3 | | |
| | LINK270 | 3 | | |
| | LINK271 | 3 | | |
| | LINK272 | 3 | | |
| | LINK273 | 3 | | |
| | LINK274 | 3 | | |
| | LINK275 | 3 | | |
| | LINK276 | 3 | | |
| | LINK277 | 3 | | |
| | LINK278 | 3 | | |
| | LINK279 | 3 | | |
| | LINK280 | 3 | | |
| | LINK281 | 3 | | |
| | LINK282 | 3 | | |
| | LINK283 | 3 | | |
| | LINK284 | 3 | | |
| | LINK285 | 3 | | |
| | LINK286 | 3 | | |
| | LINK287 | 3 | | |
| | LINK288 | 3 | | |
| | LINK289 | 3 | | |
| | LINK290 | 3 | | |
| | LINK291 | 3 | | |
| | LINK292 | 3 | | |
| | LINK293 | 3 | | |
| | LINK294 | 3 | | |
| | LINK295 | 3 | | |
| | LINK296 | 3 | | |
| | LINK297 | 3 | | |
| | LINK298 | 3 | | |
| | LINK299 | 3 | | |
| | LINK300 | 3 | | |
| | LINK301 | 3 | | </ |

Table VI
Data Deck for Case IV (cont)

03/02/77

.5543
0.6
0.0
.1913
.3536
.4619
0.5
1.0
.1531
.2828
.3496
0.4
0.0
.0557
.1768
.2910
0.25

1.0E15

COMTITL

5 DOME
DESCRPT 204 T ENGLISH-MIXER

6 DOME
DESCRPT 332 T ENGLISH-MIXER

7 DOME
DESCRPT 332 T ENGLISH-MIXER
REFERENCE M-K-S
LENGTH
VELOCITY
DENSITY
TEMPERATURE
ENTHALPY
FRQZ. SPEC. HEAT
VISCOSITY
PRES. GRADIENT
LOCAL PRESSURE
X1/LREF
PCISE
TCRR

DCNE
IONUMB -1

999
5*200
999
200 4*43
200 27 200 2*27
200 10 200 2*10
200 58 200 58 200
200 97 200 57 200
200 30 200 30 200
200 38 200 2*38
999
39 4*36

8

Table VI
Data Deck for Case IV (cont)

| 8 | HT | HTOT/HREF | U1/UREF | U2/UREF | U3/UREF | U1 PRIME | STAT./T/OFINF |
|----|-----------|-----------|---------|-----------|---------|----------|---------------|
| | 200 | 100 | 3*200 | | | | |
| | 11 | 12 | 14 | 85 | | | |
| | MPARA | -1 | | | | | |
| | 5*2 | | | | | | |
| | 2 | 162 | 164 | 163 | | | |
| | 2 | 2 | 164 | 163 | | | |
| | 2 | 2 | 170 | 174 | | | |
| | 2 | 2 | 165 | 2 | | | |
| | 2 | 2 | 2 | 2 | | | |
| | 2 | -175 | 2 | 2 | | | |
| | 2 | 2 | 2 | 176 | | | |
| | 2 | 2 | 2 | 177 | 178 | | |
| | 2 | 2 | 169 | 168 | 167 | | |
| | 2 | 2 | 2 | 2 | 2 | | |
| | 2 | 2 | 2 | 2 | 2 | | |
| | 2 | 2 | 2 | 2 | 2 | | |
| | DESCRIPT | 203 | T | | | | |
| 10 | U1/UREF | | | | | | |
| | HTOT/HREF | | | | | | |
| | DCNE | | | | | | |
| | IOSAVE | -1 | | | | | |
| | 1248 | 2248 | 3248 | 1249 | 285 | | |
| | 424E | 284 | | | | | |
| 11 | | | | | | | |
| | DCNE | | | | | | |
| | VX3ST | | | | | | |
| 12 | TOMULT | -1 | | | | | |
| | 7*2 | T | | | | | |
| 13 | COMOC | | | | | | |
| | DESCRIPT | | | | | | |
| 14 | DCNE | | | | | | |
| | VX3ST | | | | | | |
| | 0.0 | 5.0 | T | | | | |
| 15 | VPVSK | | | | | | |
| | 863.9 | 863.9 | T | | | | |
| 16 | IPINT | -1 | | | | | |
| | 1 | 4 | 2 | 8 | 9 | 10 | T |
| | KEND | 1 | | | | | |
| | ACD | | | | | | |
| 17 | DCNE | | | | | | |
| | 1 | 2 | 3 | 4 | 5 | 36 | 37 |
| | 38 | 39 | 40 | T | | | |
| | VTMP | | | | | | |
| | 5*600.0 | 1270.0 | 600.0 | 1270.0 | 600.0 | 1270.0 | 600.0 |
| | 600.0 | 1270.0 | 600.0 | 21*1270.0 | T | | |
| | VYY | | | | | | |
| | 5*0.0 | 854.4 | 586.2 | 854.4 | 586.2 | 2*854.4 | 586.2 |
| | 586.2 | 854.4 | 586.2 | 16*854.4 | 5*0.0 | T | |
| | VYYEND | 1 | | | | | |
| | VYY | | | | | | |
| | 55*0.767 | T | | | | | |
| | VYYEND | 8 | | | | | |

Table VII
Output from Case I (cont)

| E I | TKE/EKNINF | E -1 | TKEP*ALC/EKNIKE | E -3 |
|---------|--------------|---------|------------------|----------|
| 0.1C001 | C.C | C.C | 0.00000 | 0.00000 |
| 0.05231 | C.C | C.C | 0.00000 | 0.00000 |
| 0.0E462 | C.C | C.C | -0.00000 | 0.00000 |
| 0.07692 | C.C | C.C | -0.00000 | 0.00000 |
| 0.0E524 | C.C | C.C | -0.00000 | 0.00000 |
| 0.0E154 | C.CCCC | C.CCCC | 0.00000 | 0.00000 |
| 0.05385 | C.CCCC | C.CCCC | 0.00007 | 0.00013 |
| 0.04616 | 0.0C227 | 0.0C227 | 0.00251 | 0.00407 |
| 0.03846 | C.C2181 | C.C2181 | 0.01461 | 0.019C1 |
| 0.02077 | 0.07212 | 0.07212 | 0.01573 | 0.01432 |
| 0.02308 | C.11865 | C.11865 | -0.3955 | -0.5515 |
| 0.01523 | C.05886 | C.05886 | 0.07304 | 0.07C51 |
| 0.01539 | C.11C84 | C.11C84 | -0.9177 | -0.8855 |
| 0.01154 | C.08C14 | C.08C14 | 0.02115 | 0.02458 |
| 0.0C765 | C.0485C | C.0485C | 0.05603 | 0.05658 |
| 0.0C577 | 0.04474 | 0.04474 | -0.3527 | -0.2751 |
| 0.0C385 | C.02856 | C.02856 | 0.05390 | 0.04458 |
| 0.0C231 | C.03002 | 0.03002 | 0.0077C | 0.0C740 |
| 0.0C154 | C.02654 | C.02654 | -0.14415 | -0.12340 |
| 0.0C077 | C.02356 | C.02356 | 0.0 | 0.0 |
| 0.0 | 0.0 | 0.0 | 0.0 | 0.0 |
| E-1 | C.C | C.3E465 | 0.0 | 0.3E465 |
| E I | DISS/EPISINF | E -4 | ESSP*ALC/EPISINF | E -5 |
| 0.1C001 | C.C | C.C | 0.0 | 0.0 |
| 0.05231 | C.C | C.C | 0.0 | 0.0 |
| 0.0E462 | C.C | C.C | 0.0 | 0.0 |
| 0.07692 | C.C | C.C | 0.0 | 0.0 |
| 0.0E524 | C.C | C.C | -0.00000 | 0.00000 |
| 0.0E154 | C.CCCC | C.CCCC | 0.00000 | 0.00000 |
| 0.05385 | C.CCCC | C.CCCC | 0.00000 | 0.00000 |
| 0.04616 | C.CCC85 | C.CCC89 | 0.00028 | 0.0C047 |
| 0.03846 | 0.02656 | 0.02656 | 0.00304 | 0.0C4C6 |
| 0.02077 | 0.15976 | C.15976 | 0.00408 | 0.0C327 |
| 0.02308 | C.33727 | C.33727 | -0.01616 | -0.02142 |
| 0.01523 | C.25637 | 0.25637 | 0.01804 | 0.01700 |
| 0.01539 | C.30435 | C.20435 | -0.02293 | -0.03165 |
| 0.01154 | 0.18711 | C.18711 | 0.01055 | 0.01070 |
| 0.0C765 | C.12917 | C.12917 | 0.00997 | 0.01038 |
| 0.0C577 | C.15C73 | C.15C73 | -0.02206 | -0.02019 |
| 0.0C385 | C.11531 | C.11531 | 0.01802 | 0.01121 |
| 0.0C231 | 0.2C706 | 0.2C706 | 0.02161 | 0.01450 |
| 0.0C154 | C.4172C | 0.41720 | -0.21383 | -0.24676 |
| 0.0C077 | C.43186 | C.43186 | 0.0 | 0.0 |
| 0.0 | C.C | C.C | 0.0 | 0.0 |
| E-1 | 0.0 | 0.38465 | 0.0 | 0.3E465 |

Table VII
Output from Case I (cont)

| E I | U2/U1NF | E 0 | RHO/RHOINF | E 0 |
|----------|--------------|---------|----------------|---------|
| 0.1C001 | 0.0 | G.C | 0.99626 | 0.99626 |
| 0.05231 | 0.0 | C.C | 0.99626 | 0.99626 |
| 0.0E462 | 0.0 | C.C | 0.99626 | 0.99626 |
| 0.07693 | 0.0 | C.C | 0.99626 | 0.99626 |
| 0.0E924 | 0.0 | C.C | 0.99626 | 0.99626 |
| 0.06154 | 0.0 | C.C | 0.99626 | 0.99626 |
| 0.05385 | 0.0 | C.C | 0.99625 | 0.99625 |
| 0.04616 | 0.0 | C.C | 0.99618 | 0.99618 |
| 0.0E846 | 0.0 | C.C | 0.99599 | 0.99599 |
| 0.02077 | 0.0 | C.C | 0.99573 | 0.99573 |
| 0.0E2308 | 0.0 | C.C | 0.99547 | 0.99547 |
| 0.01923 | 0.0 | C.C | 0.99535 | 0.99535 |
| 0.01539 | 0.0 | C.C | 0.99526 | 0.99526 |
| 0.01154 | 0.0 | C.C | 0.99516 | 0.99516 |
| 0.0C769 | 0.0 | C.C | 0.99508 | 0.99508 |
| 0.0C577 | 0.0 | C.C | 0.99504 | 0.99504 |
| 0.0C385 | 0.0 | C.C | 0.99500 | 0.99500 |
| 0.0C231 | 0.0 | C.C | 0.99495 | 0.99495 |
| 0.0C154 | 0.0 | C.C | 0.99492 | 0.99492 |
| 0.0C077 | 0.0 | C.C | 0.99486 | 0.99486 |
| 0.0 | 0.0 | C.C | 0.99457 | 0.99457 |
| E-1 | 0.0 | 0.38465 | 0.0 | 0.38465 |
| E I | EFF.MU/MUREF | E 3 | STAT.I/TOFINF. | E 1 |
| 0.1C001 | 0.0 | G.C | 0.05983 | 0.05983 |
| 0.05231 | 0.0 | C.C | 0.05983 | 0.05983 |
| 0.0E462 | 0.0 | C.C | 0.05983 | 0.05983 |
| 0.07693 | 0.0 | C.C | 0.05983 | 0.05983 |
| 0.0E924 | 0.0 | C.C | 0.05983 | 0.05983 |
| 0.06154 | 0.0 | C.C | 0.05983 | 0.05983 |
| 0.05385 | 0.0 | C.C | 0.05983 | 0.05983 |
| 0.04616 | 0.0 | C.C | 0.05984 | 0.05984 |
| 0.0E846 | 0.0 | C.C | 0.05986 | 0.05986 |
| 0.02077 | 0.0 | C.C | 0.05988 | 0.05988 |
| 0.0E2308 | 0.0 | C.C | 0.05991 | 0.05991 |
| 0.01923 | 0.0 | C.C | 0.05992 | 0.05992 |
| 0.01539 | 0.0 | C.C | 0.05993 | 0.05993 |
| 0.01154 | 0.0 | C.C | 0.05994 | 0.05994 |
| 0.0C769 | 0.0 | C.C | 0.05995 | 0.05995 |
| 0.0C577 | 0.0 | C.C | 0.05995 | 0.05995 |
| 0.0C385 | 0.0 | C.C | 0.05996 | 0.05996 |
| 0.0C231 | 0.0 | C.C | 0.05996 | 0.05996 |
| 0.0154 | 0.0 | C.C | 0.05996 | 0.05996 |
| 0.0C077 | 0.0 | C.C | 0.05997 | 0.05997 |
| 0.0 | 0.0 | C.C | 0.10000 | 0.10000 |
| E-1 | 0.0 | 0.38465 | 0.0 | 0.38465 |

Table VII
Output from Case I (cont)

| | | | | |
|-----------------------------------|--------------|---|--------------|--|
| SKIN FRICTION DISTRIBUTION(CF/Z) | | | | |
| 1 | C.70565E-03 | 2 | C.70565E-03 | |
| DISPLACEMENT THICKNESS./REFL | | | | |
| 1 | C.12788E 00 | 2 | C.12788E 00 | |
| MOMENTUM THICKNESS./REFL | | | | |
| 1 | C.75087E-01 | 2 | C.75087E-01 | |
| ENERGY DISSIPATION THICKNESS/REFL | | | | |
| 1 | C.1315CE CC | 2 | C.1315CE 00 | |
| ENTHALPY THICKNESS./REFL | | | | |
| 1 | -C.13037E CC | 2 | -C.13037E 00 | |
| VELOCITY THICKNESS./REFL | | | | |
| 1 | C.12766E CC | 2 | C.12766E 00 | |

23

Table VIII
Output from Case II (cont)

| E 0 | U2/UINF | E 0 | MU/XMUINF | E 1 |
|---------|---------|---------|-----------|---------|
| 0.0 | 0.0 | 0.0 | 0.10000 | 0.10000 |
| -.10000 | 0.0 | 0.0 | 0.10000 | 0.10000 |
| -.20000 | 0.0 | 0.0 | 0.10000 | 0.10000 |
| -.30000 | 0.0 | 0.0 | 0.10000 | 0.10000 |
| -.40000 | 0.0 | 0.0 | 0.10000 | 0.10000 |
| -.50000 | 0.0 | 0.0 | 0.10000 | 0.10000 |
| -.60000 | 0.0 | 0.0 | 0.10000 | 0.10000 |
| -.70000 | 0.0 | 0.0 | 0.10000 | 0.10000 |
| -.80000 | 0.0 | 0.0 | 0.10000 | 0.10000 |
| -.90000 | 0.0 | 0.0 | 0.10000 | 0.10000 |
| -.9999* | 0.0 | 0.0 | 0.10000 | 0.10000 |
| E 0 | 0.0 | 0.10000 | 0.0 | 0.10000 |

19

SKIN FRICTION DISTRIBUTION(CF/2)

1 0.47623E-01 2 0.47623E-01

23

Table IX
Output from Case III (cont)

| 10 | | E C | | U1/LINF | | E I | | U1PRIMEALC/UINF E C | |
|---------|-----|---------|---------|---------|---------|----------------|---------|---------------------|---------|
| 0.62334 | C.C | C.C135C | C.C135C | C.C135C | C.C135C | | | 0.00000 | 0.00000 |
| 0.74074 | C.C | C.C135C | C.C135C | C.C135C | C.C135C | | | 0.00000 | 0.00000 |
| 0.64815 | C.C | C.C135C | C.C135C | C.C135C | C.C135C | | | 0.00000 | 0.00000 |
| 0.55556 | C.C | C.C135C | C.C135C | C.C135C | C.C135C | | | 0.00000 | 0.00000 |
| 0.46296 | C.C | C.C135C | C.C135C | C.C135C | C.C135C | | | 0.00000 | 0.00000 |
| 0.37037 | C.C | C.C135C | C.C135C | C.C135C | C.C135C | | | 0.00000 | 0.00000 |
| 0.27408 | C.C | C.C135C | C.C135C | C.C135C | C.C135C | | | 0.00000 | 0.00000 |
| 0.27778 | C.C | C.C135C | C.C135C | C.C135C | C.C135C | | | 0.00000 | 0.00000 |
| 0.23148 | C.C | C.C135C | C.C135C | C.C135C | C.C135C | | | 0.00000 | 0.00000 |
| 0.18515 | C.C | C.C135C | C.C135C | C.C135C | C.C135C | | | 0.0 | 0.0 |
| 0.13885 | C.C | C.C135C | C.C135C | C.C135C | C.C135C | | | 0.00000 | 0.00000 |
| 0.12037 | C.C | C.C135C | C.C135C | C.C135C | C.C135C | | | 0.00000 | 0.00000 |
| 0.10185 | C.C | C.C135C | C.C135C | C.C135C | C.C135C | | | 0.00000 | 0.00000 |
| 0.08333 | C.C | C.C135C | C.C135C | C.C135C | C.C135C | | | 0.00000 | 0.00000 |
| 0.06482 | C.C | C.C135C | C.C135C | C.C135C | C.C135C | | | 0.25644 | 0.15256 |
| 0.04630 | C.C | C.C135C | C.C135C | C.C135C | C.C135C | | | 0.08744 | 0.05084 |
| 0.03704 | C.C | C.C135C | C.C135C | C.C135C | C.C135C | | | 0.00000 | 0.00000 |
| 0.02778 | C.C | C.C135C | C.C135C | C.C135C | C.C135C | | | 0.00000 | 0.00000 |
| 0.01852 | C.C | C.C135C | C.C135C | C.C135C | C.C135C | | | 0.00000 | 0.00000 |
| 0.00926 | C.C | C.C135C | C.C135C | C.C135C | C.C135C | | | 0.00000 | 0.00000 |
| 0.0 | C.C | C.C135C | C.C135C | C.C135C | C.C135C | | | 0.00000 | 0.00000 |
| E C | C.C | C.C | C.C135C | C.C135C | C.C135C | | | 0.0 | 0.10000 |
| 11 | | | | | | | | | |
| 12 | | | | | | | | | |
| 18 | | | | | | | | | |
| 4 | | | | | | | | | |
| 20 | | | | | | | | | |
| E C | | U2/LINF | | E C | | EFF.MU/XMULINF | | E 4 | |
| 0.62334 | C.C | C.C | C.C | C.C | C.C | 0.30011 | 0.30011 | 0.30011 | 0.30011 |
| 0.74074 | C.C | C.C | C.C | C.C | C.C | 0.30011 | 0.30011 | 0.30011 | 0.30011 |
| 0.64815 | C.C | C.C | C.C | C.C | C.C | 0.30011 | 0.30011 | 0.30011 | 0.30011 |
| 0.55556 | C.C | C.C | C.C | C.C | C.C | 0.30011 | 0.30011 | 0.30011 | 0.30011 |
| 0.46296 | C.C | C.C | C.C | C.C | C.C | 0.30011 | 0.30011 | 0.30011 | 0.30011 |
| 0.37037 | C.C | C.C | C.C | C.C | C.C | 0.30011 | 0.30011 | 0.30011 | 0.30011 |
| 0.27408 | C.C | C.C | C.C | C.C | C.C | 0.30011 | 0.30011 | 0.30011 | 0.30011 |
| 0.27778 | C.C | C.C | C.C | C.C | C.C | 0.30011 | 0.30011 | 0.30011 | 0.30011 |
| 0.23148 | C.C | C.C | C.C | C.C | C.C | 0.30011 | 0.30011 | 0.30011 | 0.30011 |
| 0.18515 | C.C | C.C | C.C | C.C | C.C | 0.30011 | 0.30011 | 0.30011 | 0.30011 |
| 0.13885 | C.C | C.C | C.C | C.C | C.C | 0.30011 | 0.30011 | 0.30011 | 0.30011 |
| 0.12037 | C.C | C.C | C.C | C.C | C.C | 0.30011 | 0.30011 | 0.30011 | 0.30011 |
| 0.10185 | C.C | C.C | C.C | C.C | C.C | 0.30011 | 0.30011 | 0.30011 | 0.30011 |
| 0.08333 | C.C | C.C | C.C | C.C | C.C | 0.30011 | 0.30011 | 0.30011 | 0.30011 |
| 0.06482 | C.C | C.C | C.C | C.C | C.C | 0.30011 | 0.30011 | 0.30011 | 0.30011 |
| 0.04630 | C.C | C.C | C.C | C.C | C.C | 0.30011 | 0.30011 | 0.30011 | 0.30011 |
| 0.03704 | C.C | C.C | C.C | C.C | C.C | 0.30011 | 0.30011 | 0.30011 | 0.30011 |
| 0.02778 | C.C | C.C | C.C | C.C | C.C | 0.30011 | 0.30011 | 0.30011 | 0.30011 |
| 0.01852 | C.C | C.C | C.C | C.C | C.C | 0.30011 | 0.30011 | 0.30011 | 0.30011 |
| 0.00926 | C.C | C.C | C.C | C.C | C.C | 0.30011 | 0.30011 | 0.30011 | 0.30011 |
| 0.0 | C.C | C.C | C.C | C.C | C.C | 0.30011 | 0.30011 | 0.30011 | 0.30011 |
| E C | C.C | C.C | C.C135C | C.C135C | C.C135C | 0.0 | 0.0 | 0.0 | 0.10000 |

Table X
Output from Case IV (cont)

| | | | | | |
|---------|---------|---------|---------|---------|---------|
| 0.08506 | | | | | |
| 0.08019 | | | | | |
| 0.07672 | | 0.0 | | | |
| 0.07410 | | | | | |
| 0.07089 | | | | | |
| 0.06905 | 0.10000 | | | | |
| 0.06137 | | | | | |
| 0.05670 | | | | | |
| 0.05371 | | | | | |
| 0.05012 | | | | | |
| 0.04631 | | | | | |
| 0.04603 | | | | | |
| 0.03835 | | | | | |
| 0.03544 | | | | | |
| 0.03069 | | | | | |
| 0.01919 | | | | | |
| 0.0 | 0.14575 | 0.14575 | 0.0 | | |
| E 2 | 0.16638 | 0.16670 | 0.18043 | 0.18522 | 0.20048 |
| 0.20048 | | | | | |
| 0.18522 | | | | | |
| 0.18043 | | | | | |
| 0.16670 | | | | | |
| 0.16038 | | | | | |
| 0.14817 | | | | | |
| 0.14176 | | | | | 0.0 |
| 0.14034 | | | | | |
| 0.12965 | | | | | |
| 0.12759 | | | | | 0.0 |
| 0.12029 | | | | | |
| 0.11341 | | | | | 0.0 |
| 0.11113 | | | | | |
| 0.10024 | | | | | |
| 0.09924 | | | | | 0.0 |
| 0.09260 | | | | | |
| 0.08506 | | | | | 0.0 |
| 0.08019 | | | | | |
| 0.07672 | | | | | |
| 0.07410 | | | | | |
| 0.07089 | | | | | |
| 0.06905 | | | | | |
| 0.06137 | | | | | 0.0 |
| 0.05670 | | | | | |
| 0.05371 | | | | | 0.0 |
| 0.05012 | | | | | |
| 0.04631 | | | | | |
| 0.04603 | | | | | |
| 0.03835 | | | | | 0.0 |
| 0.03544 | | | | | |
| 0.03069 | | | | | |
| 0.01919 | | | | | |
| 0.0 | 0.0 | 0.0 | 0.0 | 0.0 | 0.0 |

Table X
Output from Case IV (cont)

| | | | | | | | | | | | | | | |
|---------|---------|---------|---------|---------|---------|---------|---------|---------|---------|---------|---------|---------|---------|---------|
| E 2 | 0.07672 | 0.08019 | 0.08506 | 0.09260 | 0.09924 | 0.10024 | 0.11113 | 0.11341 | 0.12029 | 0.12759 | 0.12965 | 0.14034 | 0.14176 | 0.14817 |
| 0.20048 | | | | | | | | | | | | | | |
| 0.18522 | | | | | | | | | | | | | | |
| 0.18043 | | | | | | | | | | | | | | |
| 0.16670 | | | | | | | | | | | | | | |
| 0.16038 | | | | | | | | | | | | | | |
| 0.14817 | | | | | | | | | | | | | | |
| 0.14176 | | | | | | | | | | | | | | |
| 0.14034 | | | | | | | | | | | | | | |
| 0.12965 | | | | | | | | | | | | | | |
| 0.12759 | | | | | | | | | | | | | | |
| 0.12029 | | | | | | | | | | | | | | |
| 0.11341 | | | | | | | | | | | | | | |
| 0.11113 | | | | | | | | | | | | | | |
| 0.10024 | | | | | | | | | | | | | | |
| 0.09924 | | | | | | | | | | | | | | |
| 0.09260 | | | | | | | | | | | | | | |
| 0.08506 | | | | | | | | | | | | | | |
| 0.08019 | | | | | | | | | | | | | | |
| 0.07672 | | | | | | | | | | | | | | |
| 0.07410 | | | | | | | | | | | | | | |
| 0.07089 | | | | | | | | | | | | | | |
| 0.06905 | | | | | | | | | | | | | | |
| 0.06137 | | | | | | | | | | | | | | |
| 0.05670 | | | | | | | | | | | | | | |

| | | U2/UREF | E | 0 |
|---------|--|---------|---|---|
| E 2 | | | | |
| 0.20048 | | 0.0 | | |
| 0.18522 | | 0.0 | | |
| 0.18043 | | 0.0 | | |
| 0.16670 | | 0.0 | | |
| 0.16038 | | 0.0 | | |
| 0.14817 | | 0.0 | | |
| 0.14176 | | 0.0 | | |
| 0.14034 | | 0.0 | | |
| 0.12965 | | 0.0 | | |
| 0.12759 | | 0.0 | | |
| 0.12029 | | 0.0 | | |
| 0.11341 | | 0.0 | | |
| 0.11113 | | 0.0 | | |
| 0.10024 | | 0.0 | | |
| 0.09924 | | 0.0 | | |
| 0.09260 | | 0.0 | | |
| 0.08506 | | 0.0 | | |
| 0.08019 | | 0.0 | | |
| 0.07672 | | 0.0 | | |
| 0.07410 | | 0.0 | | |
| 0.07089 | | 0.0 | | |
| 0.06905 | | 0.0 | | |
| 0.06137 | | 0.0 | | |

Table X
Output from Case IV (cont)

| | | | | | | | | | | | | | | |
|---------|---------|---------|---------|---------|---------|---------|---------|---------|---------|---------|---------|---------|---------|---------|
| 0.04631 | | | | | | | | | | | | | | |
| 0.04603 | | | | | | | | | | | | | | |
| 0.03835 | | | | | | | | | | | | | | |
| 0.03544 | | | | | | | | | | | | | | |
| 0.03069 | | | | | | | | | | | | | | |
| 0.01919 | | | | | | | | | | | | | | |
| 0.0 | | | | | | | | | | | | | | |
| E 2 | 0.07672 | 0.08019 | 0.08506 | 0.09260 | 0.09924 | 0.10024 | 0.11113 | 0.11341 | 0.12029 | 0.12759 | 0.12965 | 0.14034 | 0.14176 | 0.14817 |
| 0.20048 | | | | | | | | | | | | | | |
| 0.18522 | | | | | | | | | | | | | | |
| 0.18043 | | | | | | | | | | | | | | |
| 0.16670 | | | | | | | | | | | | | | |
| 0.16038 | | | | | | | | | | | | | | |
| 0.14817 | | | | | | | | | | | | | | |
| 0.14176 | | | | | | | | | | | | | | |
| 0.14034 | | | | | | | | | | | | | | |
| 0.12965 | | | | | | | | | | | | | | |
| 0.12759 | | | | | | | | | | | | | | |
| 0.12029 | | | | | | | | | | | | | | |
| 0.11341 | | | | | | | | | | | | | | |
| 0.11113 | | | | | | | | | | | | | | |
| 0.10024 | | | | | | | | | | | | | | |
| 0.09924 | | | | | | | | | | | | | | |
| 0.09260 | | | | | | | | | | | | | | |
| 0.08506 | | | | | | | | | | | | | | |
| 0.08019 | | | | | | | | | | | | | | |
| 0.07672 | | | | | | | | | | | | | | |
| 0.07410 | | | | | | | | | | | | | | |
| 0.07089 | | | | | | | | | | | | | | |
| 0.06905 | | | | | | | | | | | | | | |
| 0.06137 | | | | | | | | | | | | | | |
| 0.05670 | | | | | | | | | | | | | | |
| 0.05371 | | | | | | | | | | | | | | |
| 0.05012 | | | | | | | | | | | | | | |
| 0.04631 | | | | | | | | | | | | | | |
| 0.04603 | | | | | | | | | | | | | | |
| 0.03835 | | | | | | | | | | | | | | |
| 0.03544 | | | | | | | | | | | | | | |
| 0.03069 | | | | | | | | | | | | | | |
| 0.01919 | | | | | | | | | | | | | | |
| 0.0 | | | | | | | | | | | | | | |
| E 2 | 0.16670 | 0.16670 | 0.16670 | 0.16670 | 0.16670 | 0.16670 | 0.16670 | 0.16670 | 0.16670 | 0.16670 | 0.16670 | 0.16670 | 0.16670 | 0.16670 |

Table XII
NAMEO2 Output for Case I

| INITIAL CONDITIONS | | | | | | | | | | | | | | | | | | | |
|--------------------|--------|---|------------|-----|--------|---|------------|-----|--------|---|-------------|-----|---------|---|------------|-----|--------|---|------------|
| I | FACT | = | 0.3333E-02 | 2 | ONE | = | 0.1000E 01 | 3 | ALC | = | 0.3333E-02 | 4 | THK | = | 0.3000E C3 | 5 | AJ | = | 0.7783E 03 |
| 6 | HT | = | 0.1000E-06 | 7 | HSINIT | = | 0.1000E-06 | 8 | RMIASI | = | -0.1000E 01 | 9 | PINF | = | 0.2102E C4 | 10 | RHCINF | = | 0.7025E-01 |
| 11 | XT | = | 0.0 | 12 | HT | = | 0.0 | 13 | DELP | = | 0.1500E C3 | 14 | EPS | = | 0.1000E-01 | 15 | H | = | 0.3000E-04 |
| 16 | HMAX | = | 0.0 | 17 | HMIN | = | 0.0 | 18 | CGTERS | = | 0.0 | 19 | PNTEPS | = | 0.0 | 20 | PTIM | = | 0.0 |
| 21 | RF | = | 0.2375E 04 | 22 | TF | = | 0.2375E 04 | 23 | TIME | = | 0.1175E C4 | 24 | TO | = | 0.1175E 04 | 25 | TRNC | = | 0.0 |
| 26 | TWCPI | = | 0.1122E 03 | 27 | UINF | = | 0.1122E 03 | 28 | RUNIV | = | 0.1545E C4 | 29 | ZT | = | 0.0 | 30 | CPCINF | = | 0.2400E 00 |
| 31 | G | = | 0.5008E 05 | 32 | KTCOIL | = | 0.5008E 05 | 33 | RTCCN2 | = | 0.7000E C0 | 34 | RTCIN2 | = | 0.5334E C2 | 35 | TD | = | 0.1200E 04 |
| 36 | PECCIM | = | 0.1000E 01 | 37 | XLE | = | 0.1000E 01 | 38 | XMUINF | = | 0.1250E-04 | 39 | PEDE | = | 0.7647E C2 | 40 | TRATIC | = | 0.1002E 01 |
| 41 | XSPFT | = | 0.0 | 42 | YSHFT | = | 0.0 | 43 | REFL | = | 0.4333E C0 | 44 | SC2 | = | 0.1414E C1 | 45 | HS | = | 0.0 |
| 46 | UFDE | = | 0.0 | 47 | XSCALE | = | 0.1000E 01 | 48 | REGDE | = | 0.1000E 01 | 49 | RTEST | = | 0.1000E-01 | 50 | SSINIT | = | 0.3000E-04 |
| 51 | VELU | = | 0.1000E 01 | 52 | XSCALE | = | 0.1000E 01 | 53 | YSCALE | = | 0.1000E 01 | 54 | TURB | = | 0.0 | 55 | RTCCN4 | = | 0.025E-02 |
| 56 | STODVS | = | 0.1864E-22 | 57 | XTCOIL | = | 0.1305E-01 | 58 | TCFINF | = | 0.5620E C3 | 59 | FACTMU | = | 0.2627E-01 | 60 | GAMPAF | = | 0.1400E 01 |
| 61 | XMACHO | = | 0.5655E-01 | 62 | CONV | = | 0.2538E 01 | 63 | XSAVE | = | 0.1000E 01 | 64 | YSAVE | = | 0.1000E C1 | 65 | ZTEST | = | 0.1000E-04 |
| 66 | XMF | = | 0.2540E 02 | 67 | PR | = | 0.1000E 01 | 68 | EPAND | = | 0.1000E C0 | 69 | DJSS | = | 0.0 | 70 | CCARHC | = | 0.0 |
| 71 | STLDVP | = | 0.1150E-04 | 72 | STLDTR | = | 0.4920E 03 | 73 | STLDGR | = | 0.2040E-03 | 74 | STLDX | = | 0.1500E 01 | 75 | STLCCN | = | 0.0 |
| 76 | YTT | = | 0.0 | 77 | CONI | = | 0.5287E 00 | 78 | CCN2 | = | 0.9407E-03 | 79 | FACTP | = | 0.3800E C2 | 80 | FACTH | = | 0.7414E-02 |
| 81 | XI | = | 0.0 | 82 | YI | = | 0.0 | 83 | CCMPX | = | 0.0 | 84 | COMPY | = | 0.0 | 85 | HMIN | = | 0.0 |
| 86 | AVD | = | 0.2550E 02 | 87 | ARNEW | = | 0.0 | 88 | HMIN | = | 0.0 | 89 | EPSINF | = | 0.4237E C5 | 90 | EKAINF | = | 0.1259E C5 |
| 91 | RVFL | = | 0.0 | 92 | PFSLL | = | 0.1000E 00 | 93 | PFSLL | = | 0.9000E 00 | 94 | RAT02 | = | 0.2330E C0 | 95 | EPIEST | = | 0.2360E-08 |
| 96 | PSISTR | = | 0.0 | 97 | HINF | = | 0.1573E 02 | 98 | XPRIME | = | 0.6988E-04 | 99 | PPRCOIL | = | 0.8246E C4 | 100 | PPRIME | = | 0.5762E 00 |
| 101 | YUP | = | 0.7000E 02 | 102 | VSTARY | = | 0.1200E 01 | 103 | DEPLT | = | 0.1212E C4 | 104 | VELCST | = | 0.1965E-02 | 105 | RCCST | = | 0.1337E 02 |
| 106 | | = | 0.0 | 107 | VELD | = | 0.1081E 01 | 108 | | = | 0.0 | 109 | XMA | = | 0.2897E C2 | 110 | XMH | = | 0.2016E C1 |
| 111 | DELX3 | = | 0.1175E C4 | 112 | X3LAST | = | 0.1175E 04 | 113 | CLAST | = | 0.1175E C4 | 114 | DLXMI | = | 0.0 | 115 | | = | 0.0 |
| 116 | RR | = | 0.1435E C2 | 117 | RTOHMI | = | 0.1300E 02 | 118 | XMDOF | = | 0.8525E C2 | 119 | ROUALC | = | 0.8757E-04 | 120 | SCAL | = | 0.0 |
| 121 | FDOJ | = | 0.0 | 122 | HPSDGT | = | 0.0 | 123 | GR | = | 0.1000E C1 | 124 | CON | = | 0.4350E CC | 125 | XLAM | = | 0.9000E-01 |
| 126 | XMUATK | = | 0.1150E-04 | 127 | YMINRM | = | 0.1000E 01 | 128 | XMUCRS | = | 0.1000E C1 | 129 | SCT | = | 0.1000E C1 | 130 | C4ED | = | 0.7000E-03 |
| 131 | SPLIT | = | 0.2835E-01 | 132 | HRCCA | = | 0.2913E-01 | 133 | PCNT | = | 0.1000E-01 | 134 | Q3MAX | = | 0.0 | 135 | | = | 0.0 |
| 136 | | = | 0.0 | 137 | | = | 0.0 | 138 | | = | 0.0 | 139 | VF | = | 0.0 | 140 | VK | = | 0.2000E 01 |
| 141 | VA | = | 0.1510E 01 | 142 | VB | = | 0.6750E 00 | 143 | C4ECSW | = | 0.3000E 05 | 144 | C4FACT | = | 0.1000E C1 | 145 | EIE2SM | = | 0.3000E 05 |
| 146 | T0A | = | 0.5330E C3 | 147 | T0H | = | 0.5200E 03 | 148 | CVH | = | 0.1000E C1 | 149 | CVU | = | 0.9635E-02 | 150 | CVT | = | 0.1000E 01 |
| 151 | CVP | = | 0.4725E-03 | 152 | CVRHC | = | 0.1602E 02 | 153 | CVCP | = | 0.4166E C4 | 154 | XMACFS | = | 0.9664E-01 | 155 | TSINF | = | 0.5610E 03 |
| 156 | AINF | = | 0.1191E 04 | 157 | PHOUII | = | 0.7882E 01 | 158 | CPA | = | 0.2400E C0 | 159 | CPII | = | 0.3445E C1 | 160 | CPIINF | = | 0.2400E 00 |
| 161 | | = | 0.1665E C3 | 162 | FTDIN | = | 0.1200E 02 | 163 | FTTCOM | = | 0.3048E C2 | 164 | FTTOMT | = | 0.3048E CC | 165 | DRIGDK | = | 0.5556E 00 |
| 166 | PSFT0A | = | 0.4725E-03 | 167 | PSFTCT | = | 0.3591E 00 | 168 | PSFTCN | = | 0.4788E C2 | 169 | PSFTOI | = | 0.6944E-02 | 170 | P0FTOK | = | 0.1602E 02 |
| 171 | PRSCON | = | 0.2749E 02 | 172 | XFACT | = | 0.9727E-01 | 173 | 7MAX | = | 0.0 | 174 | P0FTOC | = | 0.1602E-01 | 175 | EBTOKJ | = | 0.2325E 01 |
| 176 | CBTCKJ | = | 0.4164E C1 | 177 | VLBTCA | = | 0.1488E 01 | 178 | VLBTCP | = | 0.1488E C2 | 179 | RADCON | = | 0.1745E-01 | 180 | PRDIS | = | 0.1300E 01 |
| 181 | PRTKE | = | 0.1000E 01 | 182 | CITKE | = | 0.1440E 01 | 183 | C2TKE | = | 0.1920E C1 | 184 | CATKE | = | 0.0 | 185 | CSHZ1 | = | 0.0 |
| 186 | OSH1 | = | 0.1000E 01 | 187 | CSH2 | = | 0.1000E 01 | 188 | CSH3 | = | 0.1000E C1 | 189 | CSHZ1 | = | 0.0 | 190 | YTT | = | 0.0 |
| 191 | ACUCT | = | 0.2000E 01 | 192 | XLAST | = | 0.0 | 193 | XMGEC | = | 0.0 | 194 | XTTT | = | 0.0 | 195 | | = | 0.0 |
| 196 | FK | = | 0.0 | 197 | | = | 0.0 | 198 | | = | 0.0 | 199 | | = | 0.0 | 200 | | = | 0.0 |

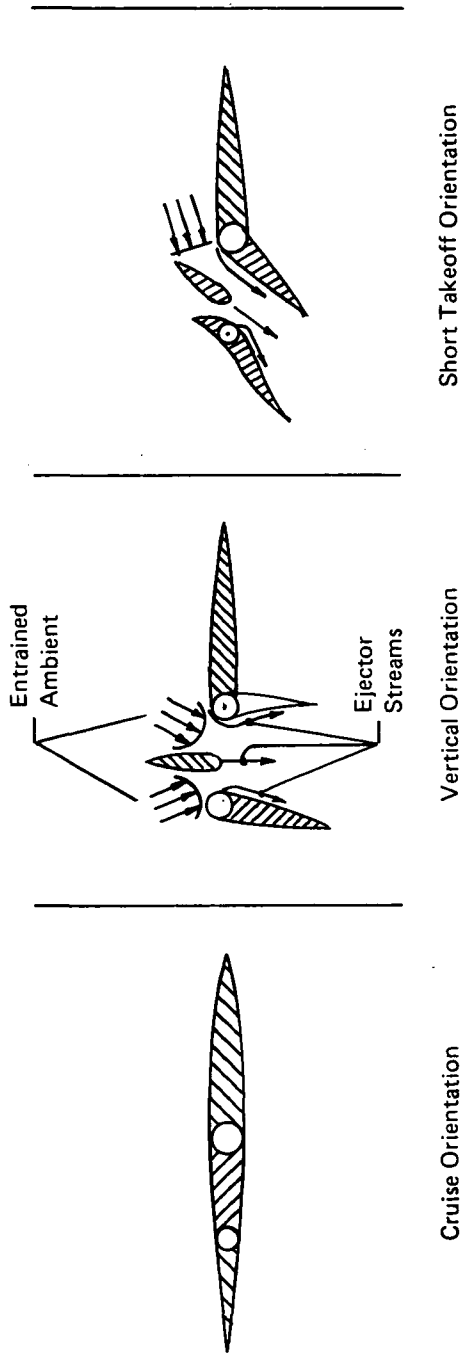


Figure 1. Schematics of Ejector in Wing Configurations

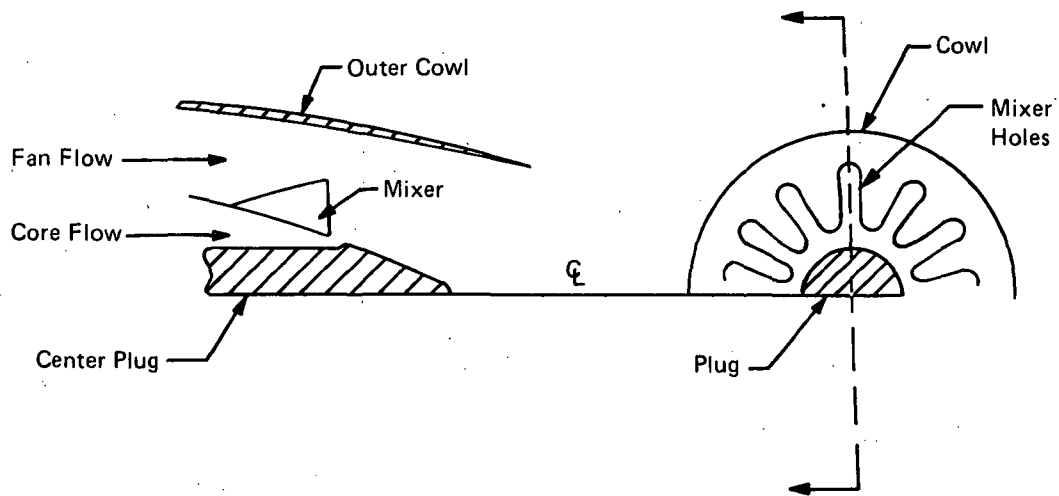


Figure 2. Axisymmetric Fluted Mixer Configuration

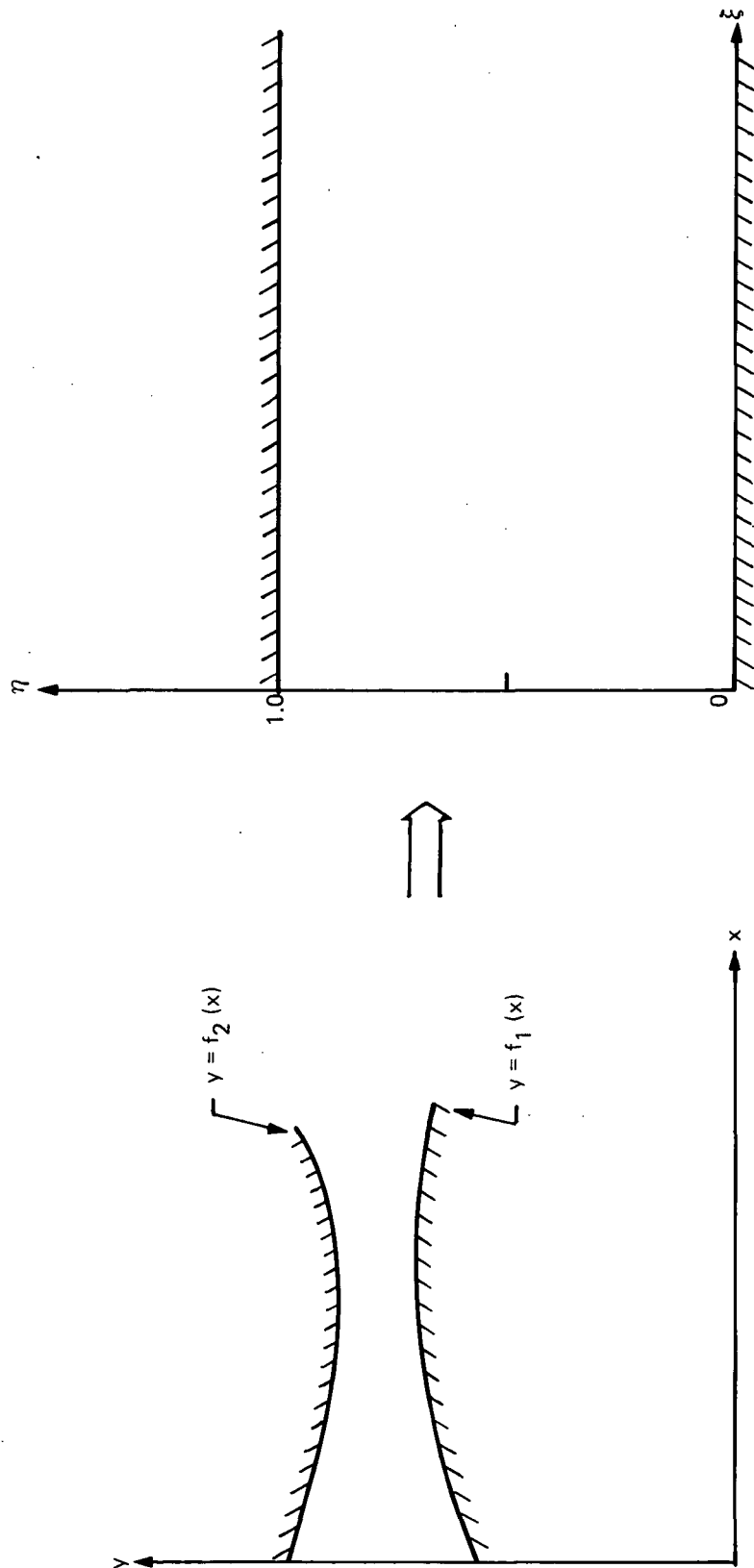


Figure 3 . Variable Geometry Transformation in the y Direction

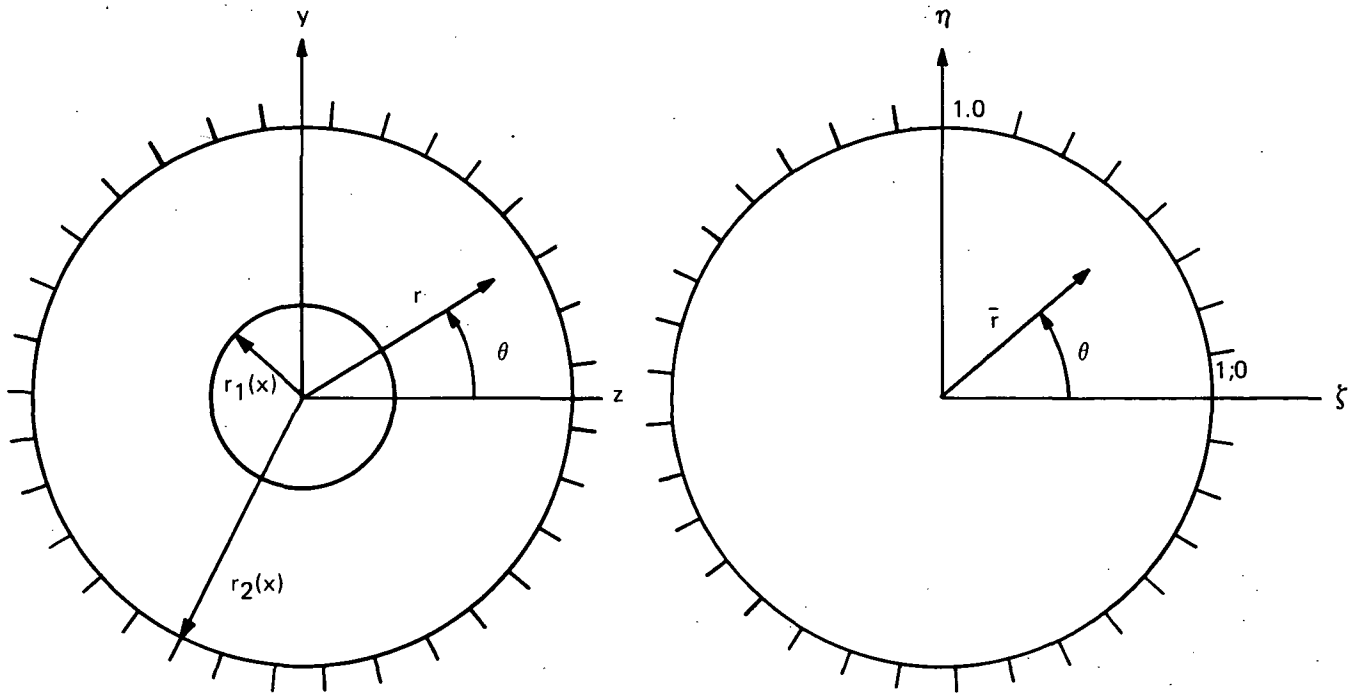


Figure 4. Coordinate Transformation for Axisymmetric Flows from (y, z) to (η, ζ) Plane

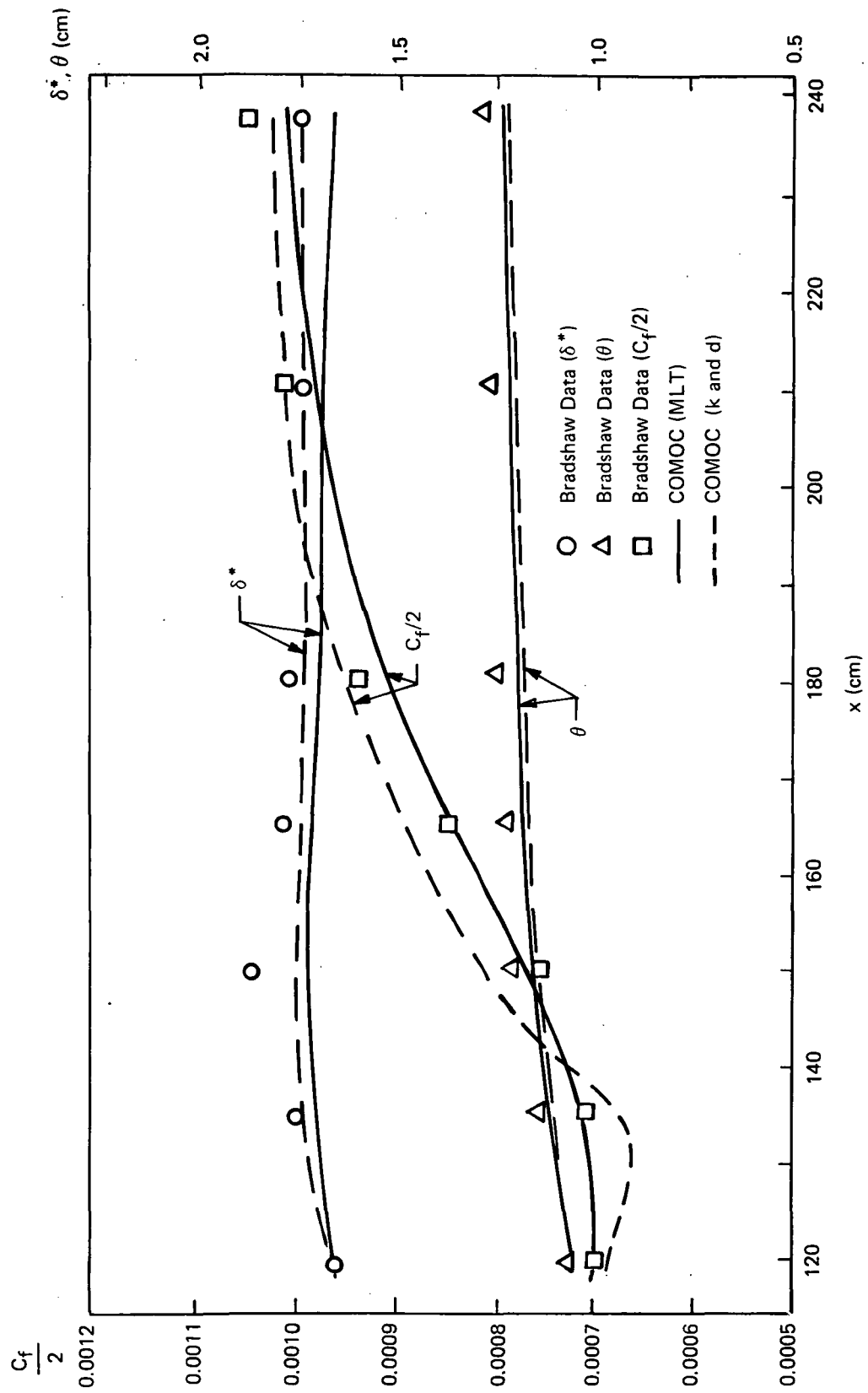


Figure 5. Comparison between COMOC Predicted and Experimental Integral Parameters for the Turbulent Boundary Layer Developing in a Duct

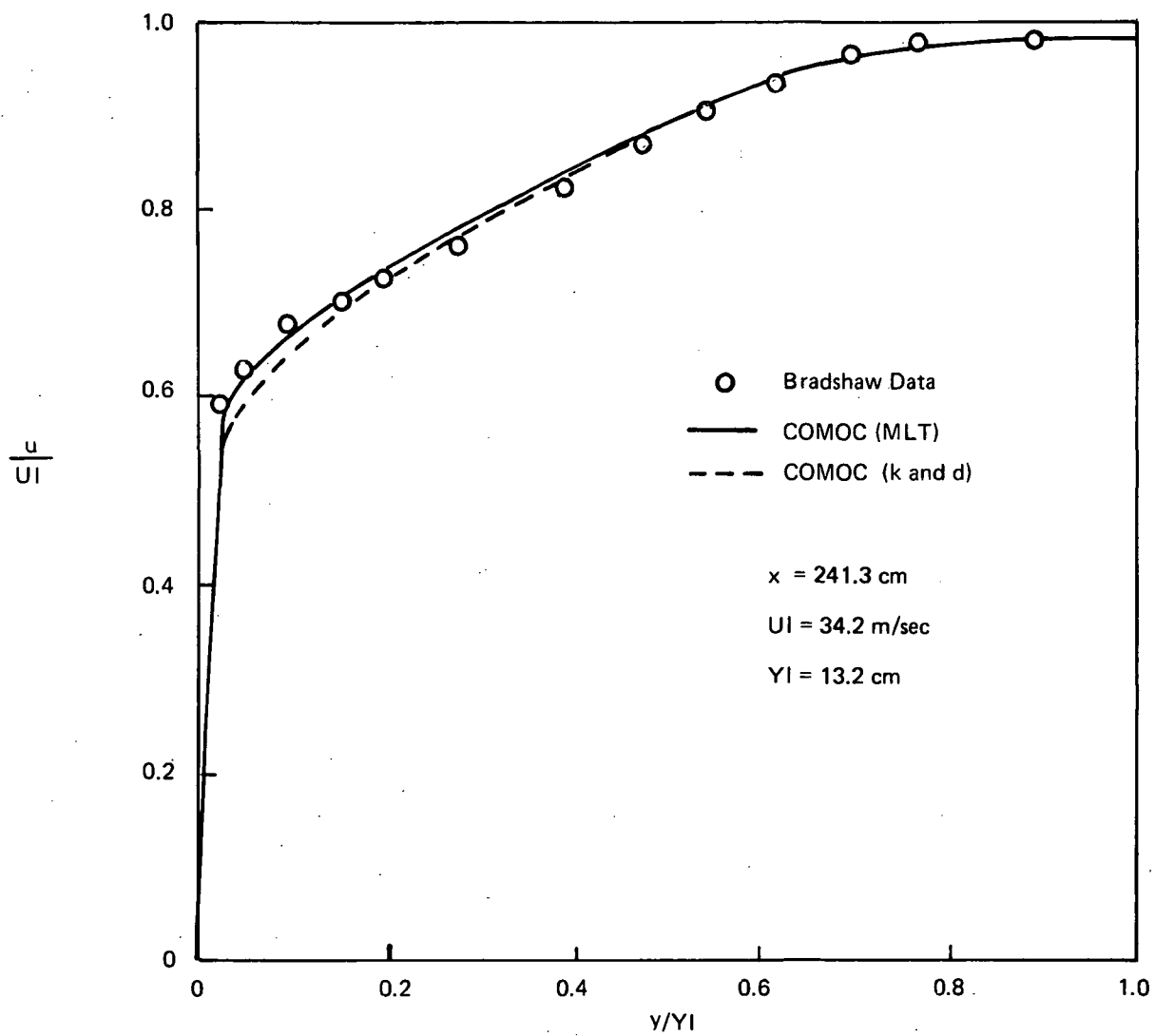


Figure 6. Comparison between COMOC Predicted and Experimental Velocity Profile at x equal 241.3 cm for the Turbulent Boundary Layer Developing in a Duct

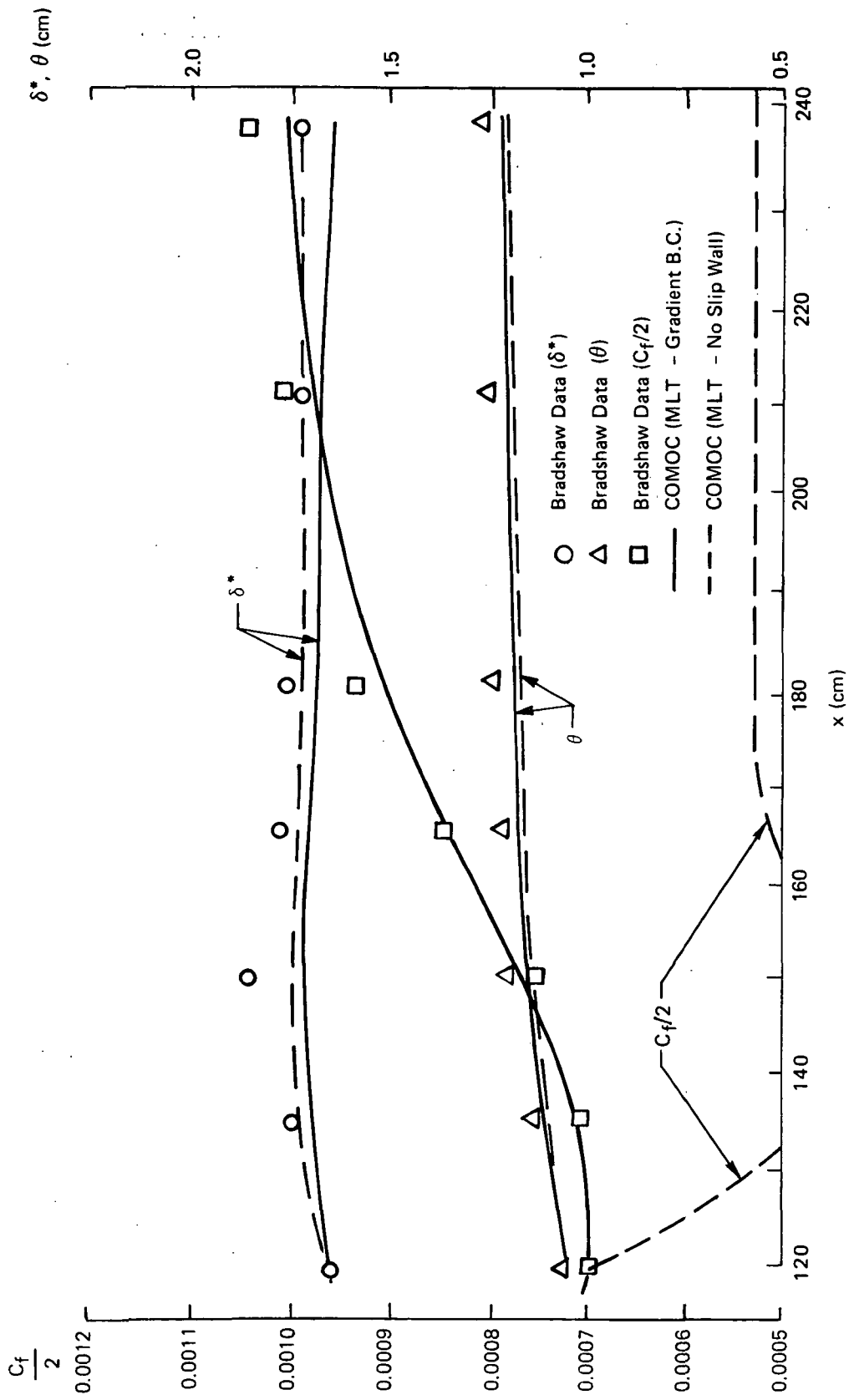


Figure 7. Comparison between COMOC Predicted and Experimental Integral Parameters for the Turbulent Boundary Layer Developing in a Duct for Gradient and No Slip Wall Boundary Conditions

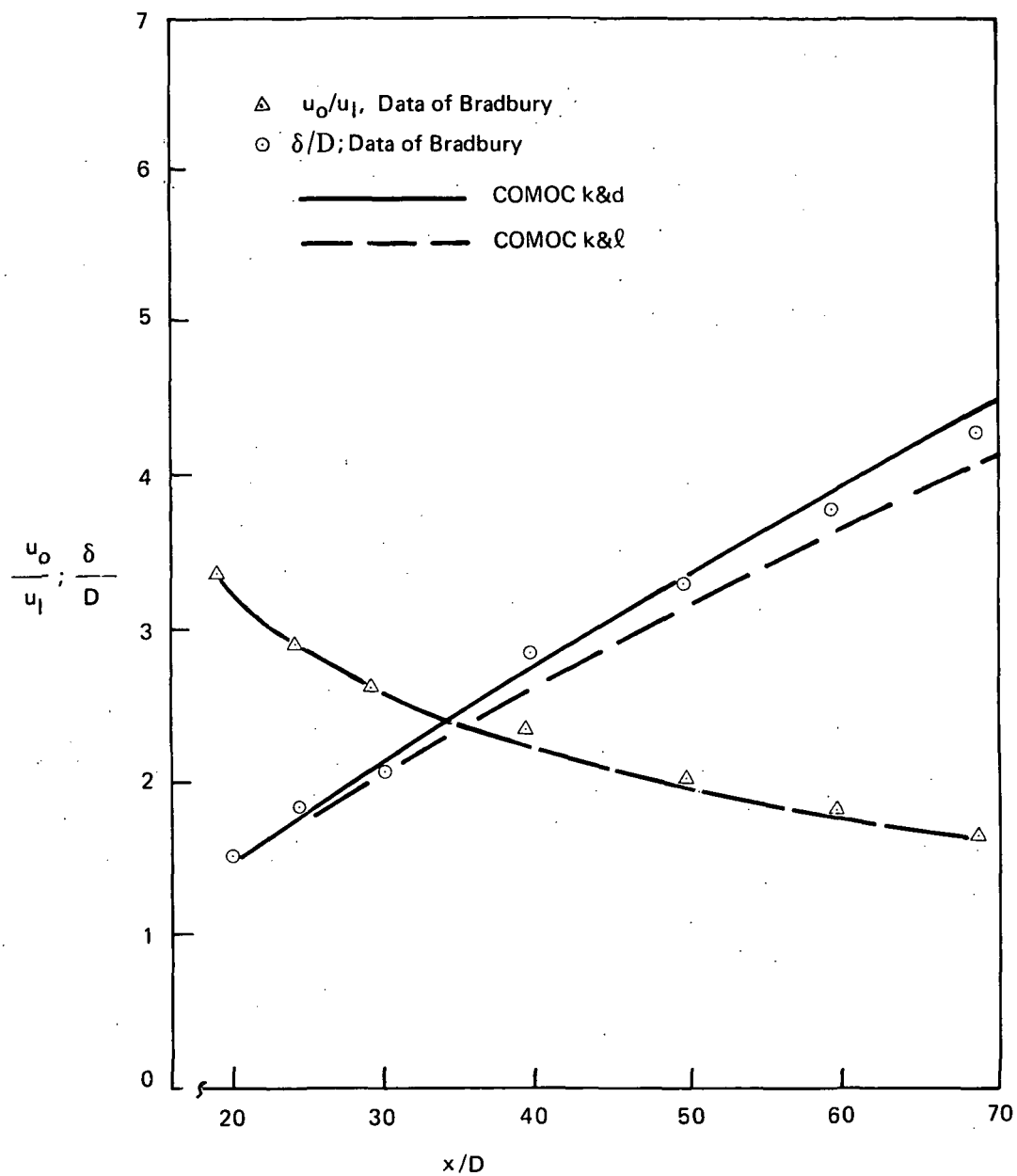


Figure 8. Comparison Between COMOC Predicted and Experimental Maximum Velocity Decay and Half-Jet Growth for the Rectangular Nozzle

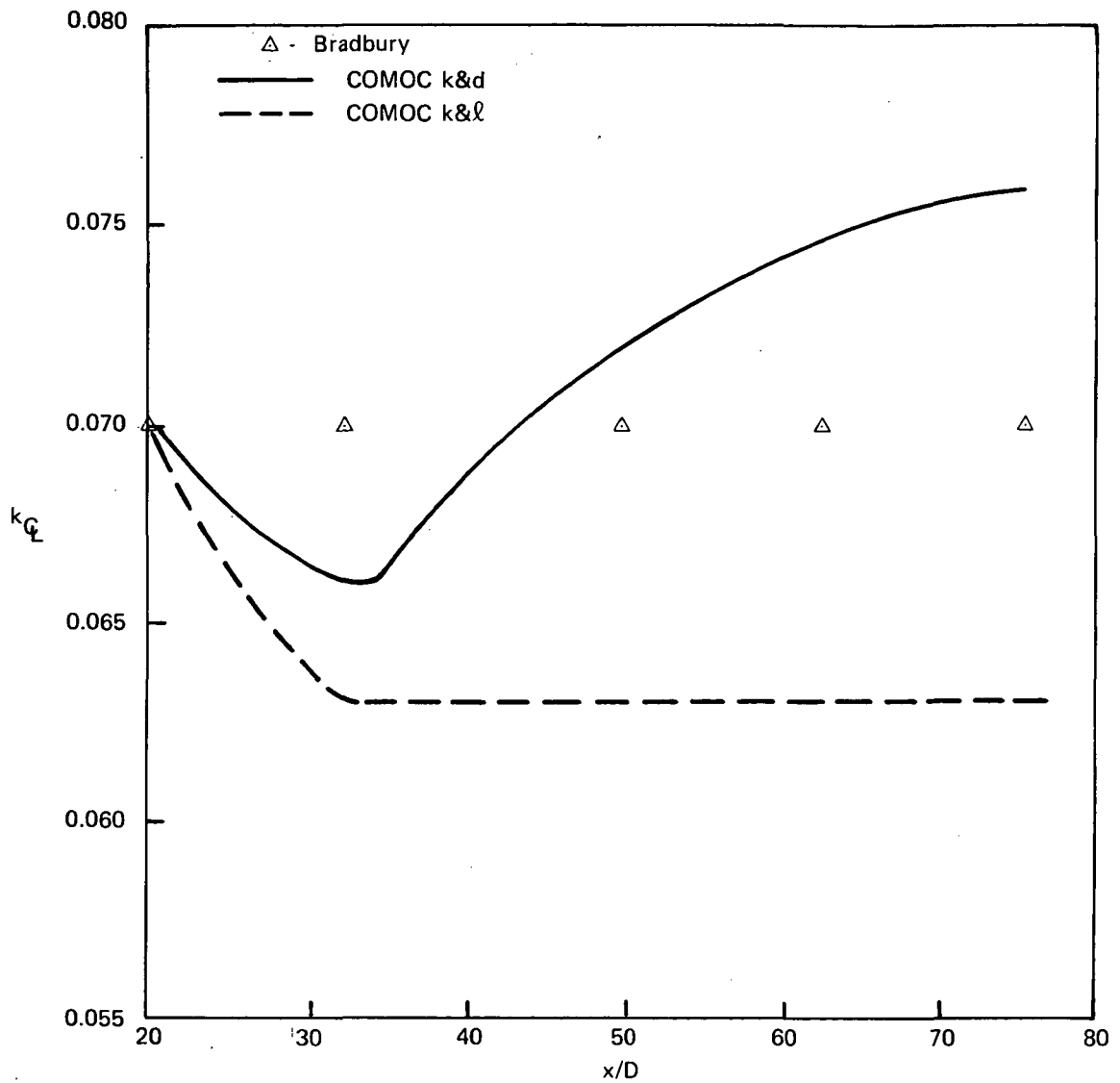


Figure 9. Comparison Between COMOC Predicted and Experimental Centerline Turbulent Kinetic Energy for the Rectangular Nozzle

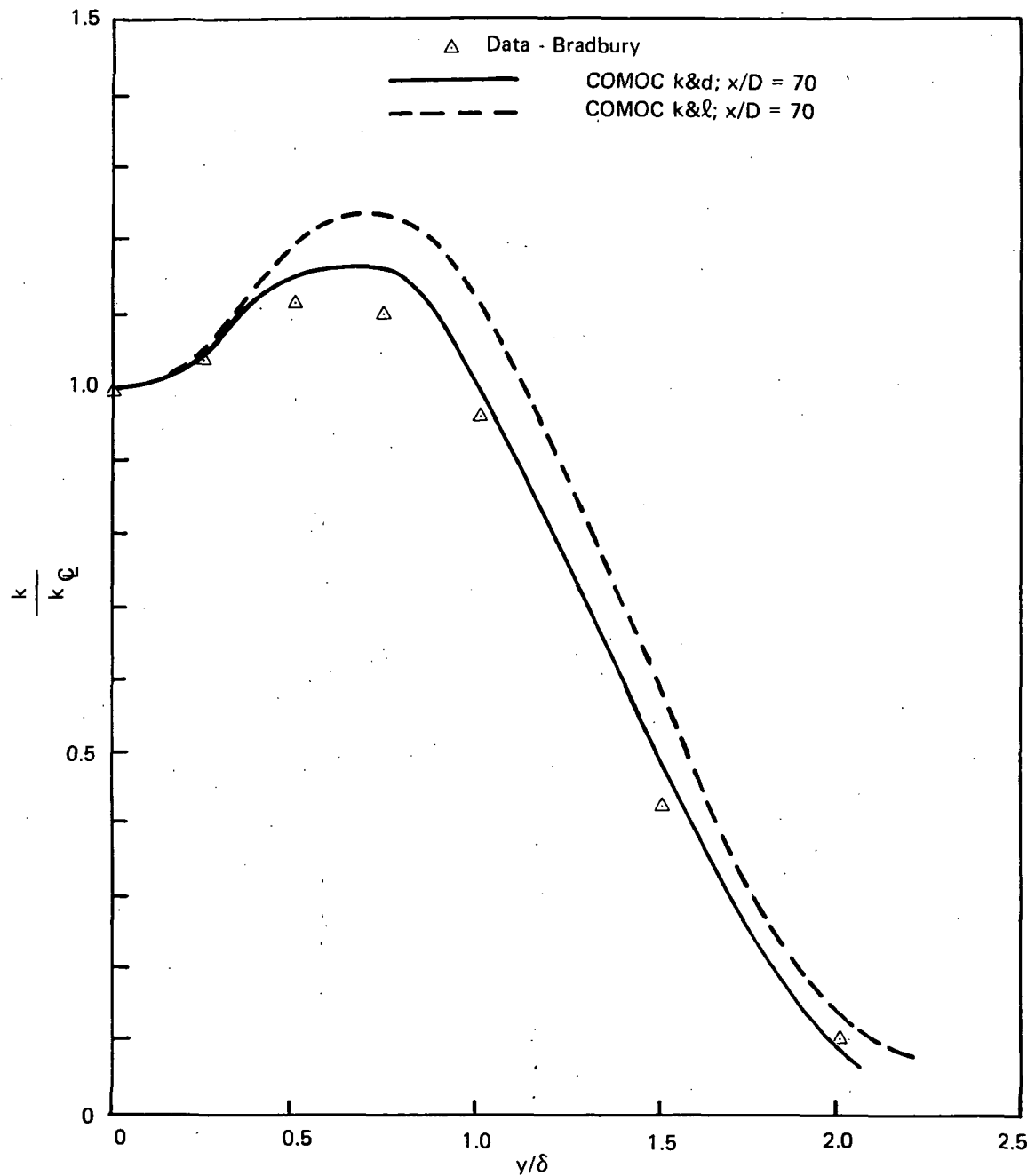


Figure 10. Comparison Between COMOC Predicted and Experimental Shape of T.K.E. Profile at x/D Equal 70 for the Rectangular Nozzle

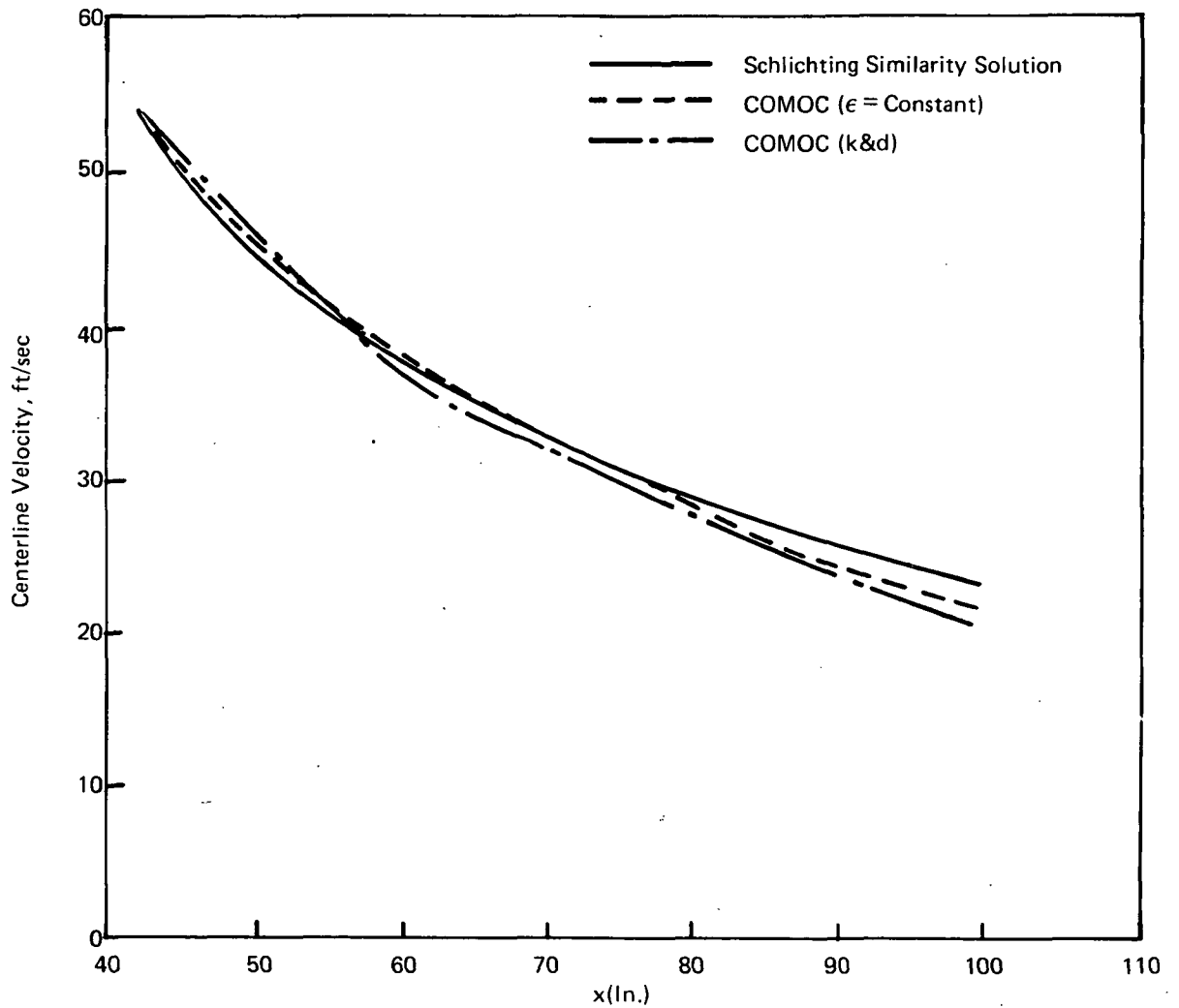


Figure 11. Comparison Between COMOC Predicted and Experimental Decay of Centerline Velocity for the Axisymmetric Nozzle

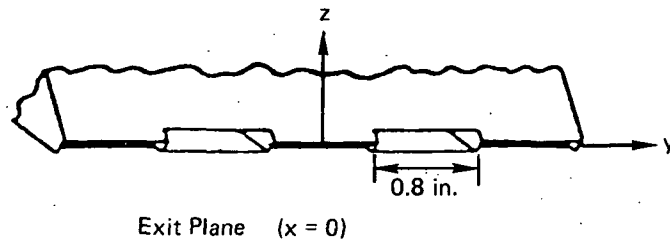


Figure 12. Hypermixing Nozzle Geometry

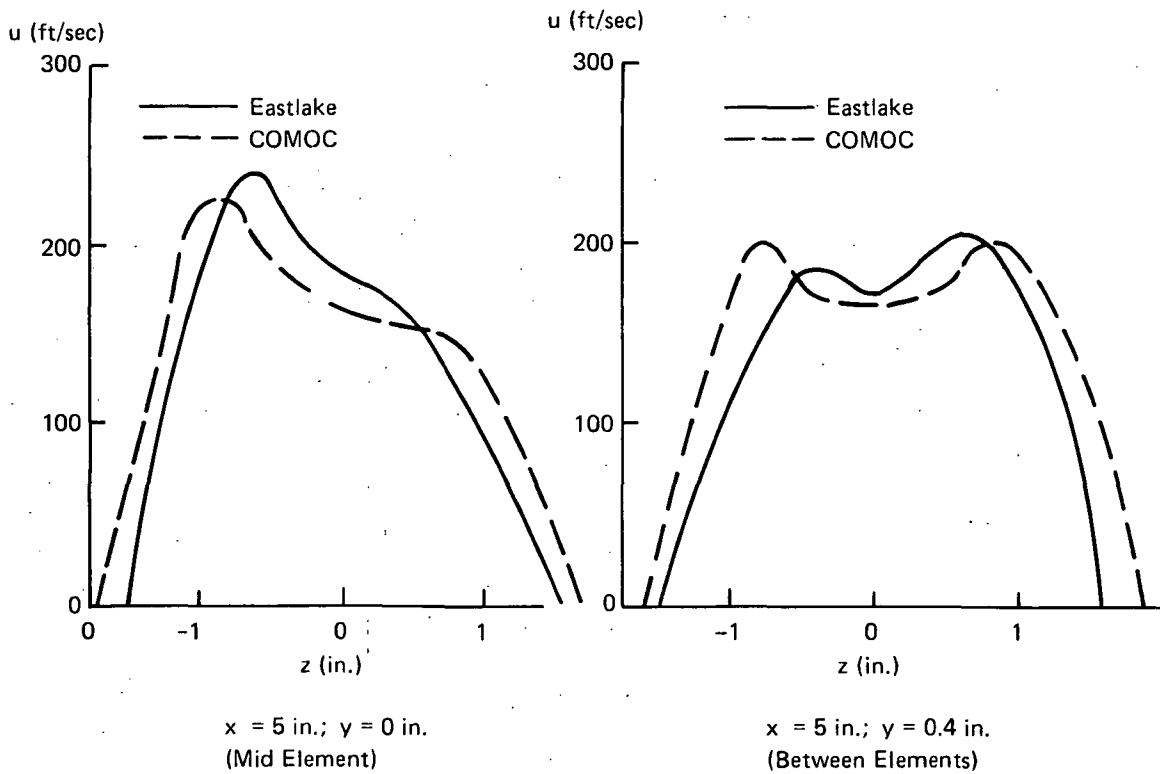


Figure 13. Comparison with Eastlake Hypermixing Data

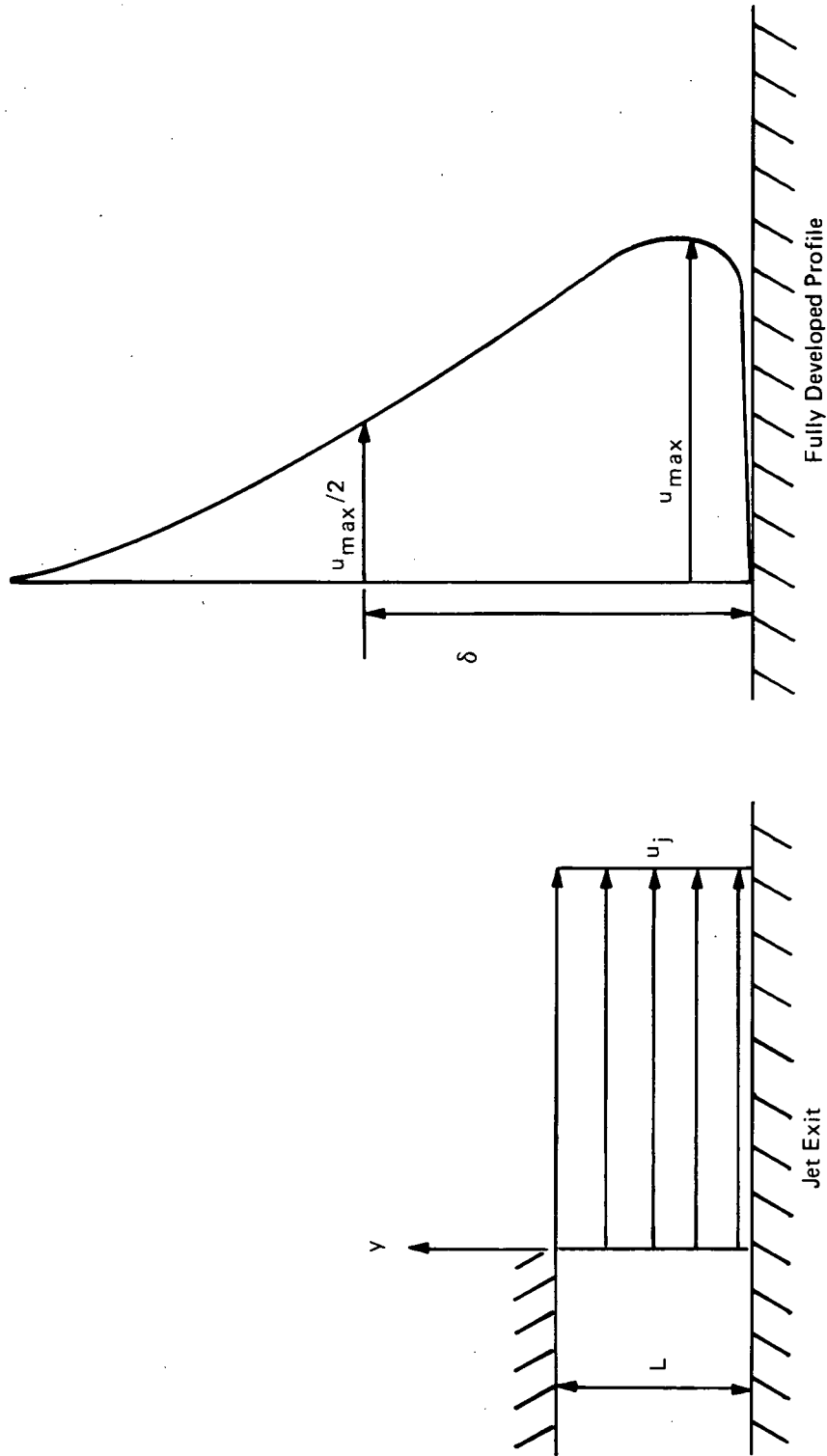


Figure 14. Configuration and Definition of Parameters for the Wall Jet Developing in a Duct

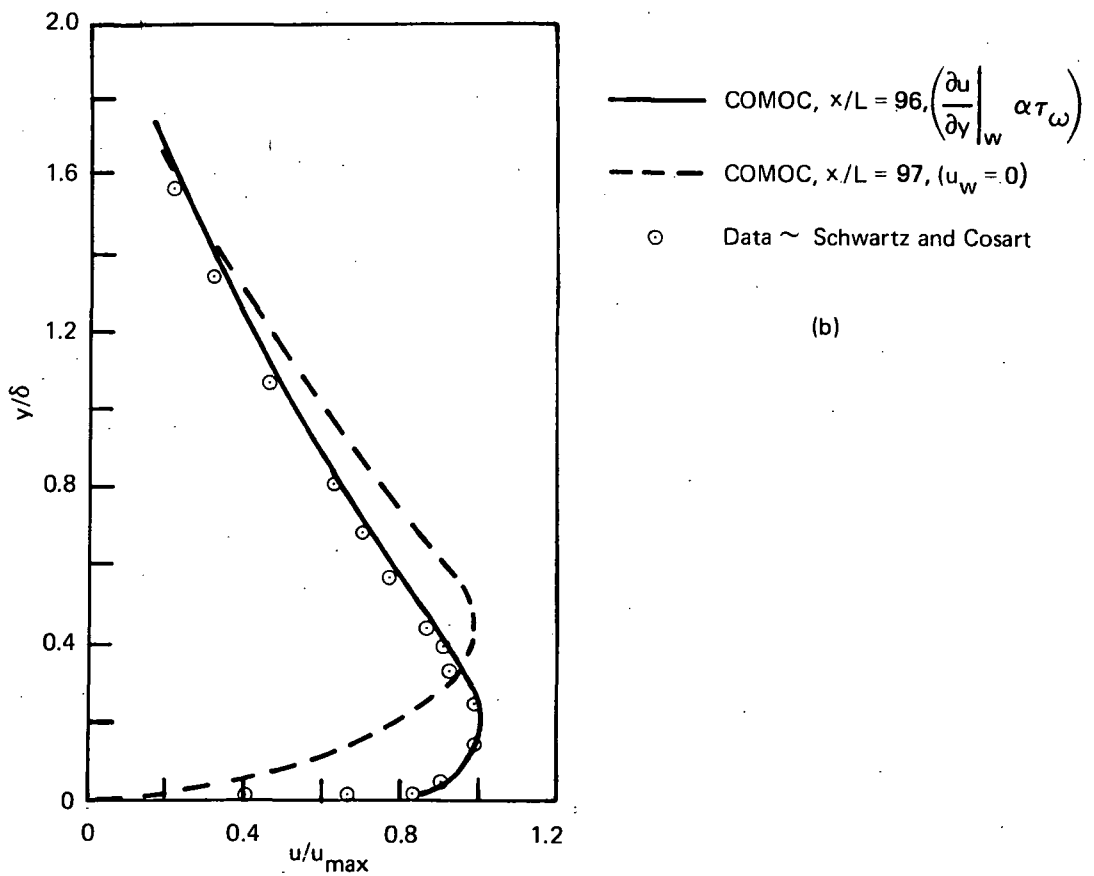
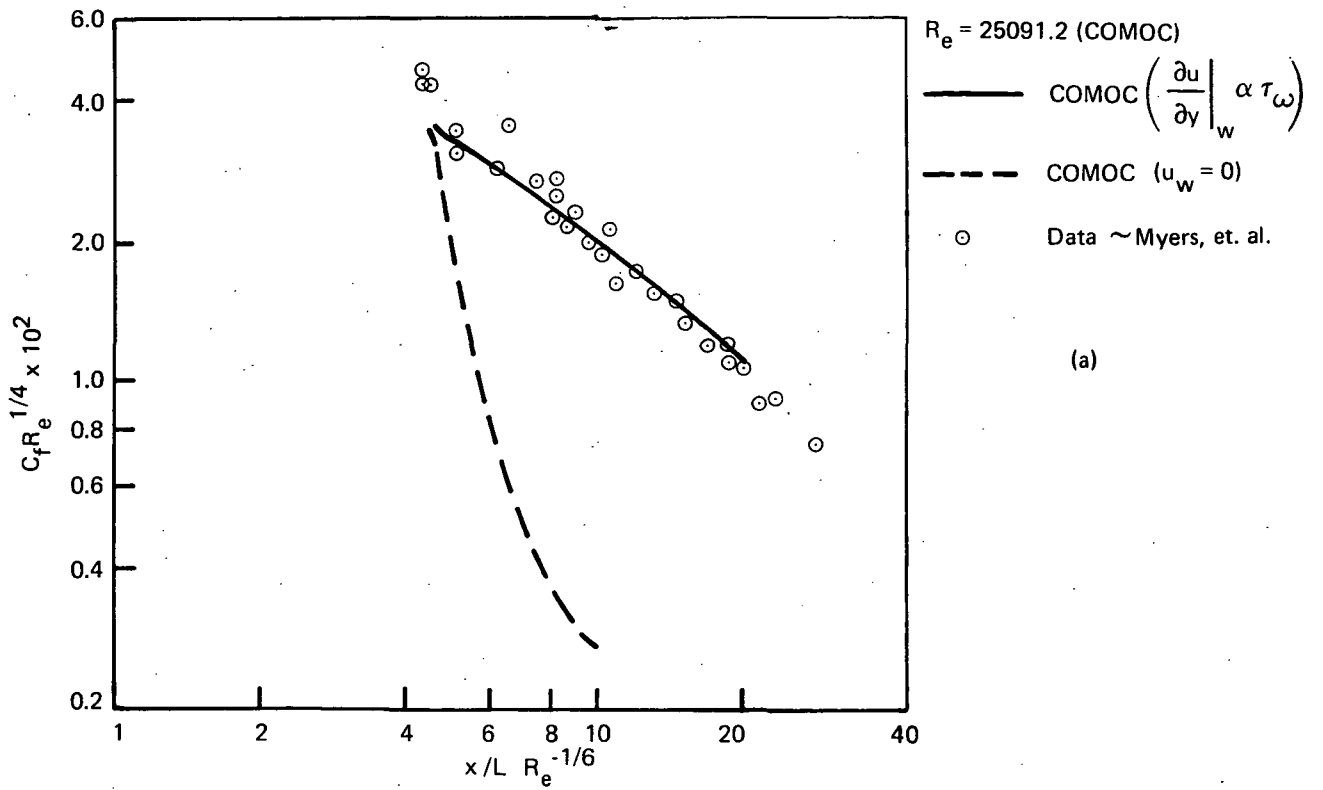


Figure 15. Comparison Between COMOC Predicted and Experimental Skin Friction and Velocity Profile The Wall Jet Developing in a Duct

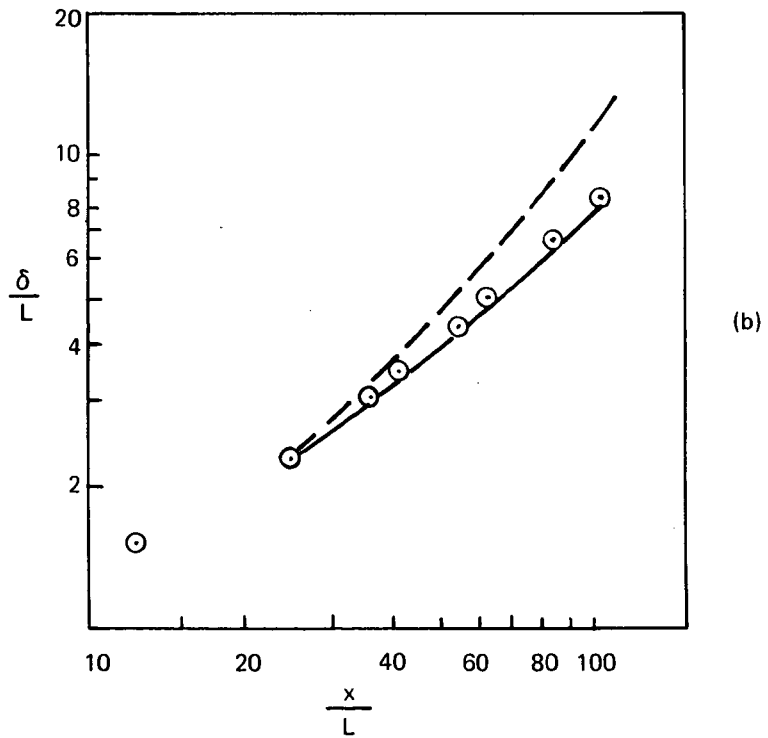
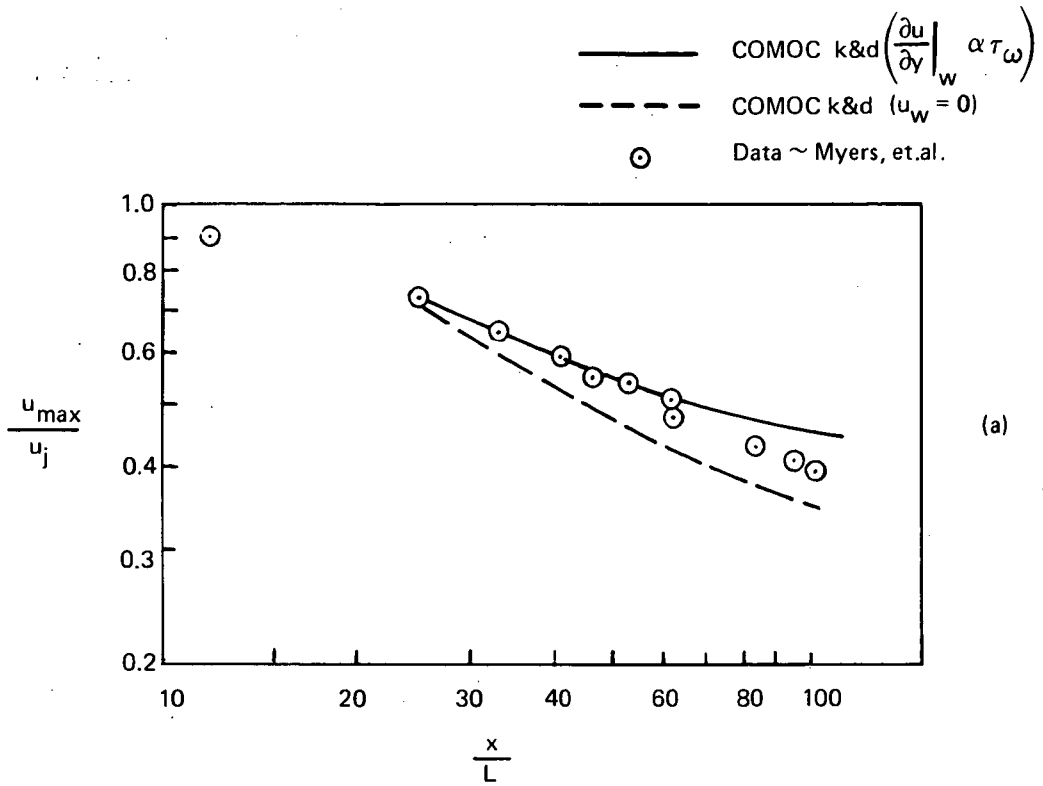
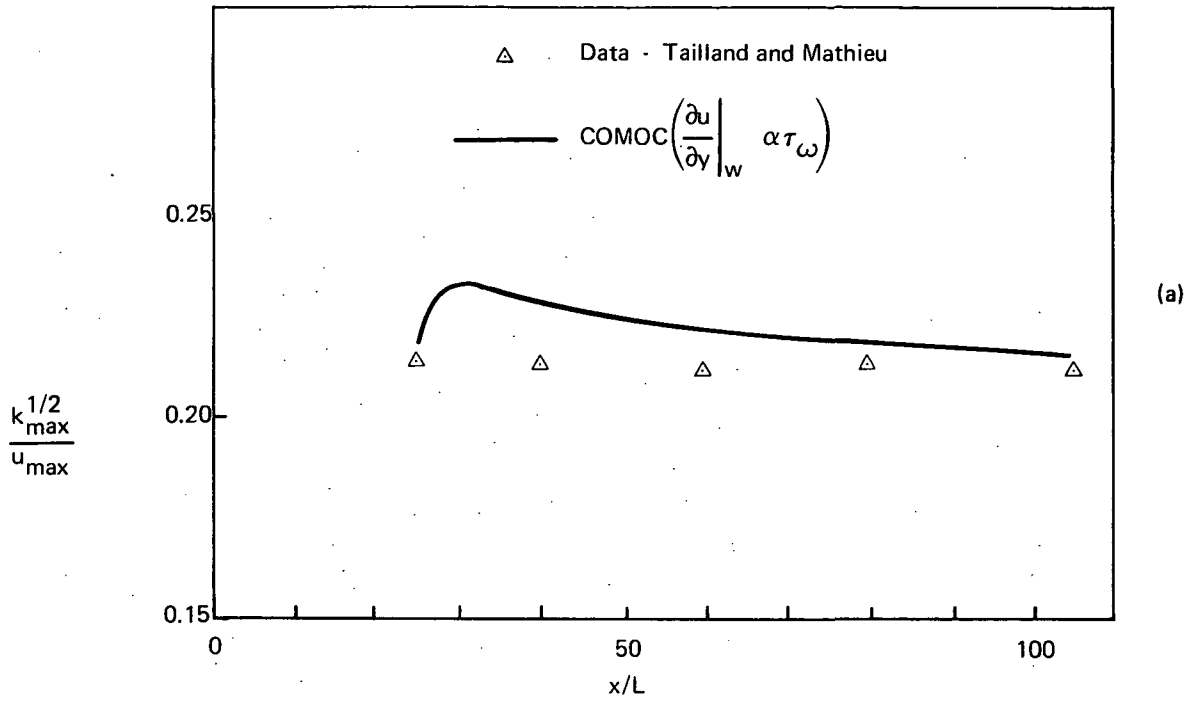


Figure 16. Comparison Between COMOC Predicted and Experimental Maximum Velocity Decay and Half-Jet Growth for the Wall Jet Developing in a Duct

(a) Maximum TKE versus x



(b) TKE profile

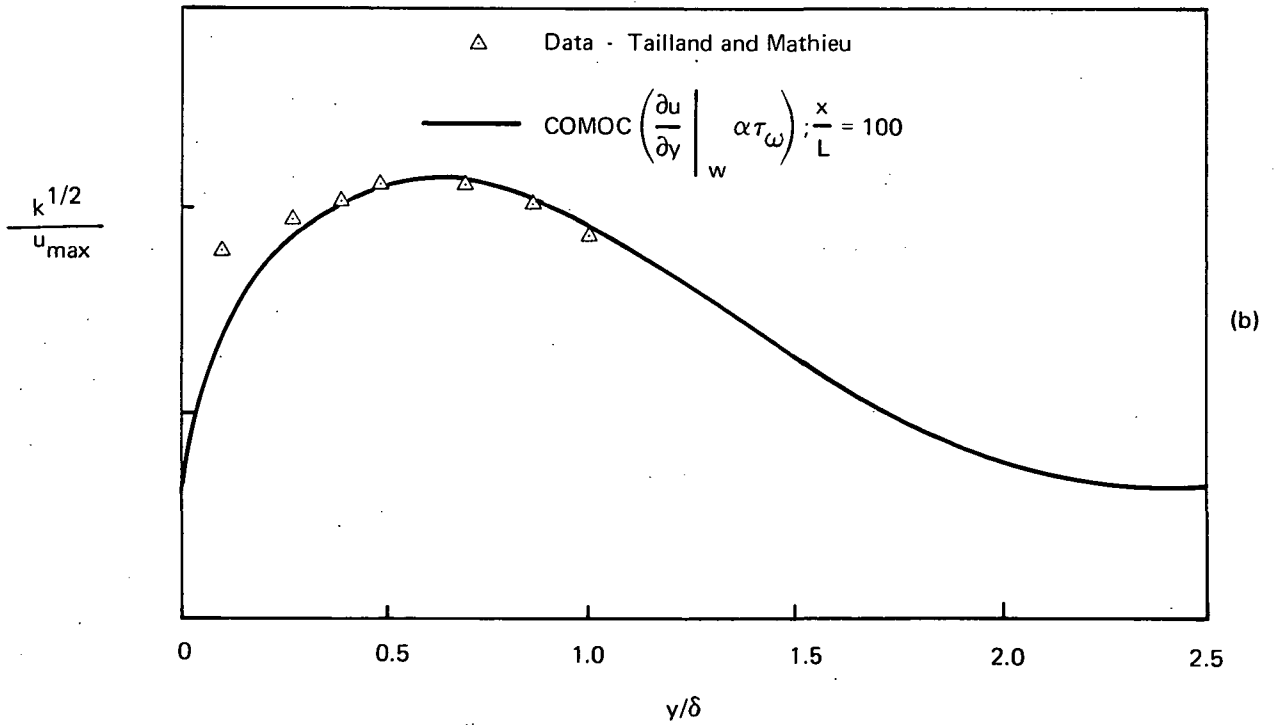


Figure 17. Comparison Between COMOC Predicted and Experimental TKE Profile for The Wall Jet Developing in a Duct

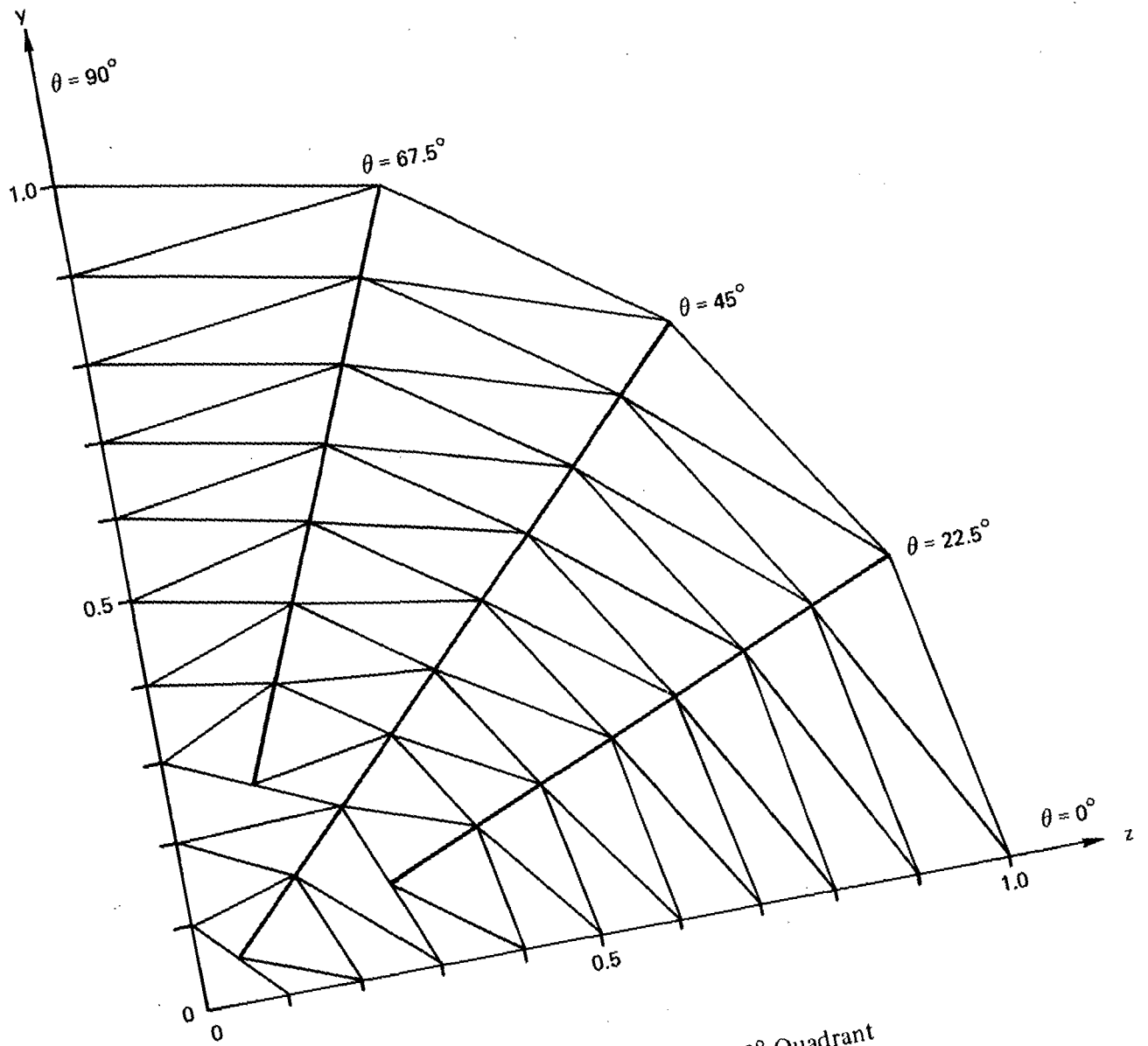


Figure 18. Finite Elements for 90° Quadrant

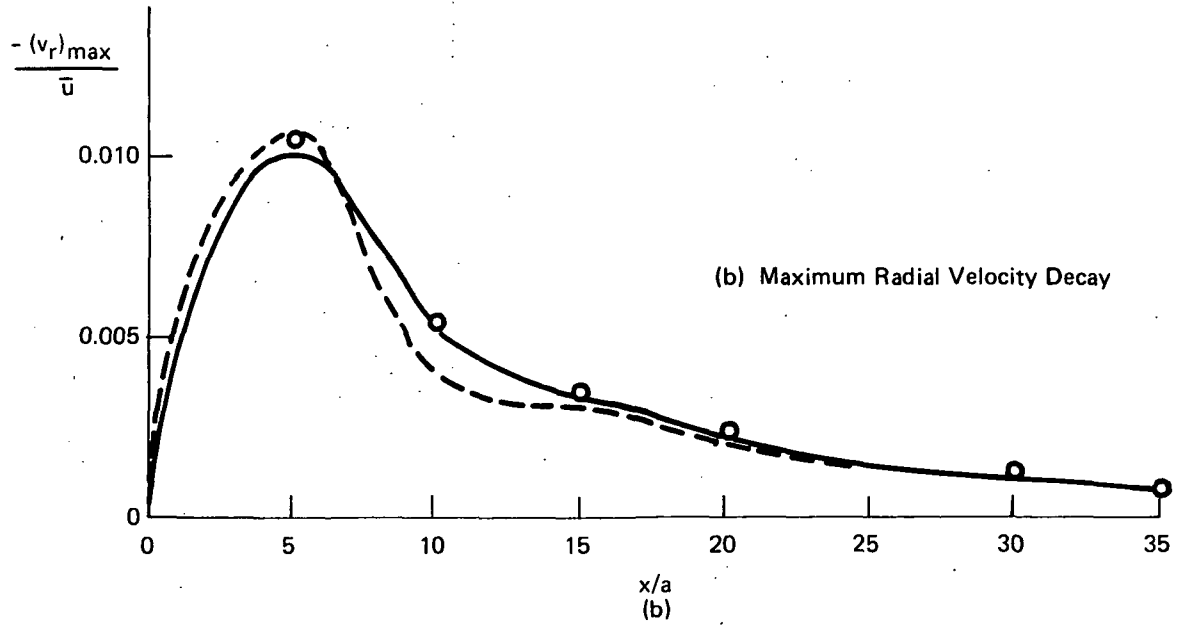
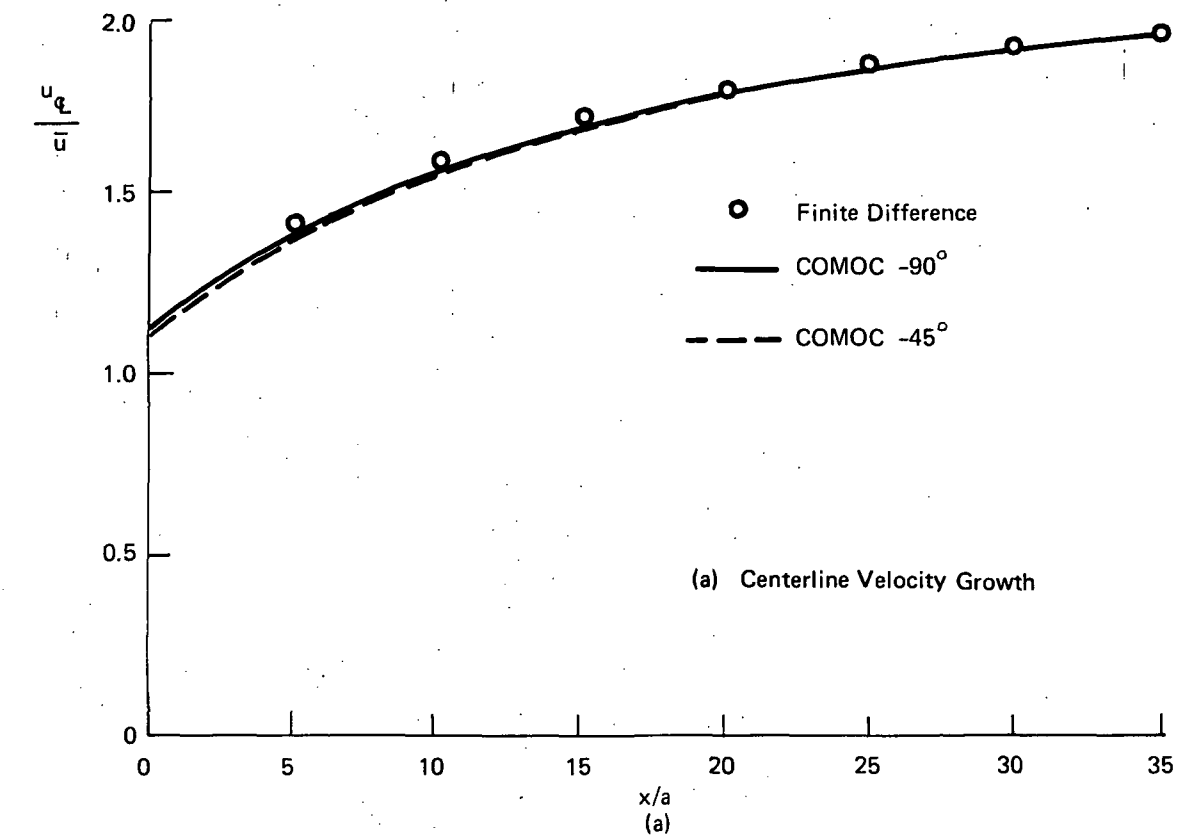


Figure 19. Developing Flow in a Pipe

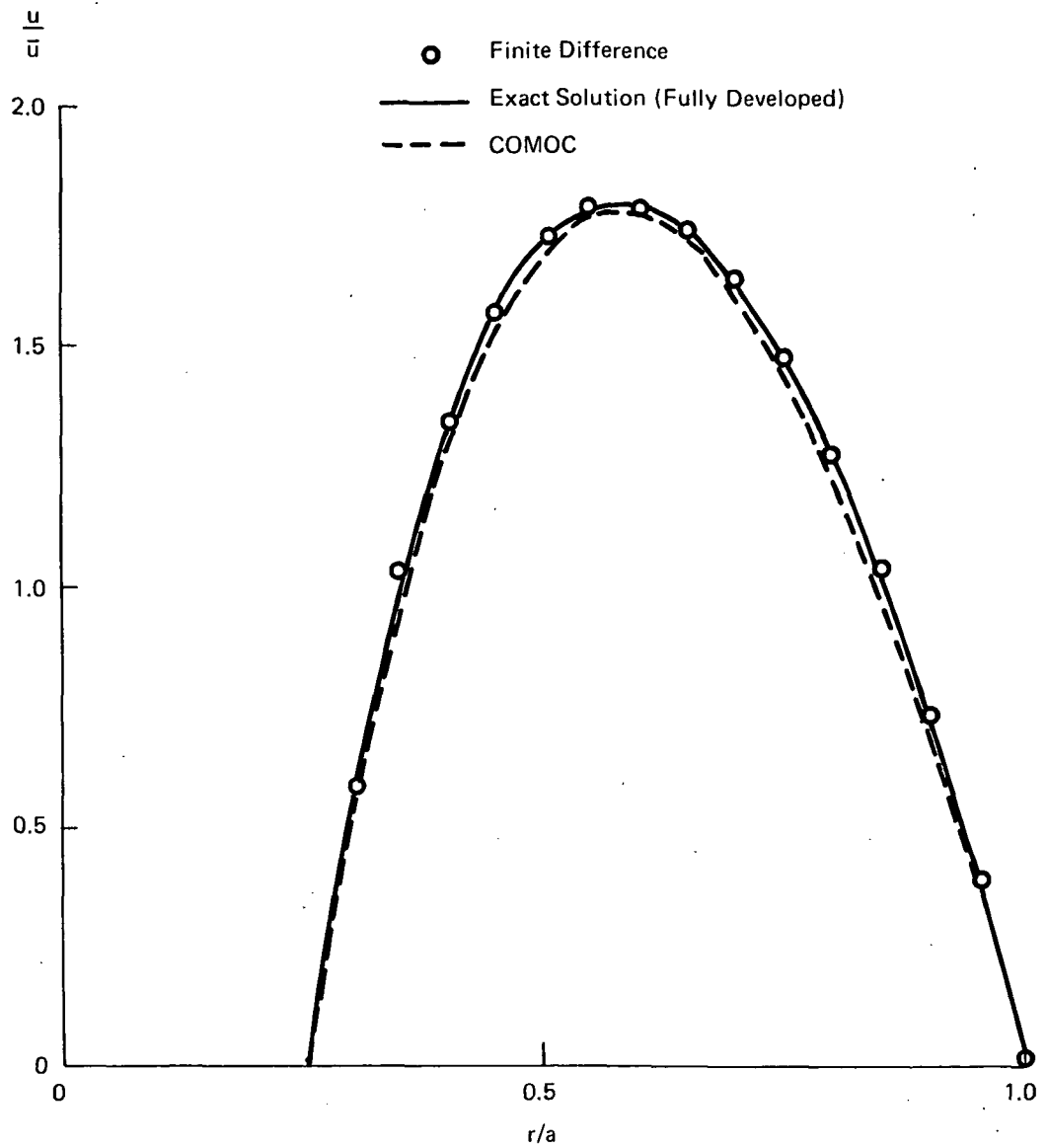


Figure 20. Fully Developed Axial Velocity Profile for Annular Pipe at $x/a = 71$.

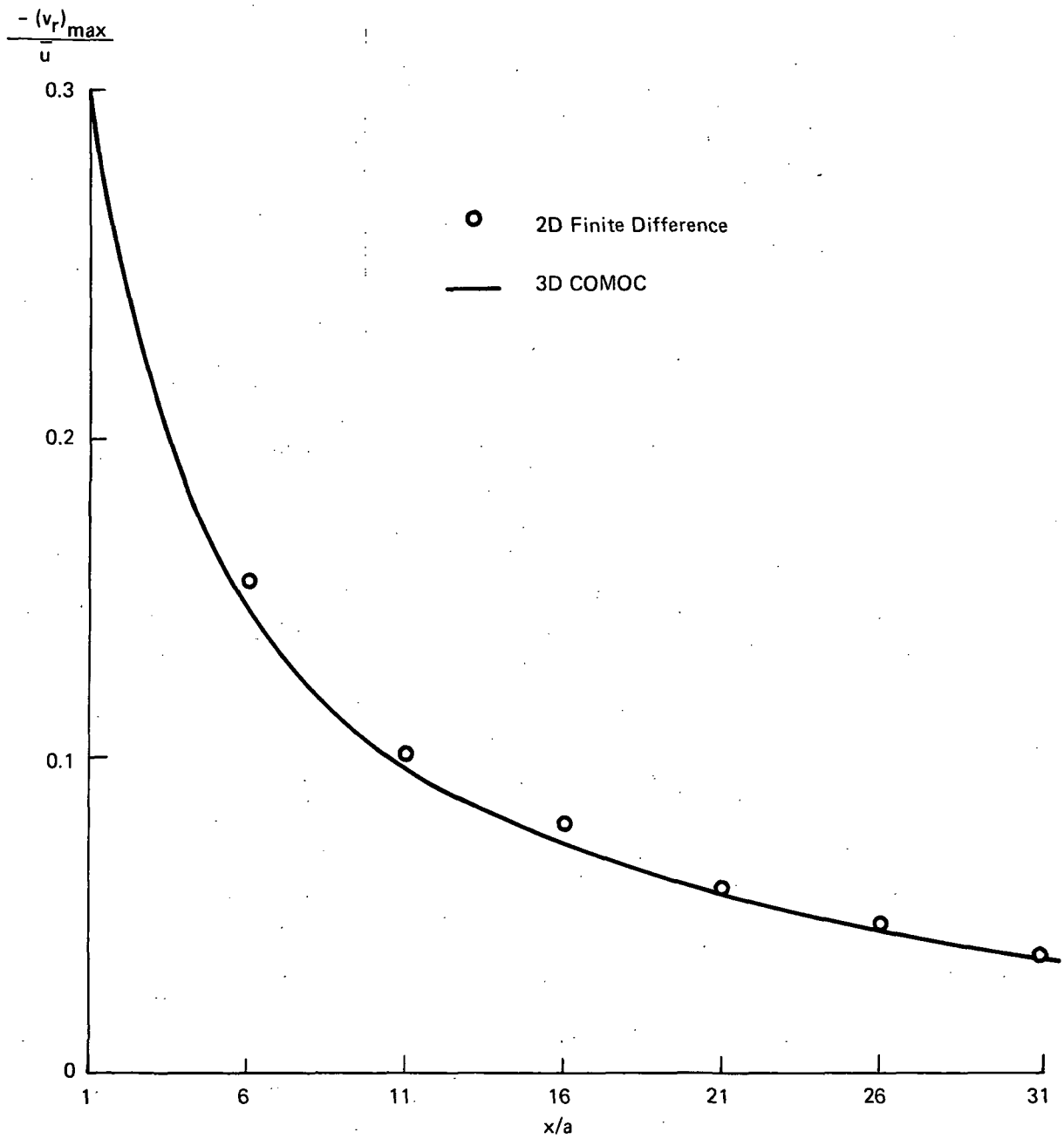


Figure 21. Decay of Maximum Radial Velocity for Annular Pipe

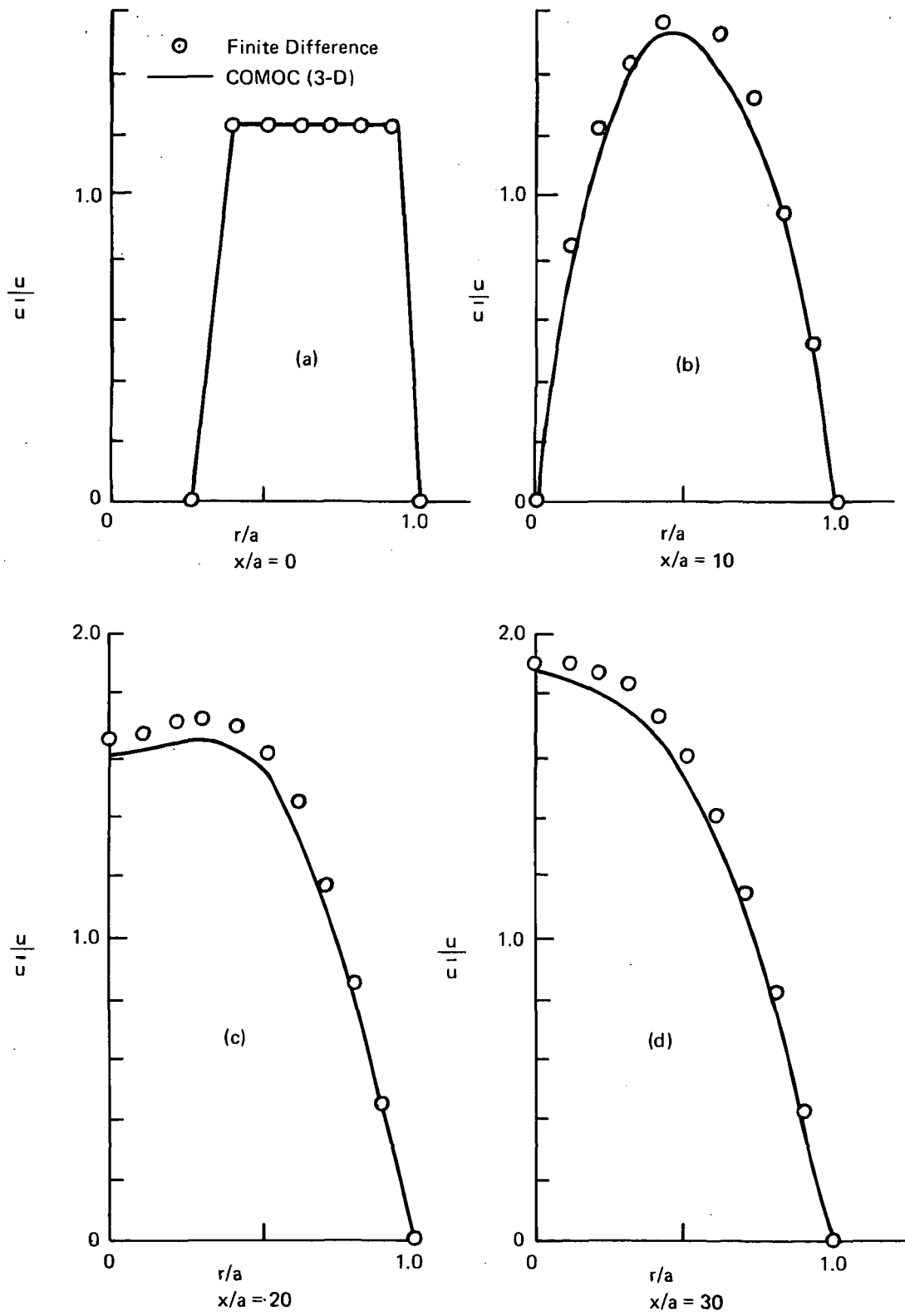


Figure 22. Axial Velocity Profiles for Conical Center Pipe Flow

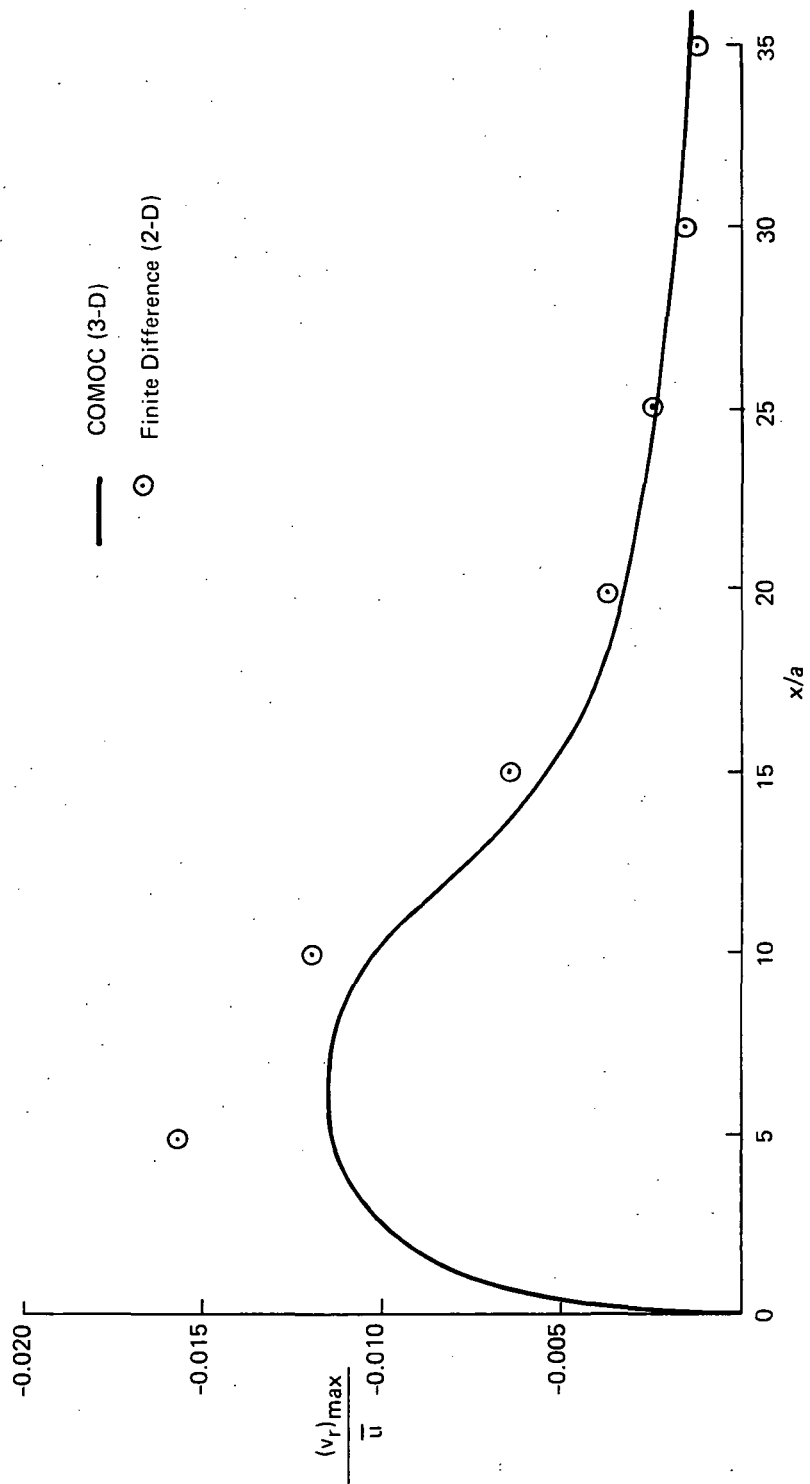


Figure 23. Maximum Secondary Velocity Comparison for Conical Center Pipe Flow. Discrepancies Between The Two Codes In the Initial Region are Due to Differences in Descretization and Axial Integration Step Size

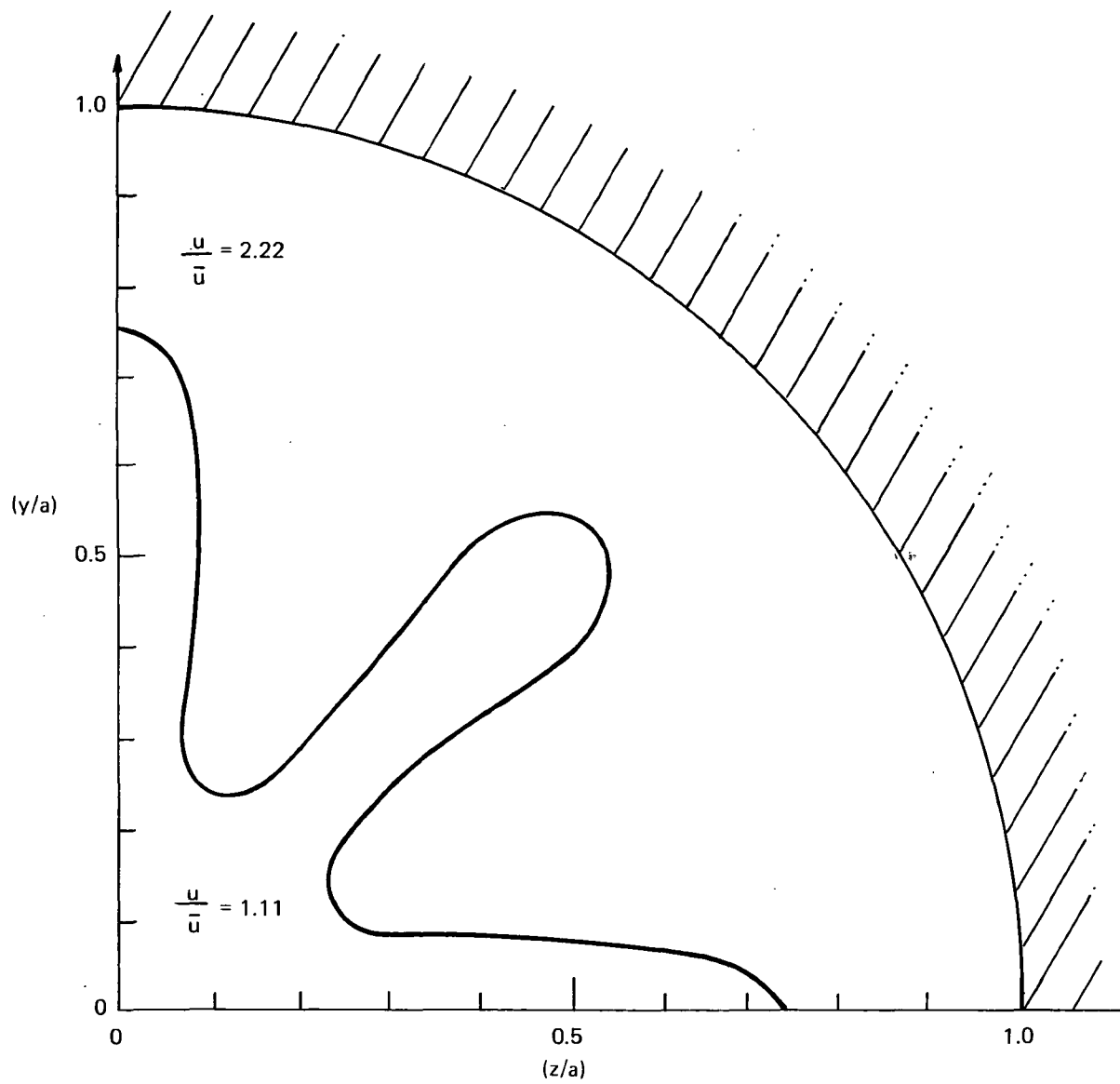


Figure 24. Fluted Pipe Geometry

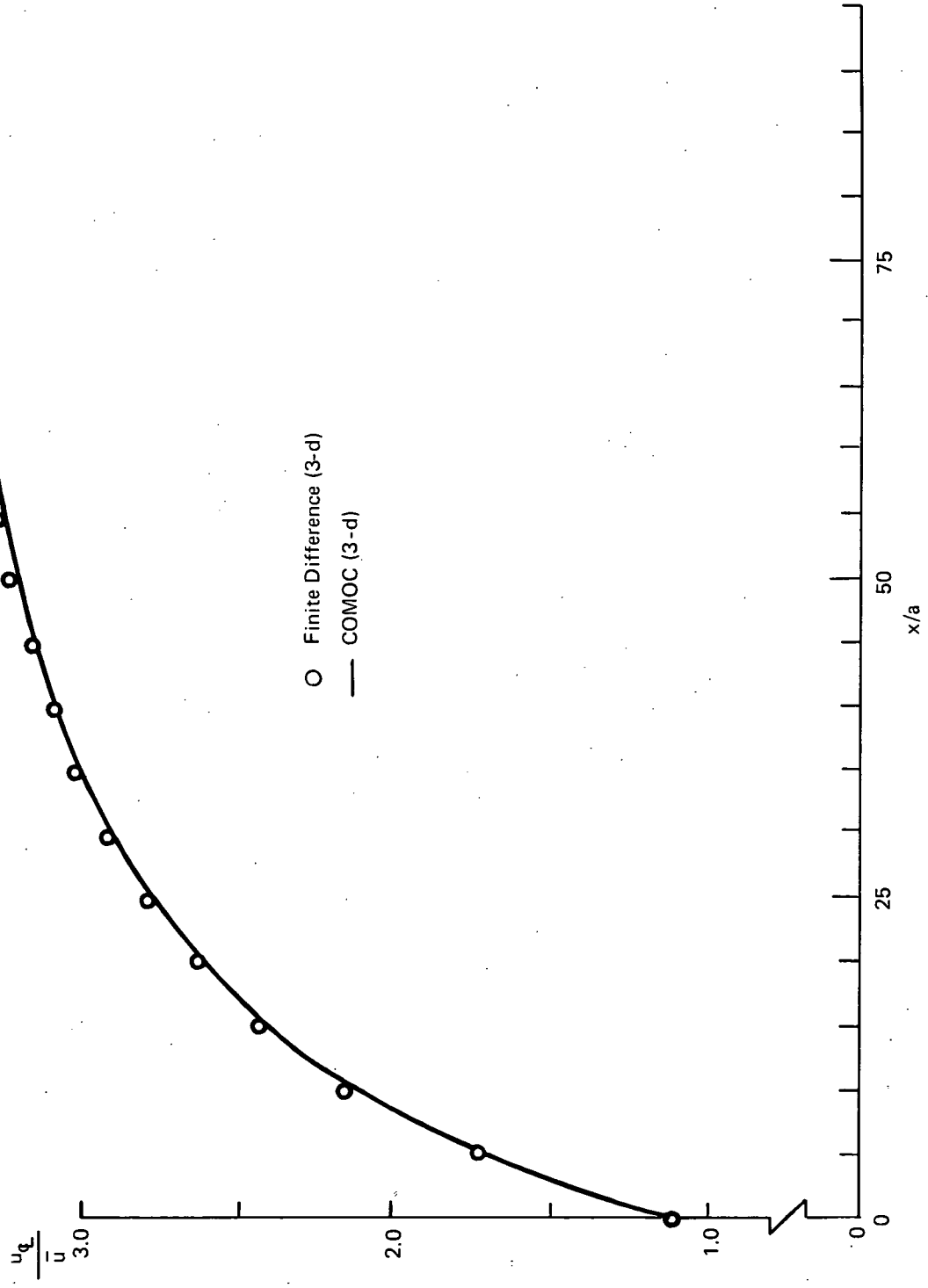


Figure 25. Growth of Centerline Velocity for Fluted Pipe Flow

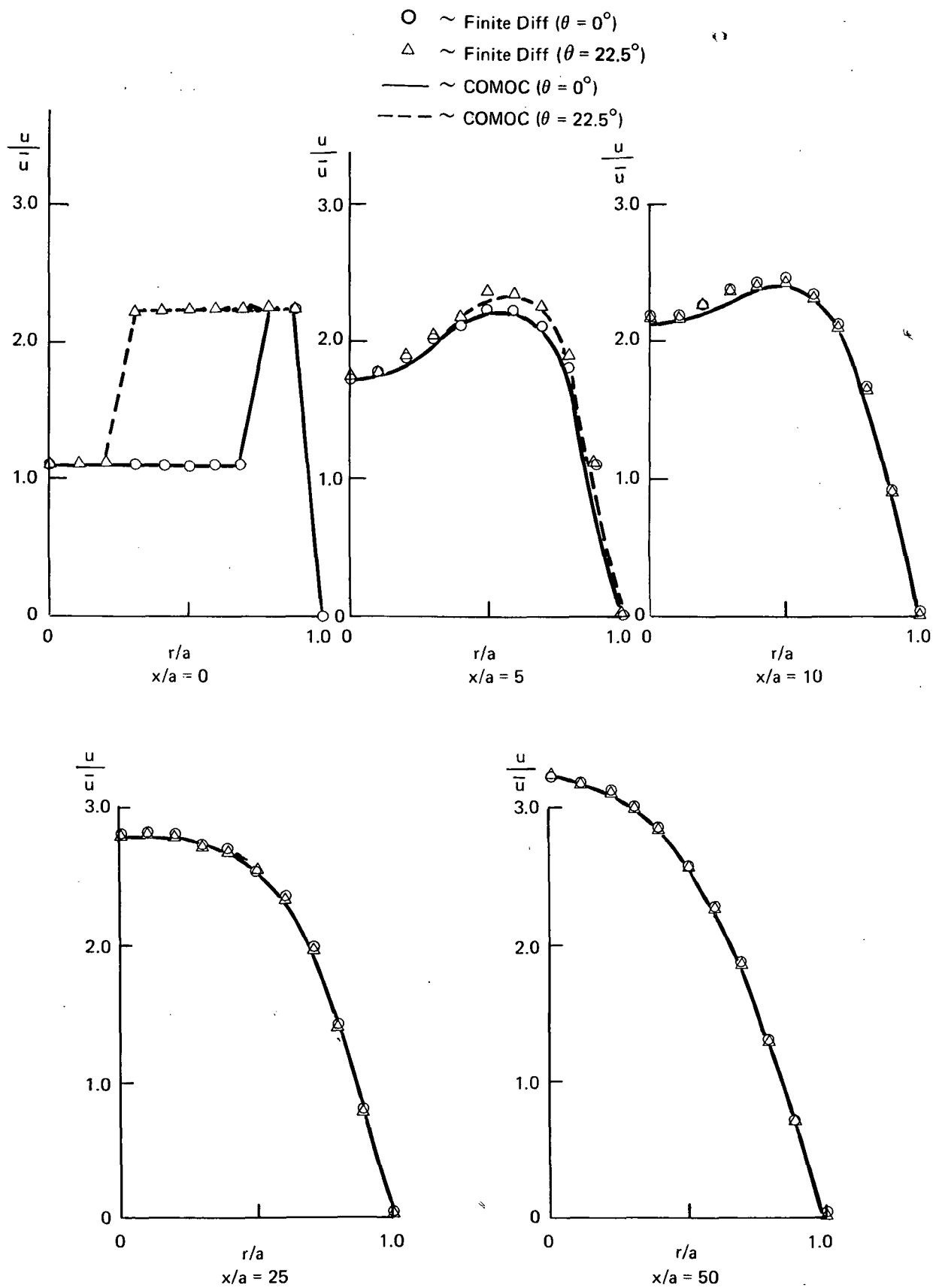


Figure 26. Axial Velocity Profiles for Fluted Pipe Flow

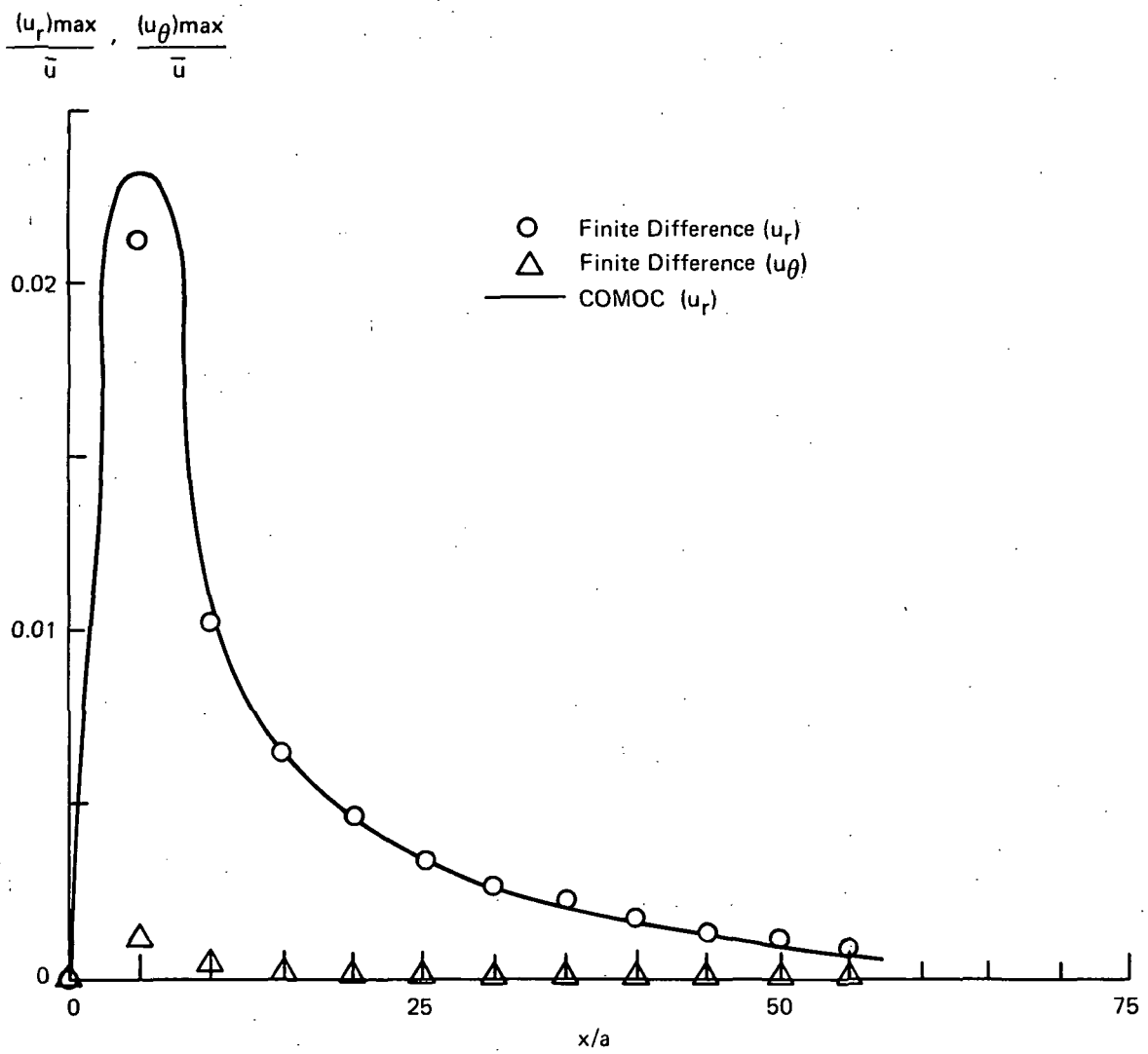
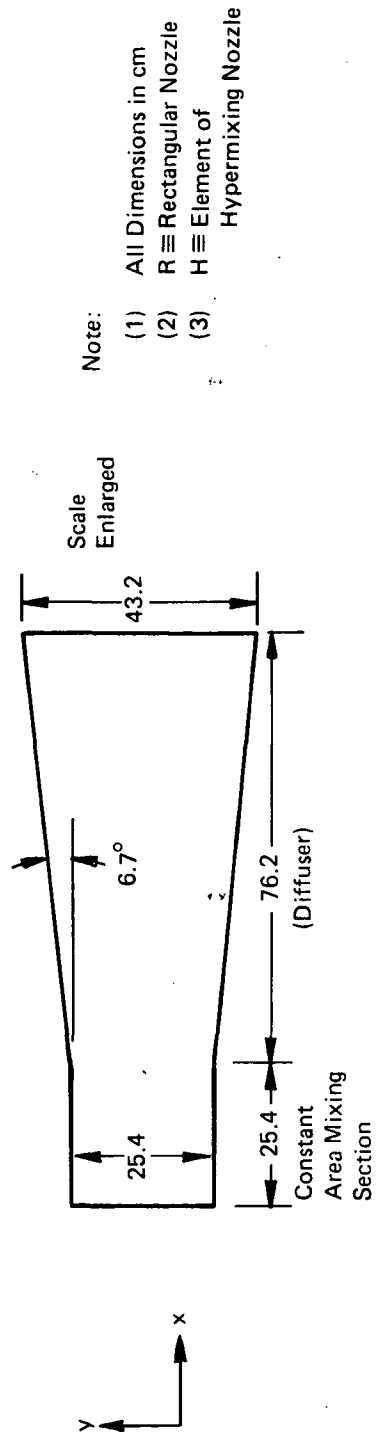
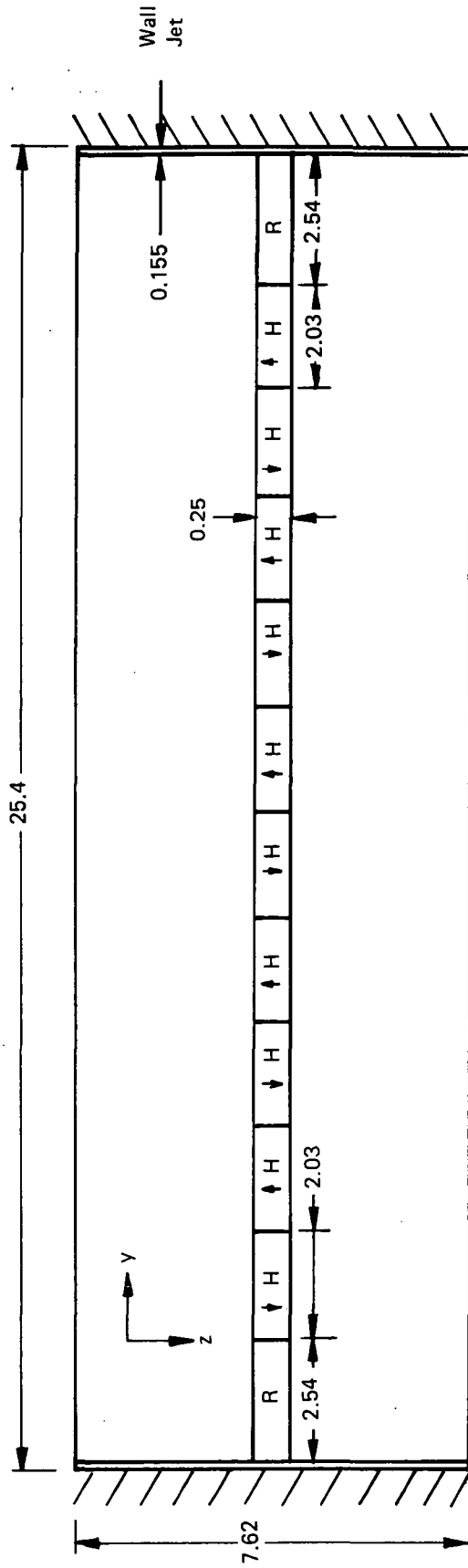


Figure 27. Maximum Secondary Velocities for Fluted Pipe Flow



Note:

- (1) All Dimensions in cm
- (2) R \equiv Rectangular Nozzle
- (3) H \equiv Element of Hypermixing Nozzle

Figure 28. Ejector/Diffuser Configuration

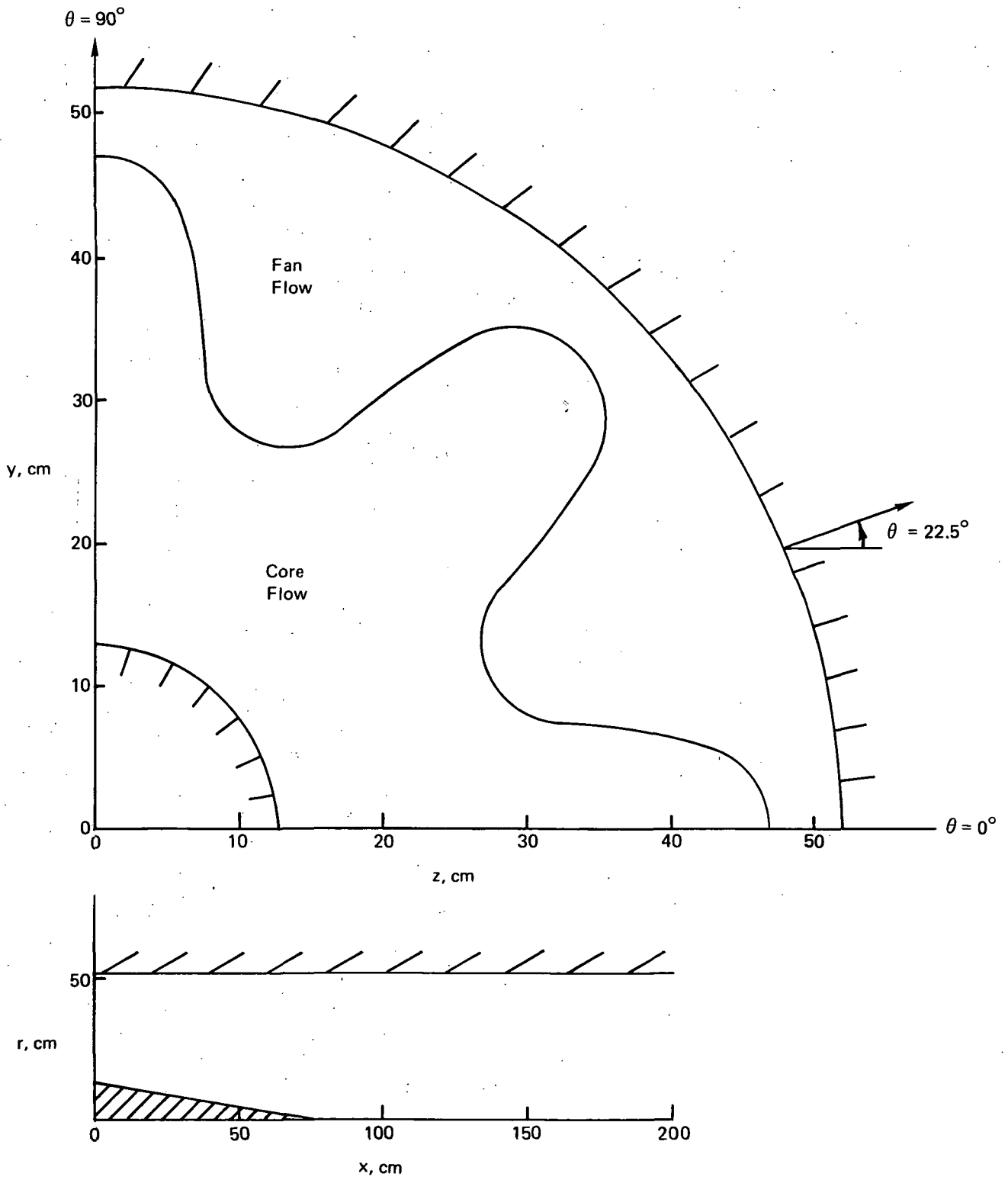


Figure 29. Axisymmetric Fluted Mixer Geometry

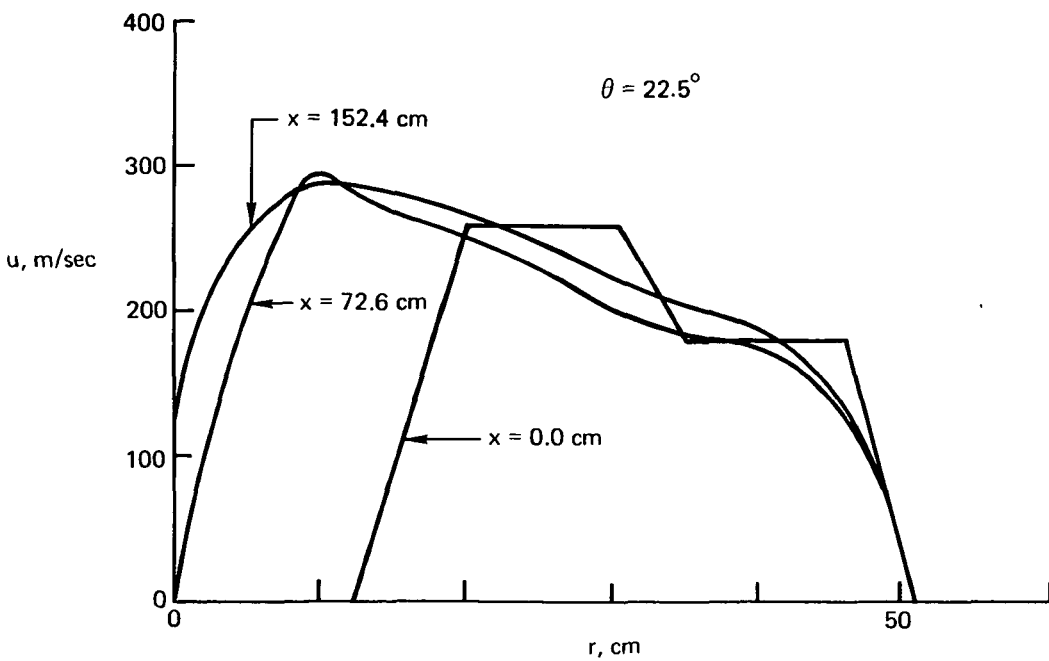
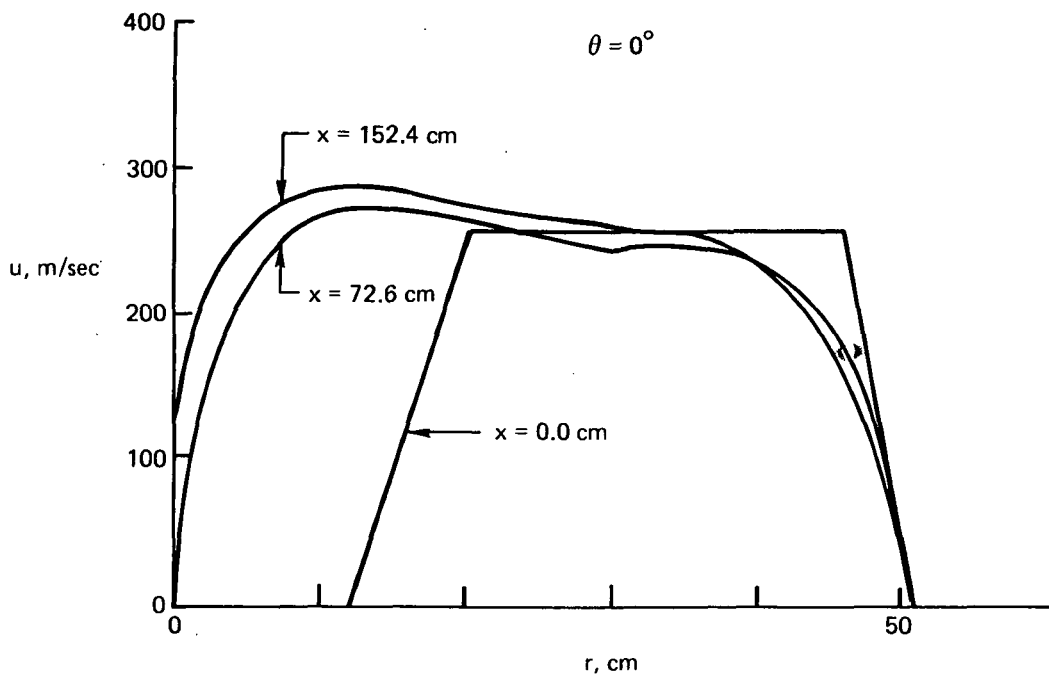


Figure 30. Axial Velocity Profiles for Fluted Mixer

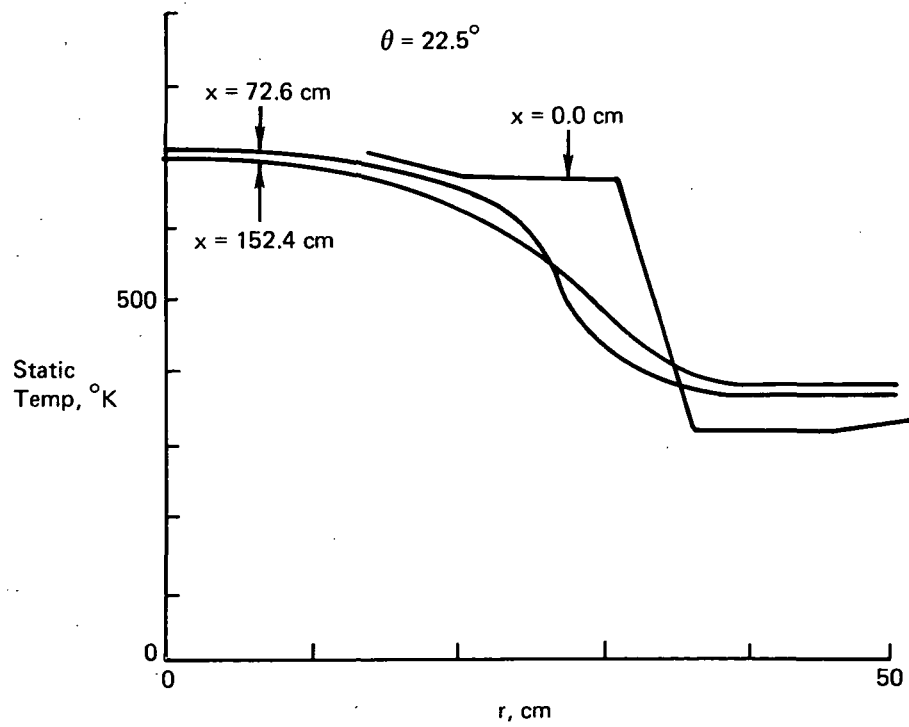
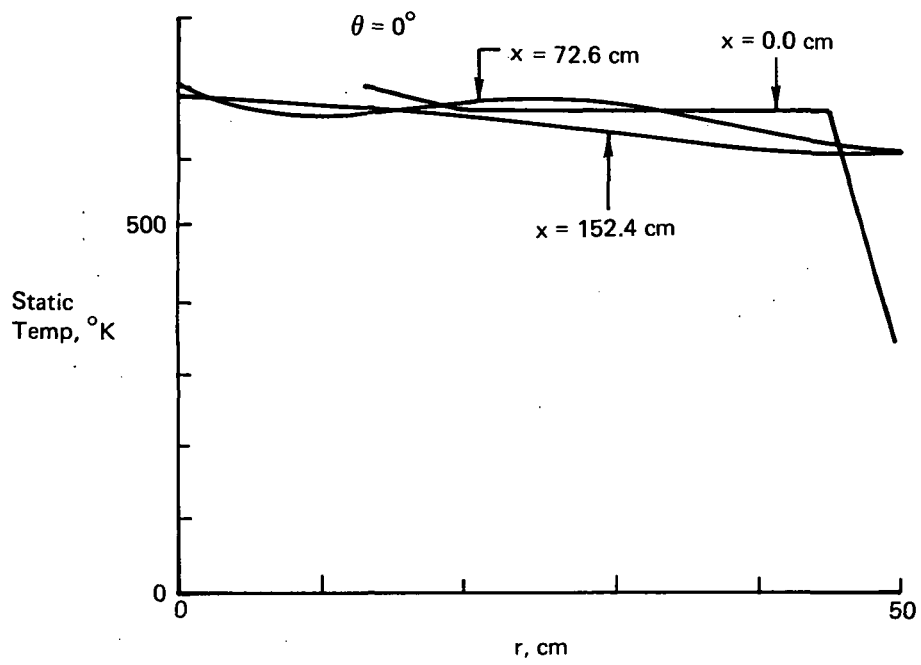


Figure 31. Static Temperature Profiles for Fluted Mixer

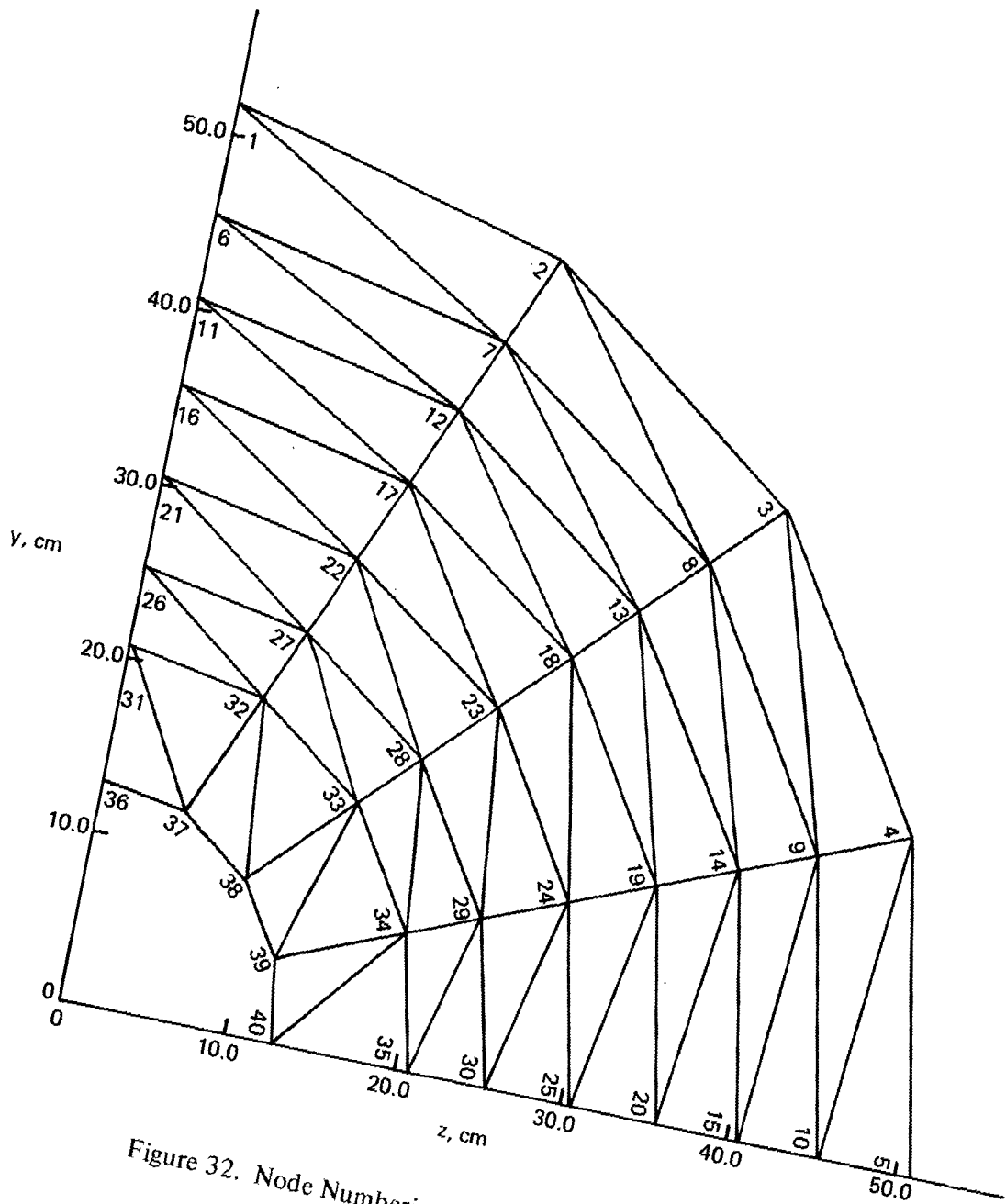


Figure 32. Node Numbering of Finite Elements for Case IV

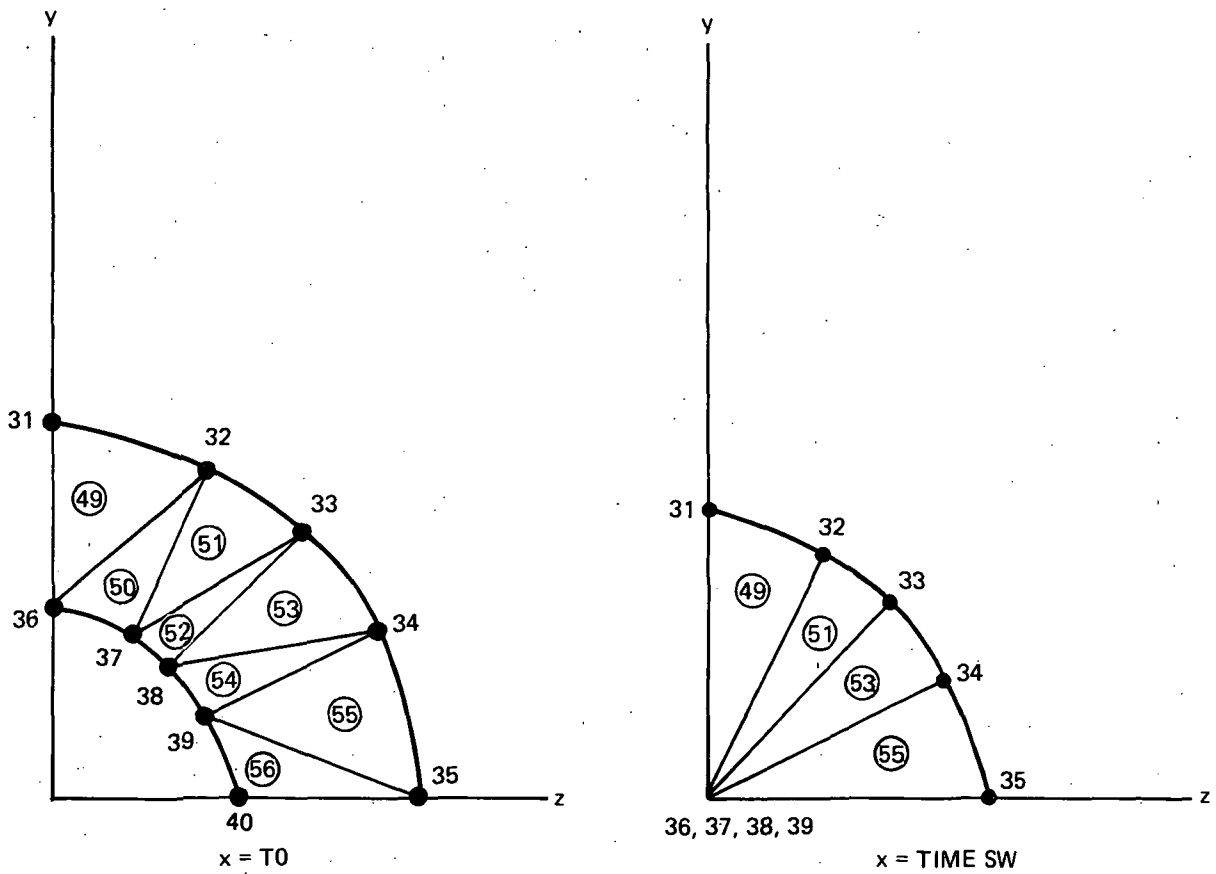


Figure 33. Finite Elements and Nodes for Changing Boundary Condition